Delft University of Technology // BioClear Earth

Engineering a horizontal layer of reduced permeability using Al-DOM precipitation

Johannes Popma

creating with the power of nature

Engineering a horizontal layer of reduced permeability using Al-DOM precipitation

Msc. Thesis

By

Johannes Popma
Student number: 4522362

To obtain the degree of **Master of Science**
in Civil Engineering at the Delft University of Technology.

Members of the thesis committee:

Prof. Dr. Ir. T.J. Heimovaara	(TU Delft – Geo-Engineering)
Dr. S.J. Laumann	(TU Delft – Geo-Engineering)
Dr. B. van Breukelen	(TU Delft – Watermanagement)
Dr. K.H.A.A. Wolf	(TU Delft – Applied Geophysics and Petrophysics)
Msc. O. Brock	(University of Amsterdam)
Msc. A. Nipshagen	(BioClear Earth)

Faculty of Civil Engineering and Geo-Sciences – Delft University of Technology

Section of Geo-Engineering

Abstract

Leakage of contaminants to the subsurface is a potential threat to groundwater and is a major problem with storage tanks. When the contaminant reaches the groundwater, it can be subjected to subsurface flow due to which a contaminant plume may form and the contaminant can spread. In this research, it was investigated if a horizontal layer of reduced permeability can be engineered by using the SoSEAL (**So**il **S**ealing by **E**nhanced **A**luminium and DOM **L**eaching) concept to prevent leakage. Within SoSEAL, Aluminium-Dissolved Organic Matter complexation is used to clog the pore space with a reduction in permeability and hydraulic conductivity as a result. The concept is based on the natural process of podsolization in which a layer of reduced permeability (a *hardpan*) is formed by decades of organic matter leaching to the subsurface while complexing with metal cations. In this research, the complexation reaction using Aluminium-Chloride Hexahydrate and HUMIN-P 775 (Organic Matter) was investigated. The study roughly consisted of two parts, one concerning a situation of ideal mixing and one where the chemicals mixed inside a porous medium. When considering ideal mixing, eleven samples were created with 40 mL of Organic Matter solution and Aluminium solution in the range of 0 to 4 ml was added. These samples were created with an initial OM pH of 5, 7 and 9 to investigate the pH effect. The precipitation was quantified on the basis of measured pH, EC, UV254 and weight. With UV254 measurements it was found that 85% of the organic matter is able to form precipitates by binding aluminium ions. Depending on the pH, the amount of aluminium which needed to be added to reach this 85% varies. At a lower pH, less aluminium salt is needed to be added to form complexes with the available organic matter.

The precipitation as a result of the complexation was also formed in the three-dimensional experimental set up. The chemicals were injected via horizontal drains and a flow was created towards an overflow drain. A narrow precipitation band of a few millimetres thick was formed at the contact interface of the aluminium and organic matter solutions. The Al-DOM precipitation was visualized with a 3D interpretation of photographs of horizontal cross-sections in Matlab. The results of this interpretation showed that it was difficult to form an area-covering layer of precipitates. Most precipitation was shown near the injection- and overflow drains, this assumes that due to separation of flow no Al-DOM precipitation took place in the middle of the set-up. Due to the lack of an area-covering layer, a significant reduction of hydraulic conductivity could not be measured. An average reduction of about 25-30% was measured. In COMSOL it was assumed that in ideal situations the precipitation band could cause a reduction in permeability of about two order of magnitude. The results of this research show that the SoSEAL concept, using HUMIN-P 775 and aluminium hexahydrate, can be used to form a horizontal layer of reduced permeability, but that it is challenging to create an area-covering layer due to separation of flow and preferential flow paths.

Contents

Appendices

List of Figures

List of Tables

Chapter 1

Introduction and Research Goals

This page is intentionally left blank

1.1 Introduction

Leakage of contaminants to the subsurface is a potential threat to groundwater and is a major problem in storage tanks (Fitts, 2012). When a storage tank is leaking and there is no impermeable layer present underneath the tank, the contaminant can infiltrate into the subsurface. The contaminant may dissolve in percolating water and potentially be a source of groundwater contamination (Bear & Cheng, 2011). When the contaminant reaches the groundwater, it is subjected to subsurface flow due to which a contaminant plume may form and the contaminant is able to spread (Fitts, 2012).

To make regulations for such potential leakage of contaminations in the Netherlands, there are the *Publicatiereeks Gevaarlijke Stoffen (PGS, Publication series for dangerous substances).* In this series of publications, guidelines are given for the production, transport, storage and use of dangerous substances (Projectbureau PGS, 2012). According to the PGS-29 guideline, for the storage of flammable liquids above ground level in vertical cylindrical tanks, a cross-section of a storage tank should look like the one depicted in Figure 1.1. The purple depicted line in the figure represents an impermeable layer which can be installed to prevent leakage from the tank to the subsoil. In existing tanks, such a layer is not compulsory and therefore often not present in the construction. It is possible that in the future such a layer, according to PGS-29, becomes compulsory for all existing tanks as a preventative measure against leakage to the subsurface flow.

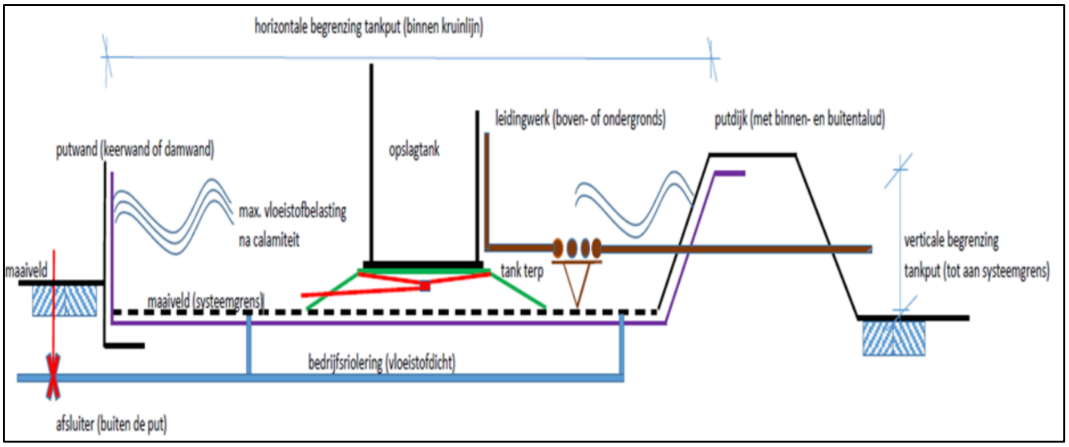

Figure 1.1: Principle cross-section of a storage tank
Figure taken from (Projectbureau PGS, 2012)

In water management and civil engineering, it is a challenging task to control subsurface flow. Rigid civil engineering structures are used as robust barriers to prevent leakage flow but require a disruption to above ground activities and are often expensive. At places where no rigid civil engineering structures are present to prevent leakage flow, the leakage is controlled by the permeability of the soil (Bear & Cheng, 2011; Fitts, 2012). Control of the permeability of the soil therefore is a tool for subsurface water management. Engineering a horizontal layer of reduced permeability underneath a storage tank potentially prevents/reduces the leakage of contaminants towards the subsurface.

1.2 Natural Layers of Reduced Permeability

In Nature, several processes take place which result in layers of reduced permeability over time. The processes which form these natural layers are an inspiration for an ecological engineering approach for infiltration and leakage problems. Examples of such processes are podsolization and calcite precipitation.

In the process of podsolization, an almost impermeable layer is formed consisting of organic/inorganic precipitates of aluminium and iron in the original pore space (Ferro-Vázquez, Nóvoa-Muñoz, Costa-Casais, Klaminder, & Martínez-Cortizas, 2014; B. Jansen, Nierop, & Verstraten, 2004). In Figure 1.2 a podzol on the Lüneberger moorland is depicted. The dark layer in the picture is the formed layer of reduced permeability which is called the B-horizon and can take decades to form (Sauer et al., 2007). Since the process of podsolization is slow, the process is not directly suitable for engineering purposes which have to be created in a short period of time.

Figure 1.2: Example of a podzol on the Lüneberger moorland
Photograph taken by Nikanos.

Another natural occurring process is MICP (Microbially Induced Carbon Precipitation) which is the formation of calcite precipitation in the pore space (Pacheco Torgal, Labrincha, Diamanti, & Lee, 2015). The two most familiar mechanisms of calcite precipitation are 1) making use of urease producing bacteria (Nemati & Voordouw, 2003) or 2) by denitrification (van Paassen et al., 2010). The process of MICP is already an inspiration for an engineering approach to enhance the strength properties of sandy soils with calcium carbonate precipitates and can potentially be used to create pore-filling precipitates (Ivanov & Chu, 2008). In Figure 1.3 the formation of calcium carbonate by microbial activity is shown on plant roots in the tropics.

Figure 1.3: CalciumCarbonate formation through microbial action
(Source: tropicalbotany.wordpress.com

1.3 SoSEAL

The SoSEAL (**So**il **S**ealing by **E**nhanced **A**luminium and DOM **L**eaching) project is inspired on the podsolization process and has the purpose to develop the foundations of a cost-effective, robust and environmentally compatible technology for in-situ permeability reduction of sub-surface systems. The SoSEAL project has as advantage that it can be carried out without any interruption to above ground activities and buildings.

Within SoSEAL, permeability reduction is studied using an aluminium solution and dissolved organic matter (DOM) which are pumped into the soil. Aluminium ions can bind to deprotonated functional groups of DOM to form Al-DOM complexes (Nierop, Jansen, & Verstraten, 2002; Tipping, 2002). The complexes are formed as a function of the pH and Metal/Carbon ratio which both influence the solubility (Ferro-Vázquez et al., 2014). The formed complexes can accumulate in the pore space leading to a reduction in permeability in the soil. Previous research on the SoSEAL concept has shown a possible reduction in permeability of 80% (Bonfiglio, 2016; Hopman, 2016; Vis, 2015).

1.4 Research Goals

Scientific research on the SoSEAL concept has been done in various previous works. In the works of Bonfiglio (2016), Hopman (2016) and Vis (2015), the SoSEAL concept was investigated as a preventive measure against piping to enhance the stability of dikes. The resulting Al-DOM precipitation layer to prevent piping was a vertical oriented layer of reduced permeability in a highly conductive aquifer. For a leakage problem, which is the main concern in this research, the layer of reduced permeability needs to be engineered horizontally. To engineer a horizontal layer of Al-DOM precipitates, a different injection strategy needs to be investigated.

In this research, it is investigated if the SoSEAL concept can be used to engineer a horizontal layer of reduced permeability. Such a horizontal layer of reduced permeability can possibility be engineered underneath a storage tank according to the PGS 29. The aims of this research are defined as:

1. Characterize the complexing behaviour of organic matter with aluminium cations as a function of:
    a. pH
    b. Aluminium/Organic Matter concentration ratio

2. Develop a three-dimensional experimental set-up in which a horizontal precipitation band is expected.

3. Visualize the Al-DOM precipitation in a three-dimensional way to get insights in three-dimensional distribution of the Al-DOM precipitation.

4. Determine the hydraulic conductivity reduction due to Al-DOM precipitation in the three-dimensional set up.

Chapter 2

Theoretical Background

This page is intentionally left blank

In this research, the possibility of engineering a horizontal layer of reduced permeability using the SoSEAL concept is investigated. In this chapter, an overview of the theoretical background of the related topics is presented. In the first part the natural process of podsolization process is described in more detail. Subsequently an overview of the Al-DOM interaction and flow properties in porous media are given.

2.1 Podzols

Podzols are defined as soils that contain amorphous organometallic complexes (Bourgault, Ross, & Bailey, 2015). They are characterized by their organic surface (O/A) horizon, underlain first by a weathered grey eluvial (E) horizon enriched in minerals with a slow weathering rate and next by a dark brownish-reddish illuvial (B) horizon, which is enriched by aluminium and iron, followed by a relatively unaffected C horizon. This sequence is illustrated in Figure 2.1. The illuvial (B) horizon in podzols where the groundwater table is high does not enrich in iron, probably because iron is reduced (Lundström, Van Breemen, & Bain, 2000). Podzol formation can take decades to develop. Various studies state that in Europe podzol formation time may range from 1000-6000 years (Sauer et al., 2007). The illuvial (B) horizon has a low permeability caused by the pore filling precipitates.

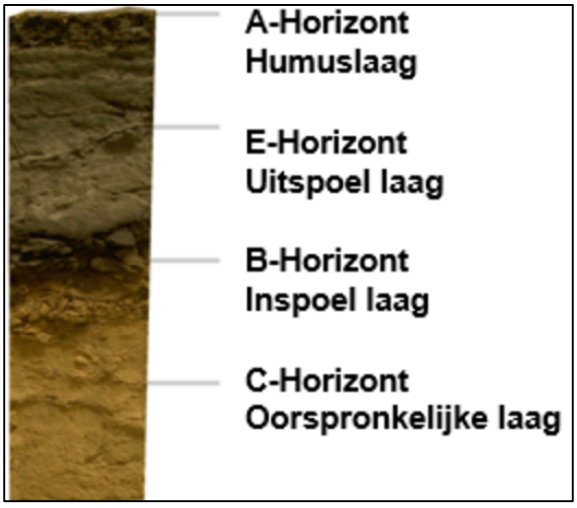

Figure 2.1: Podzol characterisation
Source: ***www.geocaching.com***

The exact mechanism for the immobilization of aluminium and iron in the B-horizon is the subject of an ongoing debate. According to Lundström, Van Breemen, Bain, et al., (2000) two main theories for the mechanisms of podsolization are now prevalent

1. In the adsorption/precipitation theory, relatively high molecular weight organic acids leached from the O horizon, form complexes with aluminium and iron. Due to continuing adsorption of metals to the complex during the downward translocation, precipitation occurs after a specific Metal/Carbon (M/C) ratio has been reached (McKeague, Brydon, & Miles, 1971). Precipitation occurs when the negatively charged organic particle is saturated with the positively adsorbed cations (De Coninck, 1980).

2. In the Biodegradation theory, mainly low molecular weight organic acids are microbially decomposed during downward migration which induces release and precipitation of the metal ions. High molecular weight organic acids, which are more resistant to microbial degradation, can then absorb on the metal ions (Lundström, Van Breemen, Bain, et al., 2000).

(Sauer et al., 2007) mentions various other mechanisms of immobilization; precipitation of complexes can occur due to an increasing pH with depth, abrupt changes in pore size and oxidation of the complexes as they are leached to greater depth. It is however generally accepted that aluminium and iron migrate downwards in the form of organic complexes and that DOM is crucial in this substance transport (Jansen, Nierop, & Verstraten, 2003; Lundström, Van Breemen, & Bain, 2000; Sauer et al., 2007). The podsolization process is therefore summarized in three interrelated steps: (1) formation of a soluble Aluminium/Iron-organic matter complex in the soil surface; (2) translocation of the complex with soil water; and (3) precipitation of the complex in the B horizon.

The above mentioned classical theory of podsolization, assumes vertical unsaturated flow and thus a horizontal B-horizon development. However, hillslope-scale lateral podsolization also occurs where lateral subsurface water fluxes predominate (Bourgault et al., 2015; Jankowski, 2014; Sommer, Halm, Weller, Zarei, & Stahr, 2000). Bourgault et al. (2015) suggests that lateral podsolization occurs via solution transport of aluminium ions and DOM downslope with groundwater, followed by complexation and immobilization. More information about lateral podsolization is found in appendix A.1.

2.1.1 Metal Cations in Podzols and SoSEAL

Iron and aluminium are the most common metal sources found in podzols. In acidic solutions iron and aluminium are present as free ions and mono- and dihydroxide ions (Nierop et al., 2002; Tipping, 2002). Other metal cations like magnesium, calcium and cupper may also form complexes with organic matter. However, due to the higher valence of iron and aluminium, their binding capacity is also higher (Nierop et al., 2002; Stevenson, 1994). Fe^{3+} ions form the strongest complexes followed by Al^{3+}- and Fe^{2+}ions (Duan & Gregory, 2003; Nierop et al., 2002). Although Fe^{3+} ions form the strongest bonds with organic matter, in the SoSEAL project aluminium is used. This is because Fe^{3+} ions can be reduced to Fe^{2+} and the latter one does not form stable complexes. Also, Fe^{3+} formed complexes can be reduced to unstable Fe^{2+} complexes by microbial activity (Eusterhues et al., 2014).

2.2 Organic Matter

Humic substances are complex, acidic organic molecules formed by the decomposition of plants, animals and microbial materials (Matilainen, Vepsäläinen, & Sillanpää, 2010). Besides incomplete litter decomposition as source of organic complexing agents, also exudates of plant roots, fungi and microorganisms may provide organic complexing agents (Lundström, Van Breemen, Bain, et al., 2000; Sauer et al., 2007). Humic substances are abundant and persistent in the biosphere and immediate subsurface, being present in particulate and dissolved forms in soils, waters and sediments. The majority of the organic carbon is present in this humic matter. The carbon content of humic substances is typically just greater than 50% on weight basis. Hydrogen contents are around 5% and oxygen in the range of 30-40% on weight basis. (Tipping, 2002). Approximately 80% of the hydrogen is bonded to carbon, the rest to oxygen. These latter bindings form the functional groups in organic matter. The major oxygen-containing functional groups present in organic matter are carboxylic acid groups and phenolic groups (Rashid & King, 1970; Tipping, 2002). These functional groups can be seen in a proposed molecular structure of organic matter in Figure 2.2.

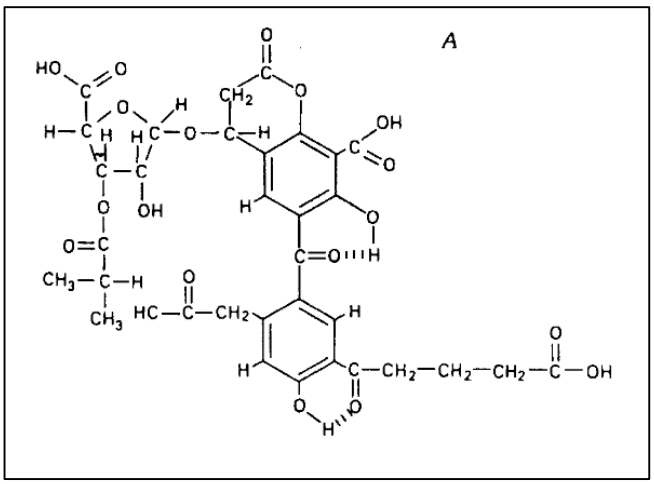

Figure 2.2: Proposed molecular structure of organic matter
Copied from Tipping (2002)

The most mobile fraction of organic matter in soils is present in the form of dissolved organic matter (DOM). DOM is defined through filtration. The size limit, which is used to differentiate DOM from organic matter is somewhat arbitrary, but there is an almost universal consensus that it is around 0.45 microns (Zsolnay A., 2003).

A distinction, as an alternative to DOM, is often made between humic acids, fulvic acids and humin (Tipping, 2002). Humic acids are defined as a group of compounds which are extracted from the soil which precipitate upon acidification. Fulvic acids stay in solution upon acidification. Humin is the part of organic matter which is mostly insoluble. Roughly concluded, humic acids and humin occur mostly in soils as part of the solid phase, whereas fulvic acids are more mobile and are art of the DOM fraction. The chemical composition of different humic and fulvic acids is explained in appendix A.2.

2.3 Solubility

In this section, the solubility of organic matter and aluminium are discussed. The two substances need to be dissolved before the complexation interaction can take place.

2.3.1 Organic Matter Solubility

The solubility of organic matter in water depends on the polarities of its functional groups and whether they can ionize (Zsolnay A., 2003). Besides the functional groups also the aromaticy of the organic matter plays a role in the solubility. As can be seen in the proposed molecular structure of organic matter (Figure 2.2), organic matter consists of hydrophobic aliphatic and aromatic hydrocarbon parts, but also of hydrophilic functional groups. The carboxylic and phenolic functional groups can deprotonate and ionize.

Ionization of the carboxylic and phenolic groups to their conjugate base and a proton is shown in equation 2.1 and 2.2 respectively. The pH value determines the degree of deprotonation. Phenolic groups dissociate at pH>7 and carboxylic at pH<7 (Tipping, Lofts, & Sonke, 2011).. Dissociation makes the organic matter molecule more hydrophilic and therefore more soluble. High pH levels will lead to the most deprotonation and therefore increase the solubility of the organic molecule. The acid dissociation constants depend on the type of functional groups and the aromaticity of the substance. It can range from pK values of 3.9 to 9.3 for humic acids (Klučáková & Kolajová, 2014).

$$RCOOH \rightarrow RCOO^- + H^+ \qquad \boldsymbol{K_{RCOOH}} = \frac{[RCOO^-][H^+]}{[RCOOH]} \qquad Carboxylic \qquad (2.1)$$

$$ROH \rightarrow RO^- + H^+ \qquad \boldsymbol{K_{ROH}} = \frac{[RO^-][H^+]}{[ROH]} \qquad Phenolic \qquad (2.2)$$

2.3.2 Aluminium Solubility

When metals, like aluminium, are dissolved in water, the metal will react with water molecules and form metal-hydroxide (ions). This process is called hydrolysis. The hydrolysis of aluminium in water with corresponding solubility constants are represented by equations 2.3 till 2.6. The solubility constant for the metal hydroxide is given in equation 2.7. Values for the solubility constants are given in Table 2.1.

$$Me^{3+} + H_2O \leftrightarrow Me(OH)^{2+} + H^+ \qquad \boldsymbol{K_1} \qquad (2.3)$$

$$Me(OH)^{2+} + H_2O \leftrightarrow Me(OH)_2^+ + H^+ \qquad \boldsymbol{K_2} \qquad (2.4)$$

$$Me(OH)_2^+ + H_2O \leftrightarrow Me(OH)_3 + H^+ \qquad \boldsymbol{K_3} \qquad (2.5)$$

$$Me(OH)_3 + H_2O \leftrightarrow Me(OH)_4^- + H^+ \qquad \boldsymbol{K_4} \qquad (2.6)$$

$$Me(OH)_3 \leftrightarrow Me^{3+} + 3OH^- \qquad \boldsymbol{K_s} \qquad (2.7)$$

Table 2.1: Equilibrium constants for metal hydrolosis.
Copied from Duan & Gregory (2003)

	pK_1	pK_2	pK_3	pK_4	pK_s
Al	4.95	5.6	6.7	5.6	31.5

In Figure 2.3 the aluminium speciation at different pH values is depicted. It can be seen that the solubility of aluminium is lowest at neutral pH (around pH=6) where the precipitate $Al(OH)_3$ is mostly present. For complexation purposes, free Al^{3+}-ions are most of interest, these are most available at lower pH.

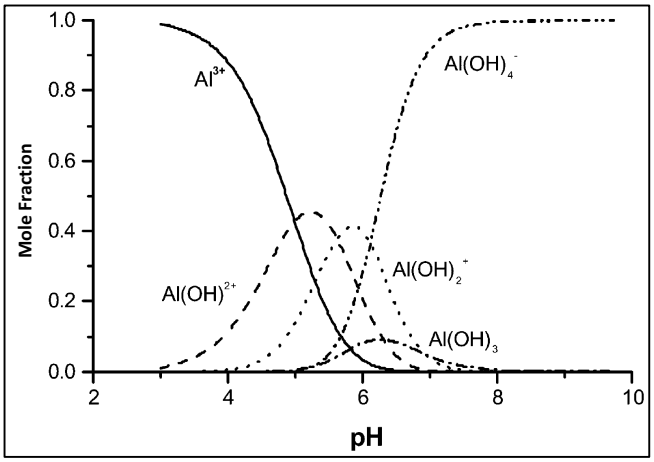

Figure 2.3: Solubility of Aluminium at various pH
Copied from Duan & Gregory (2003)

2.4 Al-DOM Complexation

The interaction of dissolved metal species with other types of solutes is known as complexation. Complexation between metal cations and organic matter is studied in many researches. In appendix A.3 an example of complexation with cupper cations is given, which illustrates the effect of organic matter. The complexation between aluminium cations and organic matter is also studied by many authors. It is found that 80-85% of soluble aluminium in E horizon of podzols can form complexes with organic matter (Lundström, 1993).

Complexation can occur in two ways; outer-sphere and inner-sphere complexation (Tipping, 2002). In outer-sphere complexes, the ligand is situated in the outer coordination sphere, forming no direct bonds to the metal ion and held by the relatively weak forces of electrostatic attraction and hydrogen bonding. Inner-sphere complexes involve the displacement of one or more water molecules from the inner coordination sphere to form a direct metal ligand bond by sharing the ligand's free electron pair. For this research, the complexation reaction is not worked out in inner and outer-sphere complexation but is simplified. The complexation reaction between aluminium and dissolved organic matter is described in three different ways; (1) by an equilibrium equation, (2) the law of actions and (3) by a mass balance.

In the complexation reaction between aluminium and DOM, a metal cation binds to a deprotonated functional group. The deprotonation of the functional groups is described in equation 2.1 and 2.2. The positively charged metal ion binds to the negatively charged functional group. The equilibrium reaction for and aluminium ion and a carboxylic functional group is given in equation 2.8. Because aluminium has a valence of 3+, it can bind to three deprotonated functional groups and therefore can form rigid ring structures (Duan & Gregory, 2003). In equation 2.9 a simplified equilibrium between DOM and aluminium is given. The equilibrium constant pK_{AlDOM} ($\log(K_{AlDOM})$) is approximately equal to 2.67 (Tipping, 2002).

$$Al^{3+} + 3RCOO^- \rightarrow Al(RCOO)_3 \quad (2.8)$$

$$Al + DOM \leftrightarrow AlDOM \qquad \boldsymbol{K_{AlDOM}} = \frac{[AlDOM]}{[Al][DOM]} \quad (2.9)$$

The law of actions can be expressed in reaction rates. In these equations (equation 2.10 and 2.11), the formation (forward reaction) and dissociation (backward reaction) of complexes are expressed. Rate constants for the forward reaction are in the range of 10^3 – 10^9 $dm^3mol^{-1}s^{-1}$ which implies that complexation happens in seconds after the solutes are mixed (Tipping, 2002). The backward rate constants for Al^{3+} and Fe^{3+} are appreciably slower and around 10 – 100 s^{-1} (Tipping, 2002). Much smaller values of the backward reaction can apply to chelates, which are compounds in which a metal ion is bound to a ligand. This means that stable complexes dissociate very slowly.

$$Al + DOM \rightarrow AlDOM \qquad \frac{\partial AlDOM}{\partial t} = k_f[Al][DOM] \quad (2.10)$$

$$AlDOM \rightarrow Al + DOM \qquad \frac{\partial AlDOM}{\partial t} = -k_b[AlDOM] \quad (2.11)$$

The mass balances for aluminium and DOM are given in equation 2.12 and 2.13. In these equations, it is assumed that aluminium only occurs in free ion or complexed form.

$$T_{DOM} = [DOM^-][DOM][AlDOM] \quad (2.12)$$

$$T_{Al} = [Al][AlDOM] \quad (2.13)$$

In Vis (2015) and Tipping (2002) a variable is introduced which is the average amount of metal bound per mole/gram of ligand. The expression for v is given in equation 2.14. From this equation is becomes clear that at a given pH value (constant H^+ concentration), v is a unique function of the concentration of the metal ions. In other words, it does not depend upon the total ligand concentration.

$$v = \frac{[AlDOM]}{T_{DOM}} = \frac{K_{AlDOM}[Al]}{1 + K_{AlDOM}[Al] + \left(\frac{[H^+]}{K_{RCOOH}}\right)} \quad (2.14)$$

When aluminium and DOM solutions are put together, the complexation happens instantly and insoluble flocs are formed (Vis, 2015). The M/C ratio and pH are the two main factors which influence the complexation and precipitation behaviour (Ferro-Vázquez et al., 2014)(Stevenson, 1994). The pH determines the equilibrium with insoluble inorganic metal phases (metal oxides as a result of metal hydrolysis), as well as the degree of deprotonation of carboxylic acid and phenolic hydroxyl groups on DOM involved in metal binding (Jansen, Nierop, & Verstraten, 2002). The M/C ratio determines to what extent the negative charge on the DOM molecules resulting from deprotonation is compensated by the positive charge on metal cations, with a net zero charge inducing precipitation of the complex. At higher M/C ratios, it will be increasingly difficult for cations to find unoccupied binding sites, also there will be an increasing electrostatic repulsion by residual positive charge left on cations that are already bound to organic matter (Jansen et al., 2002).

In Nierop et al. (2002), the pH and M/C dependency of aluminium and carbon precipitation has been investigated by titration experiments. In Figure 2.4 the results of these experiments are shown. In Figure 2.5 the results of a similar research conducted by Jansen et al. (2003) are shown in which the distribution of aluminium species as function of pH and M/C ratio is investigated. The fraction of free aluminium ions is highest at the lowest pH value due to the highest solubility of aluminium at lower pH (Figure 2.3) and because less functional groups have deprotonated (section 2.3.1). Highest precipitation amounts occur at high M/C ratios and higher pH since the most binding sites are present. Soluble Al-DOM complexes are present at M/C ratios lower than 0.03 where no pH differences are seen. At higher M/C ratios, a strong pH effect was observed.

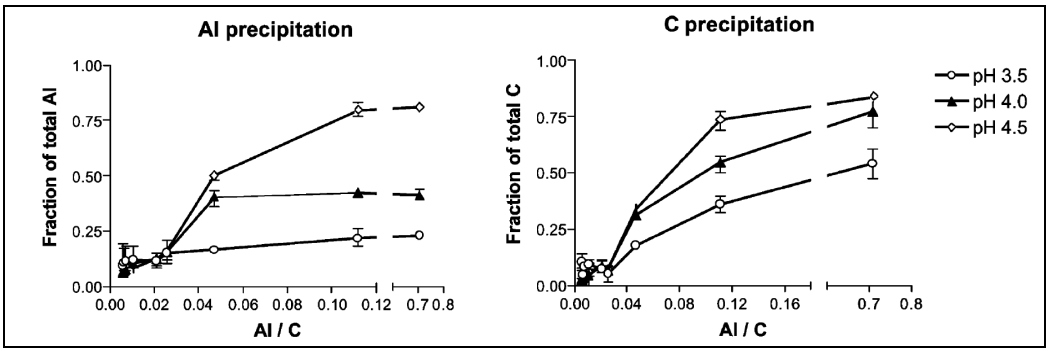

Figure 2.4: Precipitation of aluminium and carbon as function of pH and M/C ratio
Copied from Nierop et al (2002).

The size of the formed complexes is related to stirring rates/turbulence and the pH. A low pH leads to smaller flocs (Scheel, Haumaier, Ellerbrock, Rühlmann, & Kalbitz, 2008). This is because less binding sites are available and therefore the aluminium cannot react with multiple binding sites leading to smaller flocs. The effect of turbulence was investigated in experiments conducted by Hopman (2016). High stirring rates resulted in smaller flocs.

Complexation reduces the solubility of aluminium and organic matter. When organic matter is complexed with aluminium, protection mechanisms operate and (microbial) degradation rates are reduced significantly compared to organic matter itself (Scheel et al., 2008; Tipping, 2002). This phenomenon is already explained in section 2.4. Stevenson (1994) summarizes other factors which influence the stability of a complex; (1) the number of atoms which form a bond with the metal ion, (2) the number of rings formed, (3) the nature and concentrations of metal ions and (4) the pH.

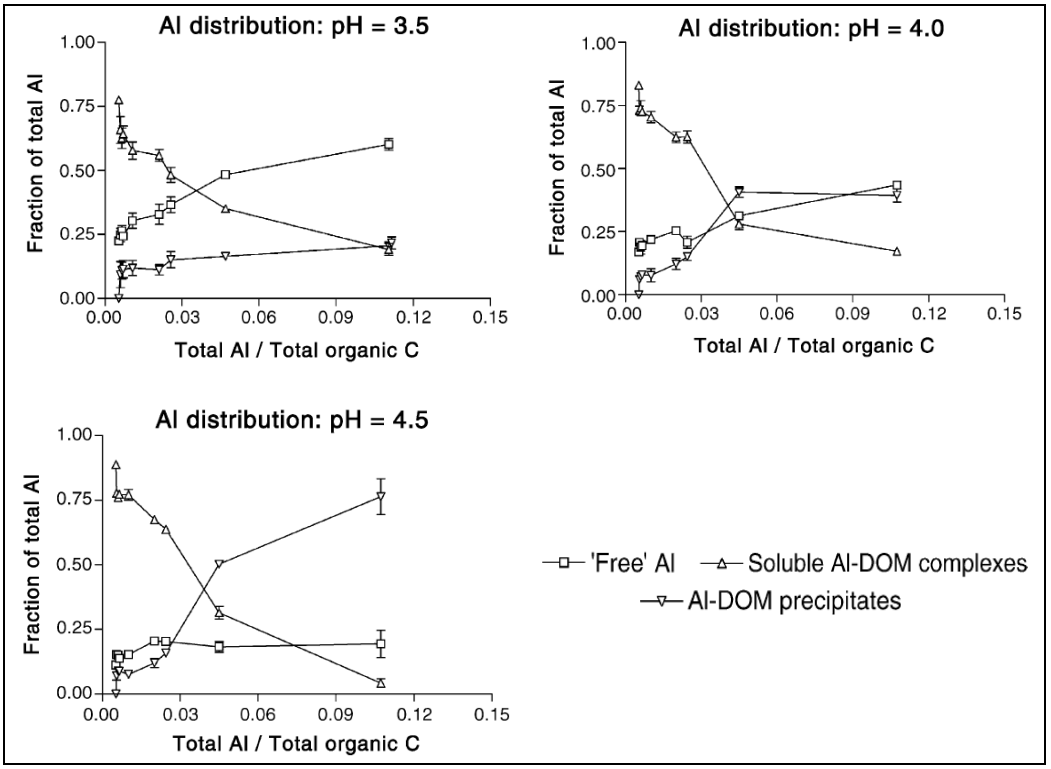

Figure 2.5: Distribution of aluminium species as function of pH and M/C ratio
Copied from Jansen et al. (2003).

2.5 Solute Movement Through Porous Media

In this section, the movement of solutes is described. In the first part the (unsaturated) water flow is described by the Richard's equation. In the second part the movement of solutes with the water flow is described by de Advection-Dispersion equation.

2.5.1 Richard's Equation for Unsaturated Flow

The flow through (unsaturated) porous media can be described by the Richard's equation (Fitts, 2012). The mixed form of the Richard's equation is given in equation 2.15.

$$\frac{\partial \theta_w}{\partial t} = -\nabla q = \nabla \cdot [K_{sat} k_{rw} (\nabla h_w + \nabla z)] \tag{2.15}$$

In which θ_w is the volumetric water content [L^3/L^3], q the specific discharge [m/s], K_{sat} the saturated hydraulic conductivity [L/T], k_{rw} the relative permeability based on the degree of saturation [-], h_w the hydraulic head [L] and z the elevation above the horizontal datum [L].

The relative permeability based on the degree of saturation can be calculated with different relationships. One possibility is by making use of the Van Genuchten equations, which are given in equation 2.16, 2.17 and 2.18. In these equations S_{eff} is the effective saturation [L^3/L^3], α [L^{-1}], n [-] and m [$1-1/n$] are the Van Genuchten parameters depending on the soil. When the relative permeability term is equal to one, complete saturation is assumed and the Richard's equation reduces to the Darcy flow equation, which is shown in appendix A.4.

$$k_{rw} = \left(S_{eff}\right)^{\frac{1}{2}} \left\{1 - \left[1 - \left(S_{eff}\right)^{\frac{1}{m}}\right]\right\}^2 \tag{2.16}$$

$$S_{eff} = [1 + (\alpha h_w)^n]^m \tag{2.17}$$

$$S_{eff} = \frac{\theta_w - \theta_{res}}{\theta_{sat} - \theta_{res}} \tag{2.18}$$

2.5.2 Advection-Dispersion Equation

The transport of solutes with groundwater is affected by four mechanisms; (1) Advection, (2) Dispersion, (3) Retardation and (4) Degradation (Fitts, 2012; Schulze-Makuch, 2009). On the short-term degradation can be neglected.

Advection is the movement of particles with the principle flow direction. Particles and flow move forward together with the same velocity. The advection equation is given in equation 2.19. In which C represents the concentration and u the average linear water flow velocity.

$$\frac{\partial C_i}{\partial t_{adv}} = -\nabla (u \cdot C_i) \tag{2.19}$$

The average linear velocity is calculated by equation 2.20. In which q is the specific discharge and n_e the effective porosity.

$$u = \frac{q}{n_e} \tag{2.20}$$

Dispersion is the movement of particles relative to the advective flow. Dispersion causes a spreading in concentration and a mixing and dilution of the solute in the bulk movement of the water and can be described by Fick's second law of Diffusion (Appelo & Postma, 2005; Bear & Cheng, 2011). The equation of Ficks's second law of diffusion is given in equation 2.21 in which D is the hydrodynamic dispersion [m^2/s]. Hydrodynamic dispersion is a combination of mechanical dispersion and molecular diffusion.

$$\frac{\partial C_i}{\partial t_{disp}} = \nabla \cdot (D \cdot \nabla C_i) \tag{2.21}$$

Mechanical dispersion is caused by different flow paths of the solutes in a porous medium. Flow paths are faster when (1) a more direct path is followed, (2) the flow flows through larger pores or (3) the flow flows through the centres of the pores where there is less friction from the grains (Schulze-Makuch, 2009). In engineering purposes, it is often assumed that the longitudinal mechanical dispersion (along with the streamlines) is ten times bigger as the transverse mechanical dispersion. Because the mechanical dispersion depends on the average linear water flow velocity it is not a constant.

Molecular diffusion is caused by random molecular motion of the particles themselves. Molecular diffusion is caused by concentration gradients within the porous medium (Schulze-Makuch, 2009). In almost all porous media, mechanical dispersion causes far more dispersion than molecular diffusion does and therefore the diffusive term can be neglected (Fitts, 2012).

Besides advection and dispersion, ***retardation*** caused by adsorption plays a role in the transport of solutes. Adsorption causes the solutes to sorb to the surface of the porous medium (Appelo & Postma, 2005). This causes that the solute is retarded compared to the water migration. The retardation factor is given in equation 2.22. In which R is the retardation factor, ρ the density [M/L^3], n the porosity [-] and K_d the distribution constant [M/L^3].

$$R = 1 + \frac{\rho}{n} K_d \tag{2.22}$$

When all the mechanisms which affect solute transport are combined, this results in the advection-dispersion equation. The advection-dispersion equation is given in equation 2.23 in which S is added as a sink term for a chemical reaction.

$$R\frac{\partial C_i}{\partial t} = \nabla \cdot (D \cdot \nabla C_i) - \nabla (u \cdot C_i) - S \tag{2.23}$$

2.6 Measuring Hydraulic Conductivity

There are several factors which influence the hydraulic conductivity; (1) Grain size distribution, (2) Degree of density, (3) Saturation, (4) Soil structure, (5) Soil texture and (6) Water Temperature (Tang, Zhou, Yang, Yan, & Zhou, 2016). In the laboratory, the hydraulic conductivity can be determined by a permeameter. In a permeameter, flow is maintained through a small sample of the material while measuring the flow rate and head loss (Fitts, 2012). The most used permeameter is a falling-head test. Other ways to measure hydraulic conductivity are thee constant-head test and Kozeny-Carman relation, these concepts are explained in appendix A.5 and A.6.

In a falling-head test the head difference and discharge through the sample decrease with time. The set-up is depicted in Figure 2.6. The level at the inlet burette must be recorded at time intervals as it falls throughout the test. The discharge is proportional to the cross-sectional area of the burette and the rate with which the burette level falls. This relationship is given in equation 2.24 in which *a* is the cross-sectional area of the burette (A1 in the figure) and *dh* the head difference. When combining equation 2.24 with the Darcy flow equation, the hydraulic conductivity can be calculated with equation 2.25 in which *A* is the cross-sectional area of the sample (A2 in the figure), *L* the flow length, dh_0 the initial head and dh_1 the head at time t_1. When assuming the Darcy flow equation is valid, the sample must be completely saturated in order to determine a valid hydraulic conductivity.

$$Q = -a\frac{d}{dt}(dh) \tag{2.24}$$

$$K = \frac{a}{A}\frac{L}{(t_1 - t_0)}\ln\left(\frac{dh_0}{dh_1}\right) \tag{2.25}$$

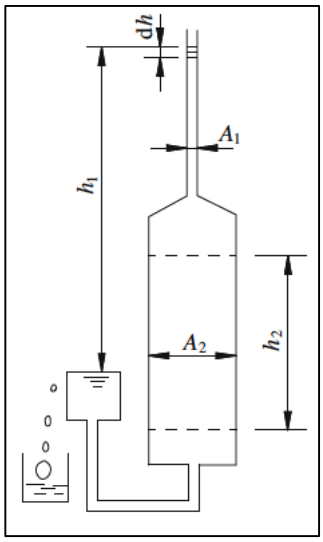

Figure 2.6: Falling-head test set-up
Copied from Fitts (2012).

This page is intentionally left blank

Chapter 3

Materials and Methods

This page is intentionally left blank

This chapter gives an overview of the used materials and experiments carried out in order to investigate the possibility to engineer a horizontal layer of reduced permeability using Al-DOM precipitation. The conducted experiments and modelling are divided into three different parts; (1) characterization of the complexation behaviour experiments, in which the complexation behaviour of the used materials is compared with literature, (2) 3D reactive transport experiments in which solutes are injected at a constant flow rate and (3) data processing for interpretation and modelling in which the experiments are interpreted in Matlab and modelled in COMSOL Multiphysics. Each part is described in this chapter after the presentation of the used chemicals and porous media.

3.1 Chemicals and Porous Media

Chemicals

As organic matter source HUMIN-P 775 was used. HUMIN-P 775 is produced by a company called HUMINTECH (see appendix B). According to the information provided by HUMINTECH, HUMIN-P 775 is a specially selected leonardite material which has been carefully reacted with potassium compounds. This reaction neutralizes the humic acids which are abundant in the raw material, converting them to water-soluble potassium humates. HUMIN-P 775 has been used in previous experiments of Hopman (2016) and Bonfiglio (2016). They had selected HUMIN-P 775 as organic matter source because the material has shown reactivity and is commercially available.

The result of a CHNS analysis on the composition of HUMIN-P 775 is shown in Table 3.1. By carrying out this analysis the amount of organic carbon was investigated. The amount of organic carbon present, influences the M/C ratio and therefore is a measure for complexation according to literature. When dissolved, HUMIN-P 775 is a dark coloured solution due to the presence of carbon and has a pH around 9.

Table 3.1: Composition of HUMIN-P 775 by CHNS analysis
conducted by the University of Amsterdam

Sample	N (%)	C (%)	H (%)	S (%)
Humic_01	1.05	41.81	3.12	0.83
Humic_02	1.00	42.54	3.83	0.88
Average	1.025	42.175	3.475	0.8545

As aluminium source, aluminium chloride hexahydrate ($AlCl_3 \cdot 6H_2O$) was used (see appendix B). This aluminium source is produced in a solid crystal form by Sigma Aldrich. When dissolved a colourless solution was created with a pH value around 4. For simplicity reasons, the aluminium chloride hexahydrate solution is referred to as an aluminium solution.

Porous Media Characterization

The main experiments are conducted with two different types of sand for the porous medium. In most experiments sand was used which was bought at a builder's merchant. The sand is described as 'play-sand' with grainsizes ranging from 0-2 mm. The main experiment was also conducted with sand sampled from the upper forty centimetres of the soil at the Oil-Tanking Amsterdam location. The sample contained some boulders which were sieved out. It was visually confirmed that the soil from Oil-Tanking Amsterdam was finer and darker coloured as the other sand. In Figure 3.1 the grain size distributions of the porous media are given. The two sands are comparable with the finest sand used in the experiments of Bonfiglio (2016). In those experiments a hydraulic conductivity reduction of 87% was measured in the area of precipitation.

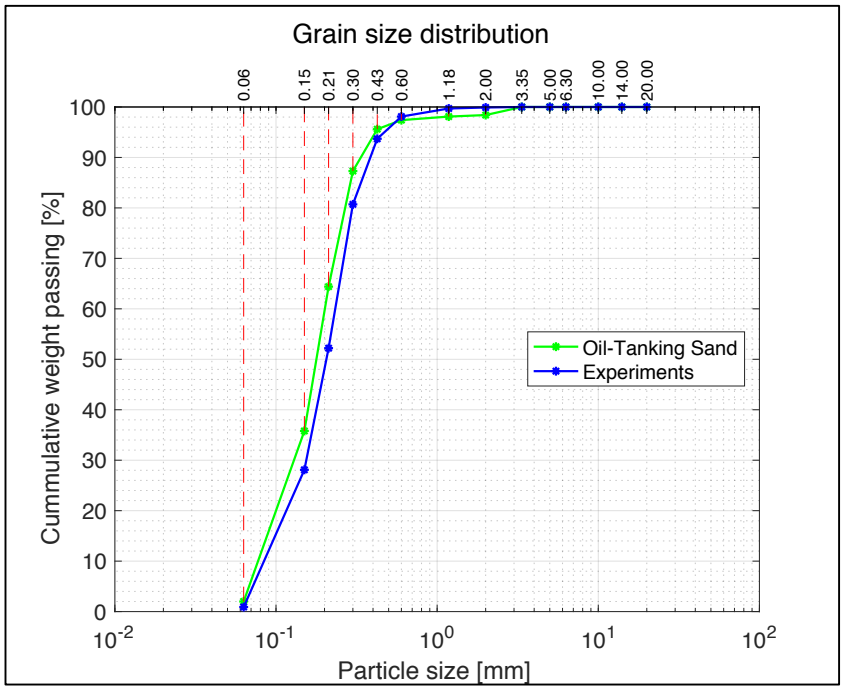

Figure 3.1: Grain size distributions of porous media

3.2 Characterization of Complexation Behaviour

The preliminary characterization experiments investigate the behaviour of the complexation/formed complexes. The characterization experiments are divided into (1) the quantification of precipitation by titration- and dilution experiments and (2) the solubility of complexes in oil compounds.

3.2.1 Quantification of Precipitation

To determine under which conditions the most complexation occurs, the complexation behaviour was examined with three variables; pH, M/C ratio and the dilution factor. From a theoretical point of view the most precipitation would occur at high pH (more deprotonation of functional groups) or at high M/C ratios (more available metal ions). Since the exact composition of HUMIN-P 775 is not known and the CHNS analysis is conducted on a dry sample, there is an uncertainty in the dissolved carbon fraction and therefore the M/C ratio. To avoid this uncertainty, the experiments were conducted with the aluminium/organic-matter concentration ratio instead of the M/C ratio.

The precipitation behaviour was quantified on pH-, EC-, UV254 values and on weight basis. In order to do these measurements, the formed precipitation and undissolved OM need to be separated from the liquid phase. This was done by putting the samples in the centrifuge for 20 minutes and by applying a filtration with 11 µm filters. The liquid phase was poured into a beaker while the solid particles were left in the tubes. The filtrates were measured on pH, EC and UV254. Since the organic matter solution has a high pH value in comparison with the aluminium solution, it was expected to see a significant decrease in pH when all organic matter has complexed. Because complexation leads to less free ions in solution, the EC was expected to rise significantly when all organic matter had complexed. Also, it was expected that the measured EC would be lower as what was expected based on individual EC measurements. In Figure 3.2 the EC values of the individual solutions are given. The y-intercept of 0.84 and 0.50 was caused by the tap water which was used instead of demineralized water.

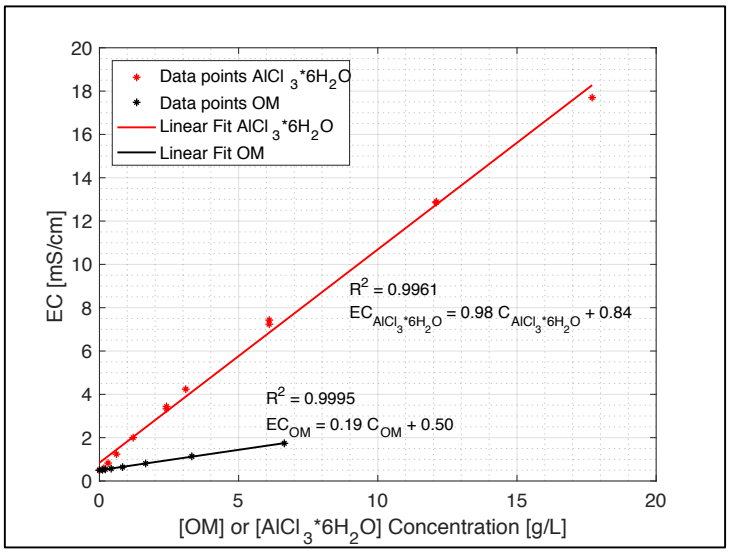

Figure 3.2: Electrical conductivity versus OM or $AlCl_3$ concentration

UV adsorption was used to quantify the remaining organic matter concentration in the filtrate. The use of UV adsorption to quantify the amount of organic matter is widely used in waste water industry (Deflandre & Gagné, 2001). The basic assumption in this approach is that the OM concentration is proportional to the UV absorption. It was found that UV absorbance at 254 nm is correlated most with Organic Matter content (Deflandre & Gagné, 2001; Zhang, 2013). Therefore, a UV-VIS spectrophotometer was used at a wavelength of 254 nm. In Figure 3.3 the correlation line between organic matter and UV254 adsorption is given for two different stock solutions. To correct for the portion of OM after filtration, the UV254 adsorption was measured after filtration. Since the UV-VIS spectrophotometer cannot measure the absorbance for high OM concentrations, all samples need to be diluted to fall in the range of the calibration line. The differences in UV254 adsorption were caused by dilution errors or a variability in OM concentration. The filtered stock lead to less UV254 adsorption since OM particles were filtered out.

For the measurement in this research, the linear fit of stock solution one was applied since this stock solution was also used in the titration experiments. This linear fit is given in equation 3.1. The filtered stock linear fit was used to quantify the uncertainty in the quantified organic matter concentration.

$$UV_{abs} = 0.028\, C_{OM} - 0.025 \tag{3.1}$$

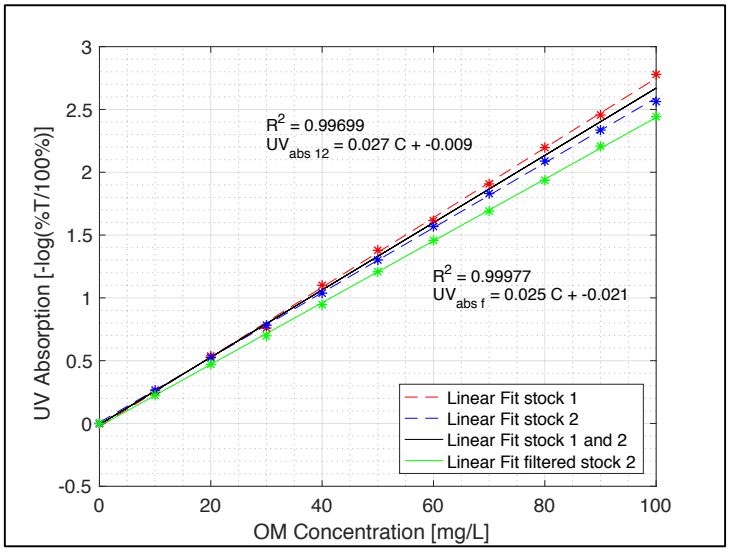

Figure 3.3: UV254 adsorption versus OM concentration

The precipitation itself was quantified on weight basis. The tubes, in which the flocs were formed, were weighed before and after the experiments. To ensure that only the weight of the flocs was measured and all liquids were evaporated, the tubes were put in a stove at 50 degrees Celsius for two nights before being measured.

Titration Experiments

In these experiments the pH and $AlCl_3$/OM ratio effect on precipitation was investigated by gradually changing the $AlCl_3$/OM ratio at three different initial pH levels. For the aluminium- and DOM solution, a stock solution of 24.14 g/L (0.1 Almol/L) and 6.64 g/L (±0.23 Cmol/L) were made respectively. The pH effect was investigated by adjusting the pH value of the DOM stock solution with 1 mol/L HCL solution.

Three cycles of experiments were conducted by creating the samples represented in Table 3.2 with the initial pH of the DOM stock equal to 9, 7 or 5. In total 33 samples were created with 40 ml of DOM and aluminium ranging from 0 to 4 ml. To ensure ideal mixing and a complete reaction, the samples were put on a shaking table for 30 minutes and let at rest for another 30 minutes. The quantification of the precipitation was based on pH, EC, UV254 values and on weight basis as explained in the previous section.

Table 3.2: Titration samples with according AlCl/OM and M/C ratio

Sample	1	2	3	4	5	6	7	8	9	10	11
OM (ml)	40	40	40	40	40	40	40	40	40	40	40
Al (ml)	0.0	0.4	0.8	1.2	1.6	2.0	2.4	2.8	3.2	3.6	4.0
AlCl/OM (g/g)	0.0	0.036	0.073	0.109	0.145	0.182	0.218	0.255	0.291	0.327	0.364
M/C (Almol/ Cmol)	0.0	0.004	0.009	0.013	0.017	0.021	0.026	0.030	0.034	0.039	0.043

Dilution Factor

In this test, the concentrations of the organic matter and aluminium solutions were changed with a constant $AlCl_3$/OM ratio. The test was conducted at a $AlCl_3$/OM concentration ratio equal to 0.364 to ensure a complete reaction. The aluminium- and organic matter stock solutions were diluted with the same factor and then mixed together. For each dilution factor, 4 ml aluminium solution was added to 40 ml of OM solution. It was expected that when increasing the concentrations linearly, the reaction products would also increase linearly. The initial pH of the DOM stock was equal to 9, therefore no HCl was needed for adjusting the pH.

Table 3.3: Dilution experiments

Sample	1	2	3	4	5
Dilution Factor	1	0.8	0.6	0.4	0.2
OM (ml)	40	40	40	40	40
Al (ml)	4	4	4	4	4
AlCl/OM (g/g)	0.364	0.364	0.364	0.364	0.364

3.2.2 Solubility of Complexes in Oil Compounds

The Al-DOM complexes are stable in water, but because in practice the Al-DOM precipitates are present underneath an oil tank, the solubility was tested in oil compounds. To test the solubility of the Al-DOM precipitation in oil compounds, the flocs created in the previous experiments were saturated with three different solutions; (1) ethanol (alcoholic compound), (2) petroleum (aliphatic compound) and (3) thinner (Aromatic compound). The samples were shaken thoroughly and let at rest for over a week.

The test was based on visual colour interpretations. When no colour change in the oil compound was identified, it was assumed that the dark coloured flocs did not dissolve significantly in the oil compounds.

3.3 Reactive Transport Experiments

In these experiments the aluminium and organic matter solution were pumped in a porous medium at a constant flow rate. The aim was to study the distribution of the Al-DOM precipitation and to quantify a reduction in hydraulic conductivity.

3.3.1 Experimental Set-up

For the 3D reactive transport experiments, a plastic aquarium box (41.3 x 26 x 29.8 cm) was used. For the injection of the chemicals, three injection drains were constructed. The input drains were made of plastic tubing with a diameter of 5 mm. The drains were about 20 cm long. In de tubes, small holes of 2 mm were drilled each centimetre. At the end of the drains, plastic caps with Teflon tape were placed to prevent the chemicals to flow out.

For the outflow- and falling head drains, a plastic tube with a diameter of 9 mm was used. In these drains, 5 mm holes were bored all over the drain so that the chemicals could flow into the drain with minimal resistance. To prevent sand from flowing into the drains, a filter stocking normally used for piezometers, was put around it. A schematic overview of the constructed box is given in Figure 3.4. A photo of the drains is depicted in Figure 3.5. In this construction, an unsaturated layer of sand is present.

The chemicals were pumped in via the injection drains. The flow was regulated via the overflow drain. This overflow drain defined the (gound)water table. The unsaturated zone is therefore situated above injection drain 1 and the outflow drain.

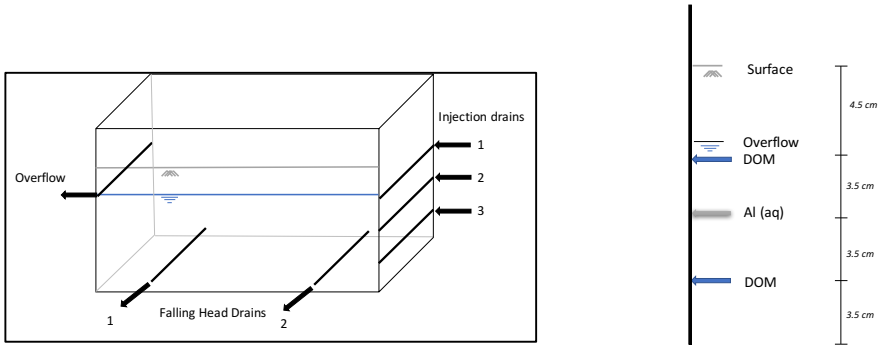

Figure 3.4: Schematic set-up 3D experiment

To estimate the hydraulic conductivity reduction, a falling head test was performed before and after each experiment. The falling head tests were conducted via the fallinghead drains, which were situatied at the bottom of the box. The falling head set-up is depicted in Figure 3.6. The column was filled with about 25 centimetres of water. Due to a difference in hydraulic head between the column and the box, the water was forced to drain into the box via the falling head drains and to flow towards the surface of the sample. The water level in the column equalized with the water level in the box. To measure the head drop in the column, a diver was placed in the column. The diver had an accuracy of ±0.5 cm H_2O, a resolution of 0.2 cm H_2O and measured the pressure every 0.5 seconds. Because the diver measured the total pressure above it, the air pressure needed to be subtracted to get a value for the (hydraulic) head. This was done by subtracting the minimum value measured by the diver, assuming that this was the air pressure.

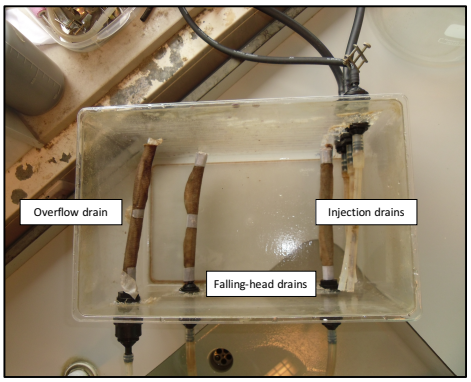

Figure 3.5: 3D set-up drains

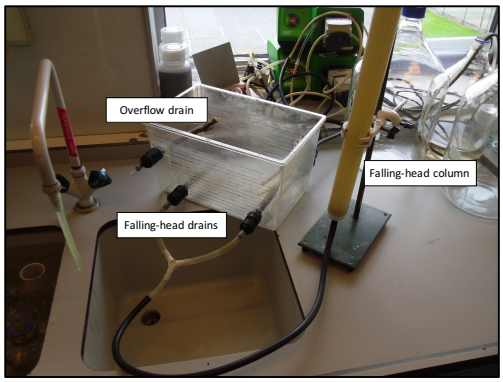

Figure 3.6: Falling Head test set-up

The hydraulic conductivity was calculated with equation 2.25. The used parameters in this equation are given in Table 3.4. The hydraulic conductivity was measured in three different ways. First the hydraulic conductivity was measured via both falling-head drains, then via both drains separately. The idea was that in this way a difference could be seen in hydraulic conductivity reduction within the two sections/halves of the box.

Table 3.4: Used parameters for the hydraulic conductivity calculation

a (cm^2)	A (cm^2)	L (cm)	dt (s)
10.2	805	13	0.5

3.3.2 Experiment Procedure

The general experiment procedure can be described with ten subsequent steps. These steps are:

1) Cleaning of the injection drains to remove undissolved organic matter and sand in the injection drains.
2) Put the caps on the injection drains to prevent an outflow at the end of the injection drains.
3) Fill the box with about 16 cm of sand.
4) Saturate the complete sample by putting a ponding layer of water on top of the sample. This step was needed in order to conduct a falling-head test
5) Conduct a falling-head test for the hydraulic conductivity calculation before the Al-DOM reaction takes place in the porous medium**.**
6) Perform a test scenario in the chemical solutions are pumped in the porous medium and Al-DOM precipitation takes place.
7) Rinse the box with about 3 L of water via the used injection drains to remove the surplus of unreacted chemicals.
8) Saturate the complete sample by putting a ponding layer of water on top of the sample.
9) Conduct a falling-head test for the hydraulic conductivity calculation after the Al-DOM reaction has taken place in the porous medium.
10) Create vertical or horizontal cross-sections of the porous medium.

In all 3D reactive transport experiments, the concentration of the organic matter stock solution was equal to 2 g/L and the concentration the of aluminium-chloride stock solution equal to 1 g/L. The solutions were pumped through the injection drains via a peristaltic pump at a flow rate equal to 5 or 10 ml/min. This flow rate was chosen because at that rates the chemicals could flow towards the outflow drain and no ponding layer of liquids was formed at the surface. To ensure that the pump stopped pumping after the timespan and no air was pumped in, a time switch was used. In each test the outflow was measured and was equal to the sum of injected chemicals which meant that the overflow drain worked correctly.

Test-scenarios

As mentioned in step 6, different test-scenarios were set-up. In these scenarios, different injection strategies were applied and at step 10 the sample was investigated vertically or horizontally. All test scenarios are given in Table 3.5.

In the *V.x* scenarios the sample was investigated on vertical cross-sections. The vertical cross sections gave insights in the horizontal distribution of the Al-DOM precipitation. In these cross sections, it can be concluded if the Al-DOM precipitation occurred over the full width of the box and if the reaction has taken place at the expected places. In scenario V.3, the volume of chemicals was doubled to see if a larger and or thicker Al-DOM layer was created. In scenario V.4, injection drain three was added. The idea of this third drain was that the aluminium solution was trapped in between the two DOM flows and therefore a reaction was inevitable. To give the reaction more time to take place, the flow rate was halved.

In the *H.x* scenarios the sample was investigated on horizontal cross-sections. In horizontal cross-sections, it is visually more difficult to see the horizontal Al-DOM precipitation layer. To make the Al-DOM precipitation visible, the horizontal cross-sectional photos can be process in an interpretation tool which is discussed in the next section. To generate multiple horizontal cross-sections, layers of 0.5 cm were removed from the top of the box. Each time a photo was taken. The photos were taken in a range of 4.0 – 15.5 centimetres measured with respect to the bottom of the box. At 3.5 cm, the falling-head drains are situated which meant that more layers of 0.5 cm could not be taken off.

For some scenarios, a pump was used at the overflow drain to simulate a suction of water in the underground. This was done since in a practical pilot it is likely that a pump is used to generate a flow of the (injected) chemicals. Using a pump at the overflow also has an influence on the streamlines in the box. Scenario H.1 till H.3 and H.7 only used two injection drains. Scenarios H.4 and H.5 used three injection drains. Scenario H.6 also used three injection drains but injected water instead of organic matter in injection drain 3. Scenario H.6 was used to investigate if the DOM injection in injection drain 3 indeed caused a different distribution of precipitation. Scenario H.7 was added to see if a noticeable difference could be seen when the solutions were pumped with a higher pump rate. In the last scenario, the soil from Oil-Tanking Amsterdam was used. In each test 5L of solutes were pumped through each drain.

Table 3.5: Test scenarios for the reactive transport experiments

Scenario	Volume	Flow rate	Injection drain			Pump at overflow
	L	ml/min	1	2	3	
V.1	5	10	-	OM	Al	No
V.2	5	10	-	Al	OM	No
V.3	10	10	-	Al	OM	No
V.4	5	5	OM	Al	OM	No
H.1	5	5	-	OM	Al	No
H.2	5	5	-	Al	OM	No
H.3	5	5	-	Al	OM	Yes
H.4	5	5	OM	Al	OM	No
H.5	5	5	OM	Al	OM	Yes
H.6	5	5	Water	Al	OM	No
H.7	5	10	-	Al	OM	No
Oil-Tanking	5	5	OM	Al	OM	Yes

3.4 Data Interpretation and Modelling

To make the Al-DOM precipitation visible from the horizontal cross-section photos, the photos are processed in Matlab. In COMSOL Multiphysics the 3D reactive transport experiments are modelled for insights in streamlines in the set-up and changes in porosity due to Al-DOM precipitation.

3.4.1 3D Matlab Interpretation

The horizontal cross-sections were used for an interpretation in Matlab. In this way, the Al-DOM precipitates were visualised in a digital form. The interpretation was based on the colour intensities of the pixels in the photographs. Al-DOM complexation leads to a change in colour when compared to 'unaffected' sand. It was assumed that the darker the colour, the more abundant the Al-DOM precipitates were at that spot. The interpretation process can be divided into three steps; (1) the loading and pre-processing of the data, (2) contrast enhancing and (3) spatial smoothing

Loading and Pre-processing

Each photo was taken with a resolution of *2448* x *3264* (8 Megapixel). This meant that each photo consisted of three *2448* x *3264* matrices which represent the Red, Green and Blue (RGB) colour intensities of each pixel. To be able to process the images based on their intensities, each photo needed to be reduced to one matrix. Therefore, the RGB images were converted to greyscale in Matlab. For this conversion, Matlab formed a weighted sum of the RGB components resulting in one matrix for each photo. For each test-scenario in which horizontal cross-sections were generated, 24 photos were taken. These 24 photos were stacked together and therefore the total 3D matrix consisted of 2448 x 3262 x 25 pixels. The loading and pre-processing steps in Matlab are summarised as following:

1) Upload the RGB image (a *m* x *n* x *3* matrix)
2) Turn the image to grayscale so each image becomes a *m* x *n* x *1* matrix.
3) Crop to image to the area of interest.
4) Process the *uint8* data type to *double* data type to enable computation
5) Stack each photo in a 3D volume data matrix.

Contrast Enhancing

To enhance to contrast between the pixel intensities, the data was discretized into classes. It was chosen to discretize the data based on the colour intensity into four classes. The first class consist of the darkest pixels and surely contained Al-DOM precipitation. The second class most likely contained Al-DOM precipitation. The third class was a mix of Al-DOM precipitation and adsorption. The fourth class represented the unaffected sand. The widths of these classes were determined by conducting a statistical analysis on the pixel data in which a normal probability function was fitted to the pixel data. By assigning probabilities for a pixel-intensity to fall in a certain class and by using the statistical parameters of the fitted probability function, the bin edges of the classes could be back-calculated.

Spatial Smoothing

When using 100% of the pixel data, light pixels were present in between the darker pixels and the Al-DOM precipitation is shown less clear. By reducing the data to 10% of the original data, the pixels get an average value of the surrounding pixels. The average pixel value of pixels containing lots of (dark) Al-DOM precipitation remain dark while dark pixels surrounded by light pixels get a lighter tint. In this way, natural dark spots in the sand were filtered out and shown as 'unaffected' sand. By using only 10% of the input data, the data could also be interpolated in z-direction with no significant effort.

3.4.2 COMSOL Multiphysics Model

In COMSOL the box experiments were modelled for an interpretation of the generated results in Matlab. The streamlines of the water flow from the separate injection drains were modelled to get an indication for the mixing zone(s). In a second run the flow, advection/diffusion and the chemical reaction were coupled to simulate the permeability reduction that could be established by Al-OM precipitation.

Boundary Conditions

Apart from the top box boundary, all box boundaries were modelled as no flow boundaries. Due to the incompressibility of water, the injection of water into a nearly fully saturated box lead to a very stiff numerical solution when assuming a no flow boundary at the top. To compensate this, the top boundary was implemented with a Robin type boundary condition. The external head was set to 10.5 cm which was equal to the initial situation. Also, a conductance term was implemented to handle the stiffness of the model. The conductance term is the reciprocal of the resistance term and therefore simulates the ease with which flow can pass the boundary. The conductance term at the top boundary was set to 1 s^{-1}.

The injection drains were modelled in such a way that it was assumed that the chemicals were injected homogeneously over the complete area of the drains. This was implemented by using a Neumann boundary condition which specified the flow rate at the position of the drains. In the case of using chemicals, the concentrations at the drains were specified by making use of a Dirichlet boundary condition. The overflow drain was modelled with a Robin type boundary condition. Since the drain was modelled as a free overflow, the conductance term was set at 10 s^{-1}. This meant that the solutes could flow in easily.

Streamlines for Each Injection Drain

The water flow from the separate injection drains was simulated by performing a stationary analysis in COMSOL. In this stationary analysis, the unsaturated layer above the drains was included to see what influence this zone had on the water flow. With help of these streamlines, an indication of the mixing zone of the chemicals could be given. The unsaturated zone was modelled by using the Richards equation and the van Genuchten parameters for unsaturated flow (Section 2.5.1). The used parameters are summarized in Table 3.6

Table 3.6: Van Genuchten parameters for Richard's equation in COMSOL Multiphysics

α (cm^{-1})	n (-)	θ_{sat} (L^3L^{-3})	θ_{res} (L^3L^{-3})
0.5	2.3	0.3	0.05

Permeability reduction due to Al-DOM precipitation

In a second run the reduction in permeability, resulting from the chemical reaction, was taken into account. In this run, it was assumed that the box was completely saturated which meant that the Richard's equation reduced to the Darcy flow equation. In this run the Darcy flow was coupled to the advection diffusion equation and the chemical reaction.

The chemical reaction was implemented with reaction rates like discussed in section 2.4. It was assumed that at low concentrations (<0.1) the reaction was taking place but that this would not result in a permeability reduction. This condition was implemented by a ramp function, which meant that when the concentrations of the chemicals were lower than 0.1, the precipitation did not influence the flow properties.

The hydrodynamic dispersivity for the advection-diffusion equation (section 2.5.2), was assumed to be α_L = 0.3 cm, which was a tenth of the distance between the injection drains. This hydrodynamic dispersity constant has a significant influence on the mixing zone of the chemicals. When choosing a higher value, the dispersion of the chemicals cause the mixing to take place over the entire volume of the box. Choosing a lower value results in less dispersion and therefore the width of the mixing zone is smaller.

3.5 Overview Experiments

For the characterization of the used materials a grain size distribution, a correlation line between EC-vale and aluminium and organic matter concentration and a correlation line between UV254 absorption and organic matter concentration were made. The lab –experiments are summarized as:

Titration experiments at pH 5, 7 and 9

Sample	1	2	3	4	5	6	7	8	9	10	11
OM (ml)	40	40	40	40	40	40	40	40	40	40	40
Al (ml)	0.0	0.4	0.8	1.2	1.6	2.0	2.4	2.8	3.2	3.6	4.0
AlCl/OM (g/g)	0.0	0.036	0.073	0.109	0.145	0.182	0.218	0.255	0.291	0.327	0.364
M/C (Almol/ Cmol)	0.0	0.004	0.009	0.013	0.017	0.021	0.026	0.030	0.034	0.039	0.043

Dilution factor

Sample	1	2	3	4	5
Dilution Factor	1	0.8	0.6	0.4	0.2
OM (ml)	40	40	40	40	40
Al (ml)	4	4	4	4	4
AlCl/OM (g/g)	0.364	0.364	0.364	0.364	0.364

Test scenarios

Scenario	Volume	Flow rate	Injection drain			Pump at overflow
	L	ml/min	1	2	3	
V.1	5	10	-	OM	Al	No
V.2	5	10	-	Al	OM	No
V.3	10	10	-	Al	OM	No
V.4	5	5	OM	Al	OM	No
H.1	5	5	-	OM	Al	No
H.2	5	5	-	Al	OM	No
H.3	5	5	-	Al	OM	Yes
H.4	5	5	OM	Al	OM	No
H.5	5	5	OM	Al	OM	Yes
H.6	5	5	Water	Al	OM	No
H.7	5	10	-	Al	OM	No
Oil-Tanking	5	5	OM	Al	OM	Yes

This page is intentionally left blank

Chapter 4

Results and Discussion

This page is intentionally left blank

In this chapter, the results of the experiments are given. In the first few sections, the results of the experiments concerning the complexation behaviour are given which show the relationship between $AlCl_3$/OM concentration ratio and pH with complexation. After these results, the main experiments are discussed concerning the 3D reactive transport experiment and the Matlab interpretation. With help of the COMSOL Multiphysics model the results of the main experiment can be explained.

4.1 Characterization of Complexation Behaviour

4.1.1 Titration Experiments

In the titration experiments a clear 'turning point' was seen in the filtrates (Figure 4.1). With an initial pH of 5, the colour of the filtrate suddenly changes from black to almost colourless between sample six and seven. This point gave an indication on the point at which all organic matter had formed complexes. This point was also observed in the precipitation size (Figure 4.2). After the point the precipitation formed larger pieces. It was observed that this turning point is dependent on the initial pH of the organic matter solution. With a lower initial pH, the turning points are reached with a smaller $AlCl_3$/OM ratio. This is due to the presence of more free Al^{3+} ions at a lower pH (section 2.3.2).

The results of the conducted experiments are subdivided based on the quantification method; pH-, EC-, UV254 values and weight basis. The results are given as a function of the $AlCl_3$/OM concentration ratio. The results as a function of the (uncertain) M/C ratio are added in appendix C.

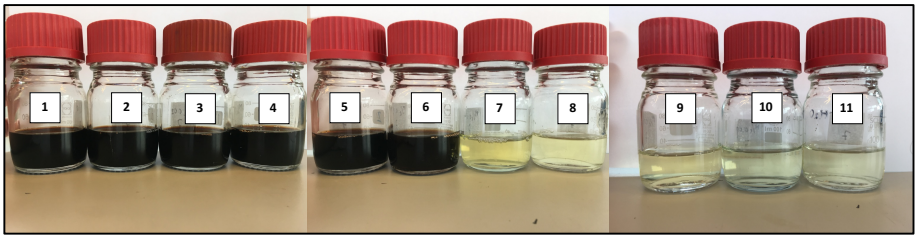

Figure 4.1: Filtrates from titration experiments with initial pH=5

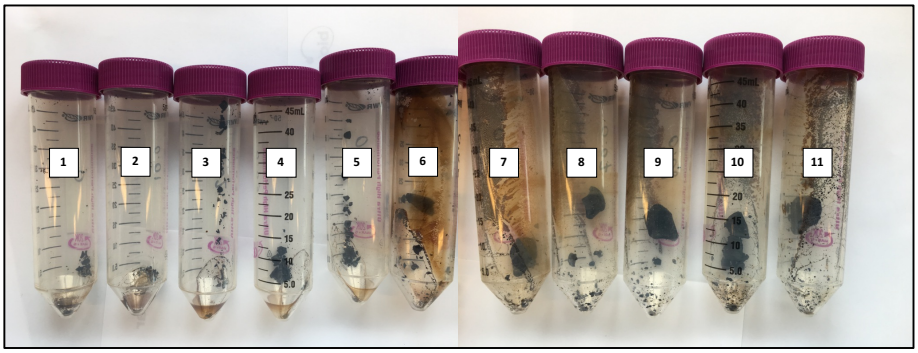

Figure 4.2: Precipitation from titration experiments with initial pH=5

pH Filtrate After Al-DOM Precipitation

The measured pH values of the filtrates after Al-DOM precipitation are shown in Figure 4.3. The measured pH decreased by increasing the $AlCl_3$/OM ratio. Therefore, adding more aluminium lead to a decrease in pH. It is observed that the slope of the measured pH decreases after the critical points at all initial pH values. The change in slope was best observed at the measurements with initial pH = 9. The experiments with initial pH = 5, almost reached a pH value equal to 3.36, which is the pH of pure aluminium-chloride solution.

In the figure the pH and $AlCl_3$/OM ratio dependency is confirmed. The pH could be used as a measure of precipitation since the measured pH was always lower then 4.5 after the turning points. At a pH value lower as 4.5, the free aluminium ion concentration is highest when looking back to Figure 2.5. The sudden drop in measured pH value can be explained by two mechanisms; (1) the adding of extra aluminium caused the total solution to reach a critical pH value beneath which the complexation reaction was favourable and (2) deprotonated negatively charged functional groups complexing with aluminium ions cause the equilibrium of equation 2.1 and 2.2 to be favourable to the right, leading to more protons in solution and therefore a drop in the pH. The sudden drop is highest at the highest initial pH experiments, probably because when starting with an initial pH equal to 7 or 5 the decrease is more smoothly and therefore no significant drop is needed to drop to a 'critical' pH value.

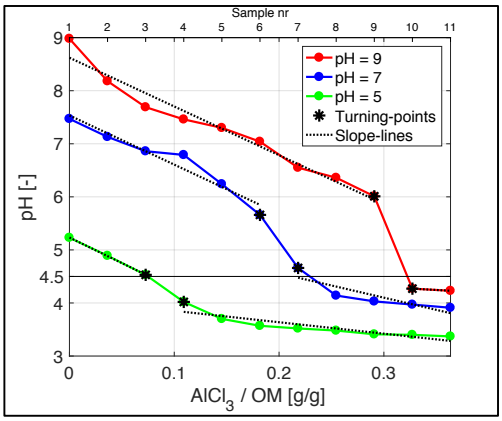

Figure 4.3: pH measurements vs $AlCl_3$/OM ratio

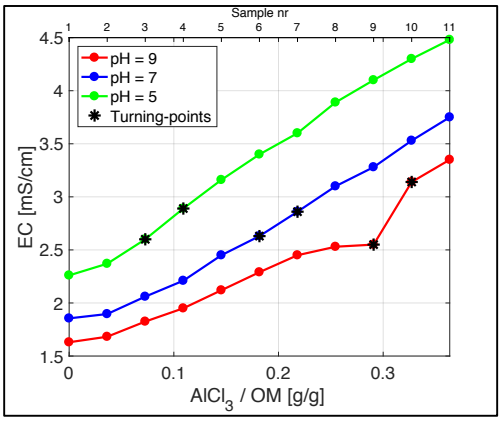

Figure 4.4: EC measurements vs $AlCl_3$/OM ratio

EC Filtrate After Al-DOM Precipitation

The measured electrical conductivity values of the filtrates after Al-DOM precipitation are shown in Figure 4.4. The initial higher EC value at lower pH was caused by the addition of HCl to adjust the initial pH value. It is observed that the measured EC increased almost linearly with increasing $AlCl_3$/OM ratio. Even at the turning points the measured EC values increases at the same slope. Only with an initial pH =9, the measured EC values show a decrease in slope till the turning point (sample nr. 9) and a sharp increase after the turning point. The slope after the turning point however is again equal to the initial slope. Therefore, it is arguable if the measurements are correct, because the experiments with lower pH do not show a change in slope.

The lack of turning points at lower initial pH may however be caused by the presence of more free aluminium ions due to a decreasing measured pH at increasing $AlCl_3$/OM ratio (Figure 4.3). With an initial pH=9 a sharp drop in pH was measured between sample nr. 9 and 10. Exactly at this place a sharp increase in EC was also measured. A sharp drop in pH causes the presence of more free aluminium ions which cause an increase in EC. An initial pH=7 or 5, such a sharp decrease in pH was not measured and therefore no turning points are visible in the EC measurements.

Because the turning points are not directly visible in the EC plot, the EC could not directly be used as a measure for complexation. To be able to use the EC as a measure of complexation, the measured EC value must be compared to the individual EC values. Correlation lines for the EC for Aluminium-Chloride and HUMIN-P 775 are given in Figure 3.2. In the correlation equations, the EC value caused by the used tap water is also included. To correct for this, the y-intercepts in the equations are neglected and the measured EC value at $AlCl_3$/OM is zero, is set equal to the calculated EC based on the correlation line. The result is seen in Figure 4.5 for an initial pH equal to nine. It is seen that the measured EC values are lower as the sum of the individual EC values of aluminium and DOM. This is a result of complexation. Due to complexation, less free ions are present in the solution leading to a lower EC value. When the same figures have to be made for the other two pH experiments. The measured EC values need to be corrected for the part of the electrical conductivity which is caused by the addition of HCl for adjusting the initial pH of the organic matter solution.

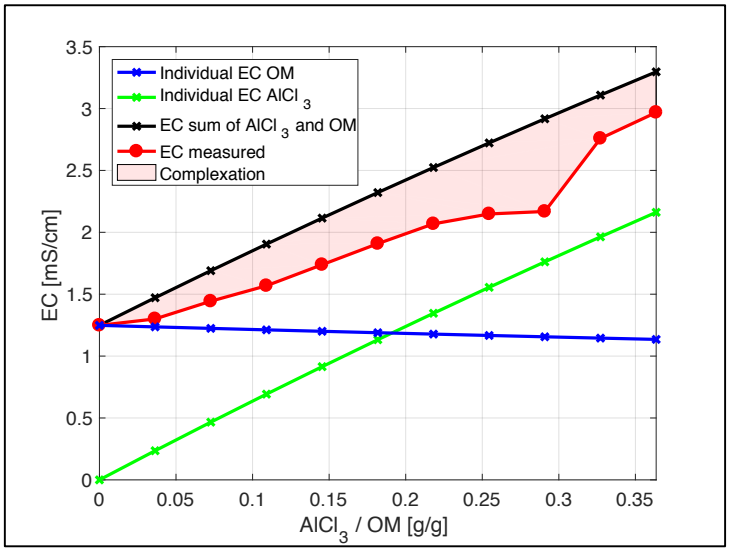

Figure 4.5: Measured EC values after complexation at initial pH =9 vs individual EC values of Al and DOM

In the figure, the individual electrical conductivity of OM is decreasing. This is caused by the dilution effect that the adding of aluminium solution had on the total volume. The individual electrical conductivity of the aluminium solution was also corrected for this dilution. As explained in the text, the correlation equation and measured EC values are corrected for the electrical conductivity of the tap water which is used in the solutions.

OM Concentration Filtrate After Al-DOM Precipitation

With UV254 adsorption measurements, the OM concentration in the filtrates was calculated with equation 3.1 based on Figure 3.3. The results are given in Figure 4.6, in which the OM concentration is depicted on the left y-axis and the complexed organic matter as a percentage of the total OM on the right y-axis. The organic matter concentration decreased almost linearly with increasing $AlCl_3$/OM ratio, which is a direct result of complexation. Which means that the reacted organic matter fraction increases almost linearly with increasing $AlCl_3$/OM ratio. The turning points are clearly visible in the figures, the slopes after the turning points were nearly equal to zero. The slope with which the OM concentration was decreasing, increased when the experiments were conducted at a lower initial pH value. This was caused by the lower pH after Al-DOM precipitation (Figure 4.3) due to which more free aluminium ions were present and therefore the conditions were more favourable for precipitation which consequently lead to a lower OM concentration.

In the figure error bars are included to give an indication of the uncertainty in the measurements. The width of the error bars was based on the different correlation lines found in Figure 3.3. Due to the applied filtration, the remaining OM concentration could be higher which is represented by the error bars. Another source for the uncertainty to become quite high before the turning points was dilution. The samples before the turning points needed to be diluted significantly to fall in the calibration range.

In sample nr. 1, the amount of undissolved organic matter was determined. In sample nr. 1 the $AlCl_3$/OM ratio is equal to zero and therefore no aluminium was added. In this sample, the organic matter concentration at all initial pH values was about 5.75±0.70 g/L. When comparing this to the initial concentration of 6.64 g/L, this means that 5-15% of the organic matter was not dissolved and was less reactive for the complexation reaction.

After the critical points, the OM concentration was approximately 0.05 g/L. Taking the undissolved fraction of OM into account, this means that 85-95% of the initial concentration has formed complexes.

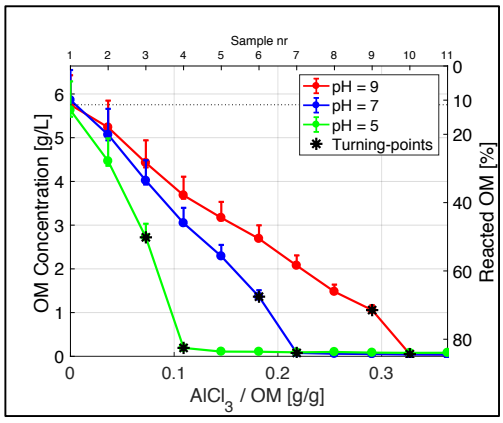

Figure 4.6: OM concentration vs $AlCl_3$/OM ratio

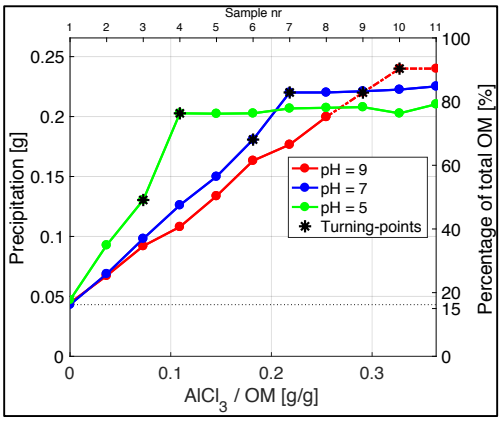

Figure 4.7: Precipitation weight vs $AlCl_3$/OM ratio

Precipitation Weight of Al-DOM Precipitation

The Al-DOM precipitation (Figure 4.2) was weighed and the results are depicted in Figure 4.7. On the left axis, the weight of the precipitates is given, on the right axis this weight is related to the weight of the input organic matter. The precipitation weight is inversely related to the OM concentration. Therefore, the figure looks like the inverse of Figure 4.6. The weight measurements of sample 9 till 11 for initial pH=9 were conducted erroneously since not all liquid had evaporated from the sample. Based on the slope before the turning point, the position of the turning point and the shape of the measurements at the other two initial pH values, values for sample nr. 9 till 11 were got via extrapolation.

In the figure, it can be seen that the weight of the precipitation in sample nr. 1 was equal to 45 mg. This weight was purely caused by undissolved organic matter since in this sample no aluminium was added. The weight of undissolved organic matter is in in the same range as found in the UV254 adsorption experiments. The undissolved weight is equal to a concentration of 45 mg/40 ml = 1.123 g/L. The OM concentration at the blank sample was approximately 6.64 – 5.75 = 0.89 g/L.

The weight of the blank sample did not vary with pH, which means that the organic matter is equally soluble at different pH values. This means that the organic matter is equally deprotonated at all initial pH values and therefore that the dissolved part consists of the same functional groups (probably carboxylic which already dissolve at pH<7). When the precipitation behaviour is not dependent on the deprotonation of the organic matter, the amount of free aluminium ions in solution is the constraining factor. Since at lower pH, more free aluminium ions are in solution, more precipitation is formed. Therefore, the maximum weight of precipitation is reached as a function of the $AlCl_3$/OM ratio.

Because there is an uncertainty in initial organic matter concentration, it is unclear if the measured difference in maximum weight of precipitation is significant. Because in every experiment the same amount of organic matter was dissolved, theoretically the same weight of precipitation must be measured. An explanation for the difference in maximum weight of precipitation might be that at higher pH and high $AlCl_3$/OM ratios, the undissolved fraction of OM might become reactive and so more precipitation is formed.

Reproducibility

The last six samples with an initial pH=9 were conducted again to access the reproducibility and compare the extrapolated precipitation values with new measurements. Figure 4.8 shows the results. It can be seen that in all quantification measurements, the reproduced values were different than the initial ones and the turning points occur at a lower $AlCl_3$/OM ratio.

The lower pH, higher EC and lower OM concentrations suggest that more aluminium ions and/or less OM was present in these samples. Since the same aluminium Salt solution was used and the fact that the aluminium ion concentration can be calculated very exactly from the aluminium Salt concentration, it is not likely that this was the cause for the variable measurements. It is more likely that the OM solution was the cause for the variability. Because a new stock solution was prepared, the input OM concentration could be slightly different initially.

Due to the organic matter not being perfectly soluble and small and large molecules are randomly present, this might have changed the initial conditions. This could have been confirmed if all the samples were done again and the blank sample gave a different measurement.

The same variability can also be seen in the previous measurements. Since for each different initial pH experiment a new stock solution was created, the initial conditions were slightly different and not exactly equal to the weighed OM. This could also explain the difference in measured maximum precipitation and the concentration measurements of the blank samples. Theoretically the difference in the concentration should be equal to the precipitation in the blank sample. Since no UV254 measurements were done on the stock solutions, it was assumed that exactly 6.64 g/L was dissolved. This however was probably not the case for all stock solutions and so there was a variability in input concentrations. Because there was a variability in input concentrations, the measurements were not exactly reproducible and small differences were measured. These differences were however small and still clear differences can be seen by changing the initial pH values.

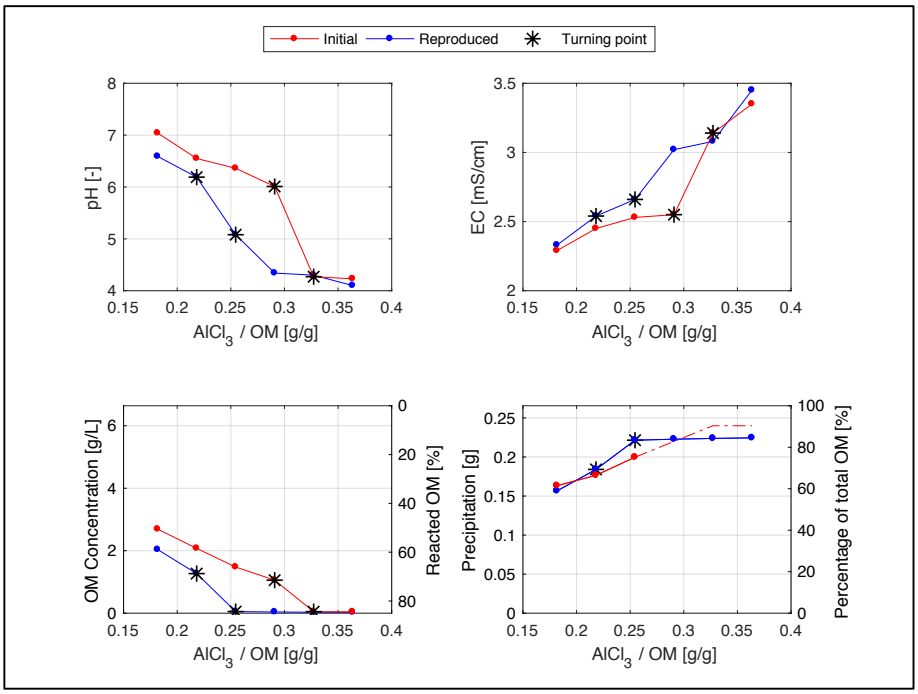

Figure 4.8: Reproducibility precipitation quantification at pH=9

4.1.2 Dilution Factor Experiments

The results of the quantification of precipitation versus the dilution factor are given in Figure 4.9. All plots but the pH measurements, show a linear relationship between the precipitation quantification and the dilution factor. The pH measurements show a sharp decrease between dilution factors 0.2 and 0.4. In Figure 4.3 it was found that the turning points, and therefore maximal precipitation, occurred at a 'critical' pH value equal or lower as 4.5. The measured pH at dilution factor 0.2 was 6.7. It was however visually confirmed that this sample was colourless and the OM concentration is almost equal to zero and therefore the turning point had already been reached. This implies that the found 'critical' pH value is not valid for solutions which are highly diluted. Apparently, the amount of free aluminium ions present at this pH value is enough the fill the small amount of deprotonated organic matter. That precipitation has taken place is shown in the precipitation weight measurements. Because even with the little amount of binding sites and aluminium ions present, 80% of the present amount of organic matter has formed complexes. Also, the measured EC values are lower as the sum of the EC values of the individual aluminium and organic matter solution, indicating that precipitation took place.

The precipitation weight measurements show that the amount of formed precipitation was always about 85% of the input concentration of organic matter. This is in accordance with wat was found in Figure 4.7. In theory, the amount of reacted organic matter should be exactly equal at each dilution factor. The variation herein was caused by the earlier described variability in OM solubility. The overall trend that at a smaller dilution factor, a lower percentage of OM has formed precipitation can be explained by the measured pH and the corresponding relative amount of free aluminium ions.

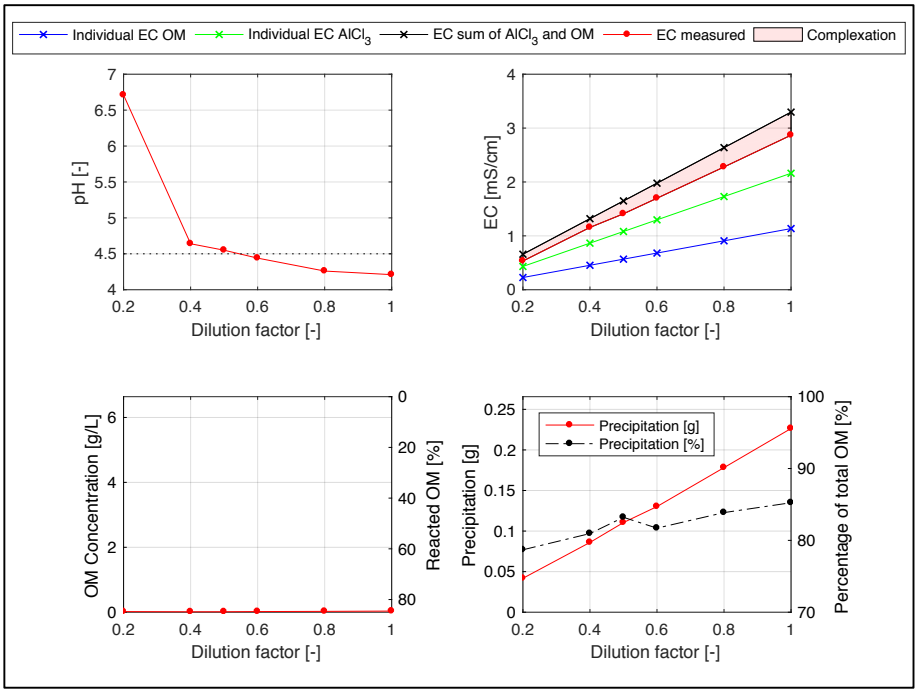

Figure 4.9: Quantification of precipitation vs dilution factor at initial pH=9

4.1.3 Solubility of Complexes in Oil Compounds

The results of the solubility test in water, petroleum (aliphatic compound), ethanol (alcoholic compound) and thinner (aromatic compound) are shown in Figure 4.10. The results show that the colour of the substances have not significantly changed. This implies that no significant dissolution of the flocs has taken place in the oil compounds. It was observed that the present Al-DOM flocs present in the oil compounds were still present in the samples and that with shaking also no colour change occurred.

After a time period of about two months a really small colour change was identified in the thinner solution. It can therefore be that Al-DOM flocs dissolute at a very slow rate in thinner. Thinner consists of aromatic compounds and so does organic matter. There may be an interaction between these components which is the cause of the colour change.

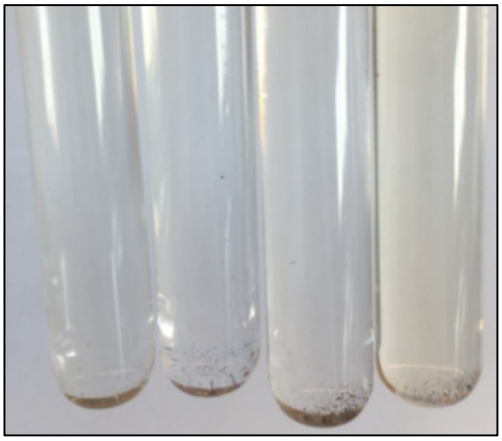

Figure 4.10: Solubility of complexes in oil compounds
(Left to right: Water, Petroleum, Ethanol and Thinner)

4.2 Reactive Transport Experiments

In this section, the results of the reactive transport experiments are presented. After seeing the first results of the reactive transport experiments, it was decided to analyse the set-up with a COMSOL Multiphysics model first. In this section, the COMSOL Multiphysics model is therefore presented first so that it can be used in explaining the results of the test-scenarios. After the visual interpretation of the Al-DOM precipitation in the set-up, the conducted falling-head tests are presented in which it is tried to quantify the hydraulic conductivity reduction.

4.2.1 COMSOL Multiphysics model

Unsaturated Zone

The result of the flow paths for each separate injection drain is shown in Figure 4.11. Due to the injection, a hydraulic gradient in the direction of the unsaturated layer is created (Figure 4.12). The hydraulic gradient causes an upwards flow though the unsaturated layer. The streamlines should flow along the simulated water table, however due to the implemented Robin-type boundary condition of the top of the set-up, it looks like streamlines flow up towards the surface. In the Robin-type boundary, the external head at the top of the set-up, was set at 10.5 m. Therefore, there will always be a hydraulic gradient and flow will occur towards the surface. Apparently, the resistivity term in the Robin Boundary type was set too low.

When it is assumed that in injection drain 1 and 3 an organic matter solution and via injection drain 2 an aluminium solution is brought in, the places where the green and red streamlines are near to each other give an indication of the mixing zone were potential Al-DOM precipitation can be formed. In reality this depends on the dispersivity of the injected chemicals, dispersion causes the chemicals to mix.

The upwards flow which is present in the set-up, causes that injection drain 1 was not as effective as thought beforehand. Due to this upwards flow, forming of precipitation in the unsaturated layer is inevitable but this does not contribute to the forming of a horizontal layer.

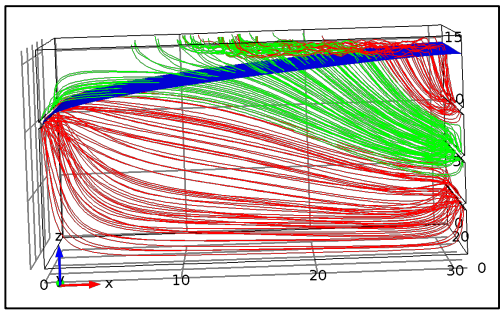

Figure 4.11: Flow paths of water for each separate drain

The blue layer represents the water table in the set-up. The red streamlines represent flow paths injected from injection drain 1 and 3. The green streamlines represent flow paths injection from injection drain 2.

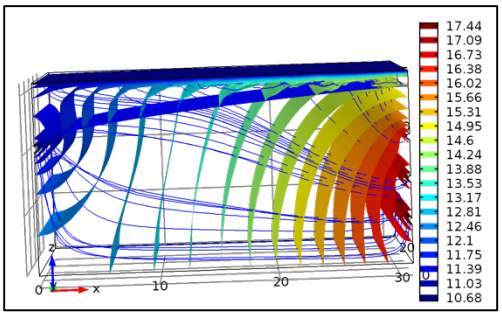

Figure 4.12: Hydraulic head distribution in the set-up

The hydraulic head difference causes the flow to flow through the unsaturated layer towards the surface.

Permeability Reduction

The results for the streamlines in initial situation and after reaction in which the Darcy equation, advection-dispersion equation and the chemical reaction are coupled is depicted in Figure 4.13 and Figure 4.14. In the figures, it was assumed that the sample was completely saturated and therefore the streamlines are more horizontal than in the case where an unsaturated zone was included. As can be seen in Figure 4.14 the Al-DOM precipitation layers form barriers between the streamlines of the different injection drains.

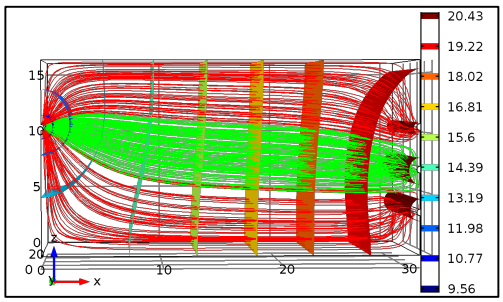

Figure 4.13: Streamlines in the initial situation with hydraulic head

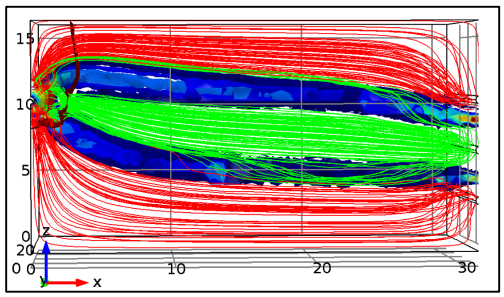

Figure 4.14: Streamlines and location of the Al-DOM precipitation band after reaction

The red streamlines represent the injection of aluminium-chloride. The green streamlines represent the organic matter injection. The dark blue layer represents the Al-DOM precipitation layer.

In Figure 4.15 the permeability reduction caused by the Al-DOM precipitation in the pore space is shown. At places where the Al-DOM precipitation band was modelled, a reduction in permeability can be seen. It has been assumed that the maximum reduction of permeability is about two order of magnitude. The maximum thickness of the Al-DOM precipitation band is near the overflow drain. This is caused by the chemicals being attracted to the overflow point and so a reaction is unavoidable at this spot. In the middle of the set-up the Al-DOM precipitation band is less thick because the streamlines can avoid each other and are separated by earlier formed Al-DOM precipitation. This mechanism is highly dependent on the dispersivity, a high dispersivity causes that the mixing will occur even when the solutes are separated. When the dispersivity is low and the flow of solutes is separated, no mixing will occur till the overflow point.

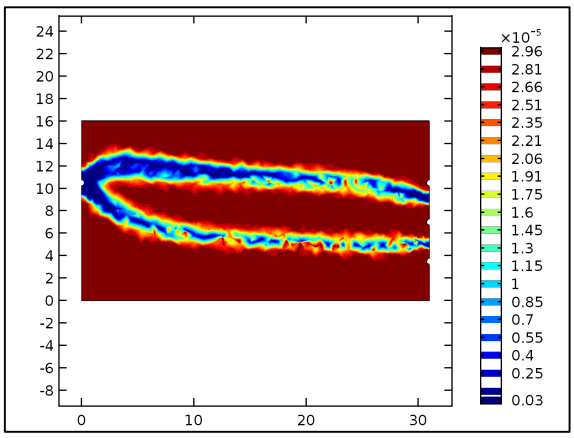

Figure 4.15: Permeability reduction by Al-OM interaction modelled in COMSOL

4.2.2 Visual Vertical Cross-sections

The results of scenario V.1 till V.4 are shown in Figure 4.16, Figure 4.17, Figure 4.18 and Figure 4.19. In the figures, four cross-sections are depicted with descending distance towards the injection drains (A-B-C-D). This distance is annotated in the text-boxes of each individual cross-section. In all scenarios, the results show that the Al-DOM precipitation took place in between the used injection drains like modelled in COMSOL Multiphysics. The Al-DOM precipitation layer was formed over the complete width of the set-up but not over the complete length of the set-up. It was found that in the container to which the overflow drain was attached, a significant amount of Al-DOM precipitates was formed in all V.x scenarios.

The Al-DOM precipitation was clearly visible because of the dark colour. The more abundant the precipitation, the darker the colour is. The highlighted areas in the figures show areas which are darker coloured as the 'normal' sand. This colour differs from the Al-DOM precipitation colour and when compared to the COMSOL Multiphysics model (Figure 4.11 injection drain 2 and 3), no real precipitation was expected in this area. Therefore, it is assumed that these areas were darker colour due to the adsorption of organic matter. This assumption is strengthened by the fact that this highlighted area was seen at the height at which OM was injected. In scenario V.1 this area is at the top of the set-up, while in scenario V.2 at the bottom.

The Al-DOM precipitation layer near the injection drains was fairly sharp and about 2-3 millimetres thick (Cross-sections D). At a larger distance from the injection drains the Al-DOM precipitation layer was vaguer and about 1 centimetre thick. The precipitation layer was not visible anymore at about half the length of the set-up. The lack of precipitation at the half of the box furthest away from the injection drains can be caused by two mechanisms; (1) the direction of the streamlines in the set-up and (2) separation of flow. The direction of the streamlines was simulated in COMSOL Multiphysics and depicted in Figure 4.11. It is shown that the streamlines of injection drain 2 and 3 reach the surface at about half the length of the set-up. During the test, it was however not observed that the chemicals reached the surface of the set-up. Mechanism two is therefore more likely. Because of the formed Al-DOM precipitation layer the flow of OM and aluminium-chloride was separated from each other. This is illustrated in Figure 4.20. The dispersion of the two chemicals does not lead to a high intensity of mixing when the flows are separated and therefore to less to no precipitation. Due to dispersion, the mixing of the chemicals starts again near the overflow, where precipitation is observed. Most of the chemicals could flow in the overflow drain without mixing. Therefore, the flocculation occurred in the container attached to the overflow.

The separation of flow does also explain why the Al-DOM precipitation line is observed to be 'sharper' near the injection drains. The flows were close to each other due to which dispersion caused higher concentrations to mix with each other. Further away from the injection drains, the flows are separated and due to dispersion lower concentrations of the chemicals mix with each other over a larger width. This leads to a thicker but vaguer precipitation line because the mixing intensity is not concentrated over a small width (Figure 4.20).

The results of scenario V.1 and V.2 do not differ much from each other, apart from the area in which possible adsorption of organic matter is situated. The Al-DOM precipitation lines are more or less equally thick and sharp. In scenario V.3 the precipitation line was observed sharper further away from the injection drains. The higher injected volume caused the test to have a longer duration and so the reaction could take place for a longer amount of time. Due to this more accumulation of precipitation could take place, leading to 'sharper' lines.

In scenario V.4 two precipitation lines were formed because all three injection drains were used. The lower precipitation line was observed to progress further in the set-up. This was already explained by the separation of flow in Figure 4.20. In cross-section D of scenario V.4, the effect of the boundary conditions become clear. It is seen that precipitation also took place above injection drain 1. This is probably caused by preferential flow of chemicals along backside of the injection drains.

In all presented scenarios, the most abundant Al-DOM precipitation was present closest to the organic matter injection drain. More vaguer precipitation was present close to the aluminium-chloride injection drain. This phenomenon is most clear in scenario V.4, cross-section C and caused by the $AlCl_3$/OM ratio. The $AlCl_3$/OM ratio is highest near the aluminium-chloride injection drain and lowest near the OM injection drain. As found in the characterization experiments, at lower $AlCl_3$/OM ratio the amount of aluminium is the limiting source and at high ratios this is the amount of organic matter. At the place where the Al-DOM precipitation is most abundant, the $AlCl_3$/OM ratio was most favourable. Below the line the ratio is too small for precipitation to take place or all aluminium ions have already reacted. Above the line the ratio is bigger, but less organic matter is present leading to 'vaguer' precipitation.

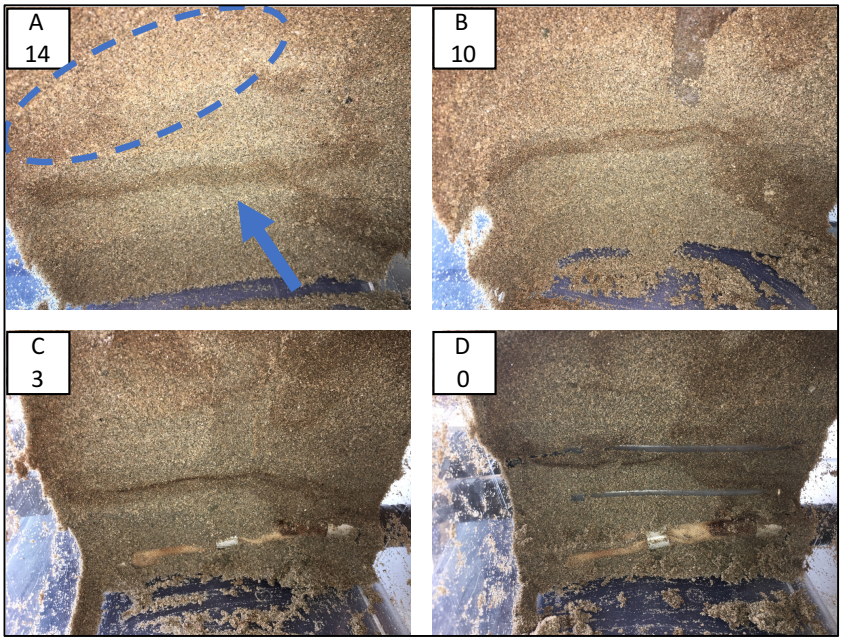

Figure 4.16: Vertical cross-sections scenario V.1

5L OM was injected via injection drain 2, 5L aluminium-chloride via injection drain 3. The injection rate was 10 ml/min for each injection drain. The blue arrow shows the Al-DOM precipitation layer. The highlighted area shows possible adsorption of organic matter.

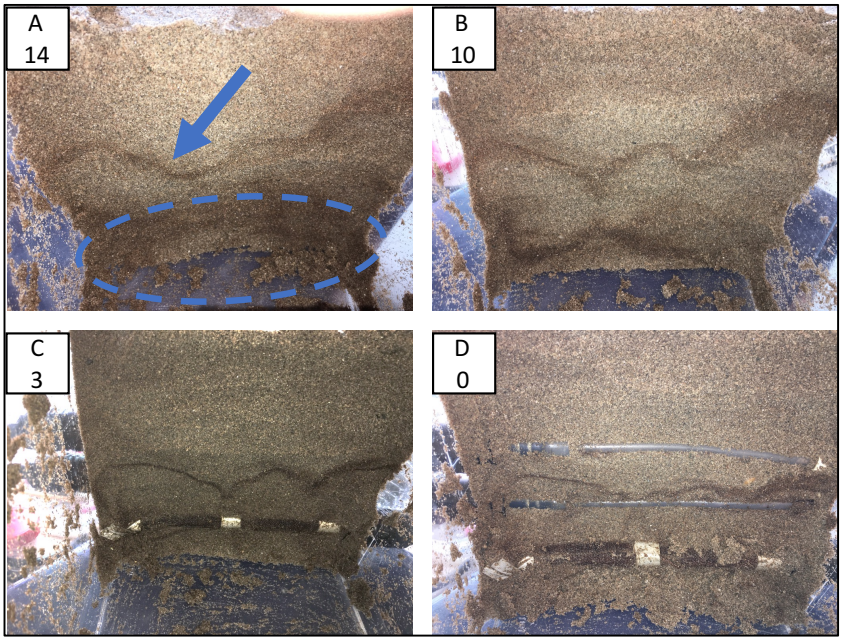

Figure 4.17: Vertical cross-sections scenario V.2

5L OM was injected via injection drain 3, 5L aluminium-chloride via injection drain 2. The injection rate was 10 ml/min for each injection drain. The blue arrow shows the Al-DOM precipitation layer. The highlighted area shows possible adsorption of organic matter.

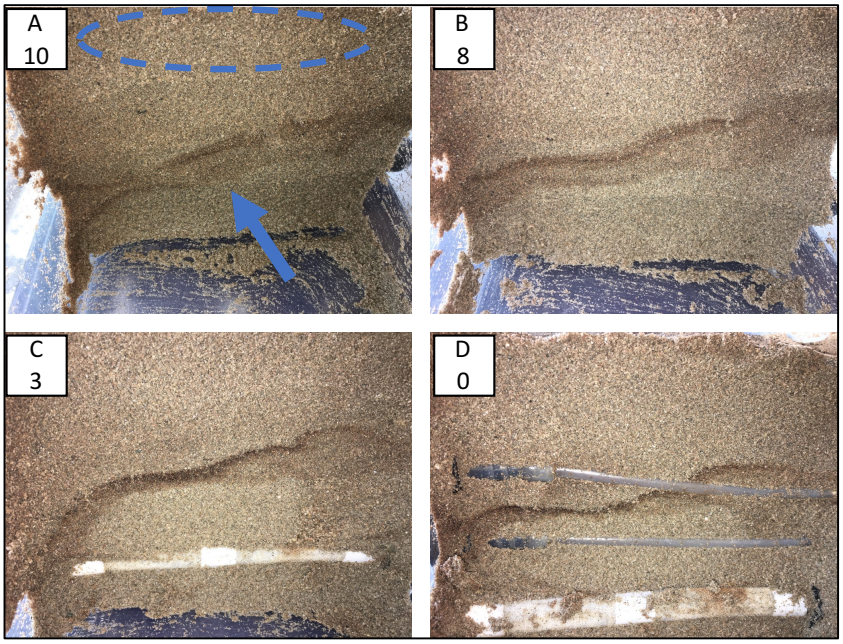

Figure 4.18: Vertical cross-sections scenario V.3

10L OM was injected via injection drain 2, 10L aluminium-chloride via injection drain 3. The injection rate was 10 ml/min for each injection drain. The blue arrow shows the Al-DOM precipitation layer. The highlighted area shows possible adsorption of organic matter.

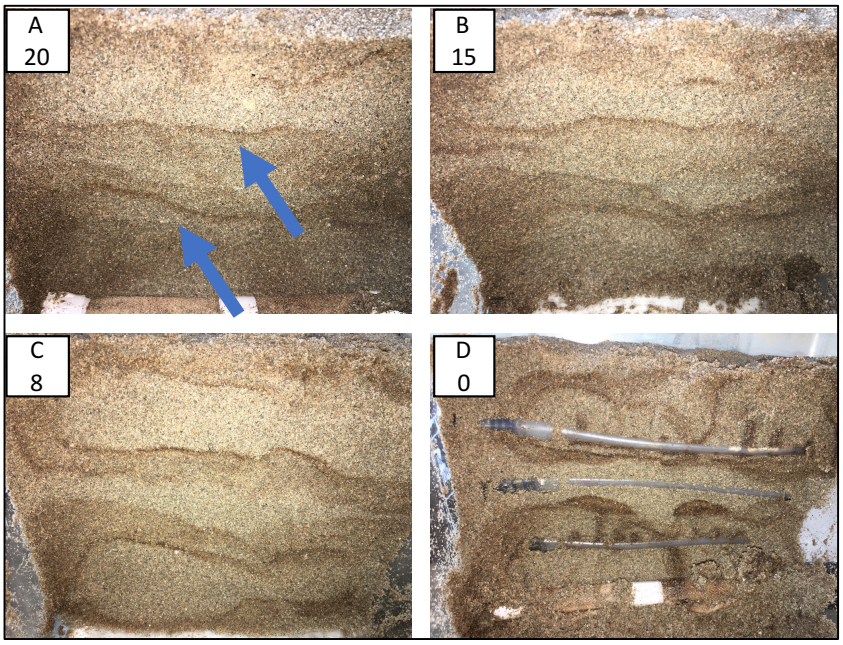

Figure 4.19: Vertical cross-sections scenario V.4

10L OM was injected via injection drain 1 and 3, 5L aluminium-chloride via injection drain 2. The injection rate was 5 ml/min for each injection drain. The blue arrows show the Al-DOM precipitation layers.

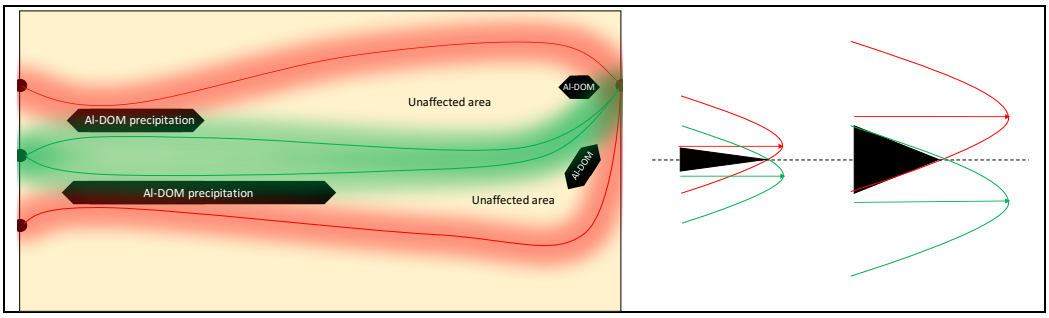

Figure 4.20: Separation of flow in the set-up

The lines represent the streamline. The highlighted area around this streamline represents the dispersion. The concentrations are represented by the parabola forms. Further away from the streamline a lower concentration yields.

4.2.3 3D Matlab interpretation

In this section, the results of the interpretation of the horizontal cross-sections are presented. The used 3D Matlab interpretation code can be found in appendix D. Before presenting the results of the test-scenarios, the contrast enhancing and spatial smoothing methods are described in more detail and an assessment of the functionality of the Matlab visualization tool is given.

Contrast Enhancement and Spatial Smoothing

To enhance the contrast, the data was discretized into four classes. The widths of these classes were determined by a statistical analysis. In this statistical analysis, the bin edges were back calculated by using the fitted distribution function parameters and by assuming a certain probability for each class. Based on the results, which were compared with the COMSOL Multiphysics model, it was assumed that the 5% darkest pixels surely contained Al-DOM precipitation the 10% above that most likely contained Al-DOM precipitation, the 15% above that was a mixture of adsorption and Al-DOM precipitation and the 70% which was left contained the unaffected sand. These assumed percentages were somewhat arbitrary and therefore a sensitivity analysis has been performed by varying the percentages ±30% of the chosen values. The results of this sensitivity analyses can be found in appendix E and are discussed in the results of the test-scenarios.

The chosen percentages resulted in the least noisy effect. Setting the percentages lower resulted in a smaller amount of pixels in which precipitation was interpreted and precipitation was not shown in places where it was observed. Setting the percentages higher resulted in a larger amount of pixels in which precipitation was interpreted but also at places where this was not expected based on the COMSOL Multiphysics model.

In Figure 4.21 the effect of spatial smoothing (by using 10% of the original data) and improving contrast (by discretizing the data into classes) is shown. In the original data, the Al-DOM precipitation is not directly clear (fig A). By discretizing the data into classes, the Al-DOM precipitation becomes better visible (fig B). When the size is reduced to only 10% of the input data, the data becomes less noisy and shows a clear interpretation of the Al-DOM precipitation layer (fig C).

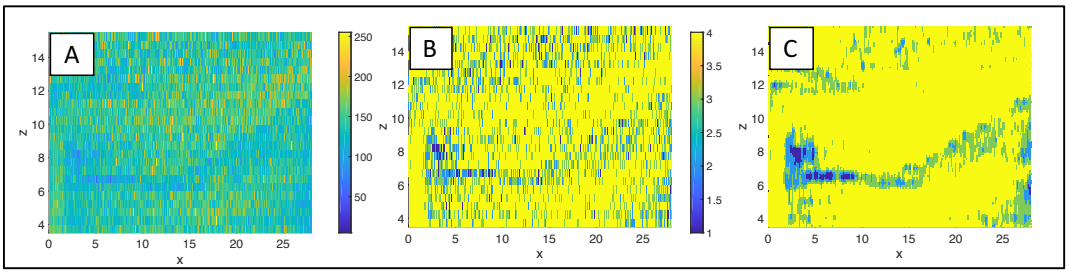

Figure 4.21: Effect of contrast enhancement and spatial smoothing in Matlab
The original data is present in fig. A. In fig. B the original data is discretized into classes. In fig. C the amount of data is reduced to spatially smooth the discretized data.

Assessment of 3D Matlab Interpretation Tool

In Figure 4.22 the Matlab interpretations of scenario H.2 and H.3 are compared with the observed vertical cross-sections near the injection drains. It can be concluded that the Matlab visualisation, and especially class 1 and 2, give good results and coincide with what was observed. Nevertheless, above the interpreted Al-DOM precipitation line, the interpretation still presents a lot of dark pixels. The cause of this effect is discussed in the next section.

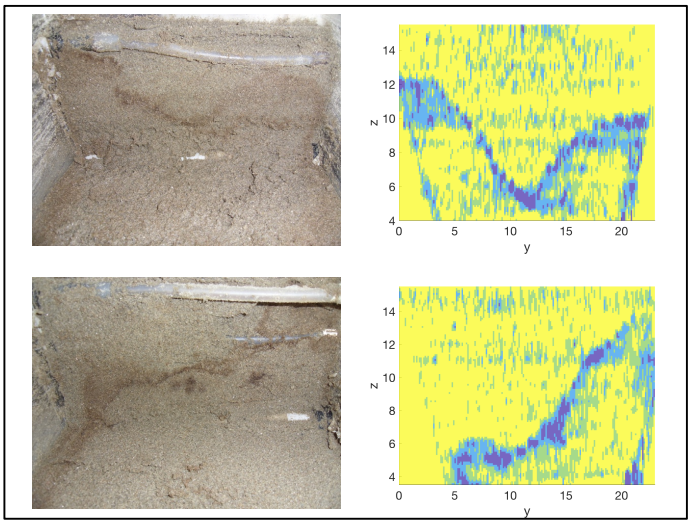

Figure 4.22: Comparison of Matlab visualisation with observations

Test-scenario Results

The 3D Matlab interpretation of the horizontal cross-sections of scenario H.2 and H.5 are depicted in Figure 4.23, Figure 4.24, Figure 4.25 and Figure 4.26. The 3D Matlab interpretations of all scenarios can be found in appendix F.

The general results in all scenarios show that Al-DOM precipitation took place over the complete width of the box but that no area-covering layer was engineered. In the precipitation plots it is seen that the most abundant Al-DOM precipitation was present in the first half of the box and near the overflow drain. This was caused by the separation of flow which was already explained in Figure 4.20.

Because the Matlab interpretation was based on colour differences, natural dark spots in the sand could influence the results. Since the organic matter solution was also dark coloured, adsorption of OM could also could lead to dark spots in the cross-sections. In the Matlab interpretation, dark spots show up at places where it was not directly expected based on the COMSOL Multiphysics model. As seen in Figure 4.22, the overall Al-DOM precipitation line can be distinguished but above and beneath this line several spots are shown. This is a direct cause of the discretization into classes. The calculated bin-edges form a boundary. A small change in chosen percentages for each class would result in a slightly different result as was shown by the sensitivity analysis in appendix E.

In the sensitivity analysis, the widths of the classes were varied by 30%. In all variations, the shape of the Al-DOM precipitation line could be distinguished clearly in between the injection drains as expected based on the COMSOL Multiphysics model. The chosen percentages therefore mostly affected the amount of interpreted precipitation which was present above and beneath the Al-DOM precipitation layer. The effect of the chosen percentages was higher in the precipitation visualisation plots. Obviously, when choosing higher percentages, more pixels are interpreted as precipitation and are therefore shown. In the sensitivity analysis, it was shown that choosing a percentage of 25% leads to an almost area-covering precipitation layer. However, when choosing 25%, it must be argued how much 'unaffected' sand is interpreted as precipitation. When comparing the 25% plots with the COMSOL Multiphysics model, it is shown that not only the area in between the drains show precipitation, but also large areas where they were not expected. Therefore, the used percentage showing the darkest 15% gives a good indication of the Al-DOM precipitation.

As became clear in the COMSOL Multiphysics model in Figure 4.11, injection drain one was not as effective as thought. The hydraulic head gradient caused an upward flow due to which the aluminium-chloride was not was not 'trapped' in between two horizontal organic matter flows. Due to the upward flow, the Al-DOM precipitation was not concentrated between two individual flows. The Al-DOM precipitation therefore occurs more or less randomly in the unsaturated layer.

Due to what was described above, the Al-DOM precipitation layer was less clear in the scenarios in which three injection drains were used compared to where chemicals were injected via two injection drains. Injection drain 2 and 3 are less influenced by the upwards flow towards the unsaturated layer. This becomes clear when looking at the results of scenario H.6. In scenario H.6, three injection drains were used but in injection drain 1, water was injected resulting in only one mixing zone for Al-DOM precipitation. In the 3D Matlab interpretation the Al-DOM precipitation layer becomes more clear in this scenario than in the scenarios in which organic matter was injected in injection drain 1.

In scenario H.2 (Figure 4.23) and H.5, curly formed Al-DOM precipitation lines are shown. This is probably caused by clogging of the injection drains which influences the flow properties in the set-up. The clogging of injection drains could either be caused by formed Al-DOM precipitation or by the insoluble part of HUMIN-P 775 which was found in Figure 4.7.

In scenario H.3 and H.5, a pump was added to the overflow drain to simulate in-situ situations. In the current set-up however the applied suction was not constant over the complete length of the overflow drain. Because the first few centimetres of the overflow were constructed of tubing, no suction was applied here. This resulted in a tilted Al-DOM line. The presence of this tubing was also the reason that no Al-DOM precipitation occurred on the left side of the overflow drain, this is seen in all precipitation plots.

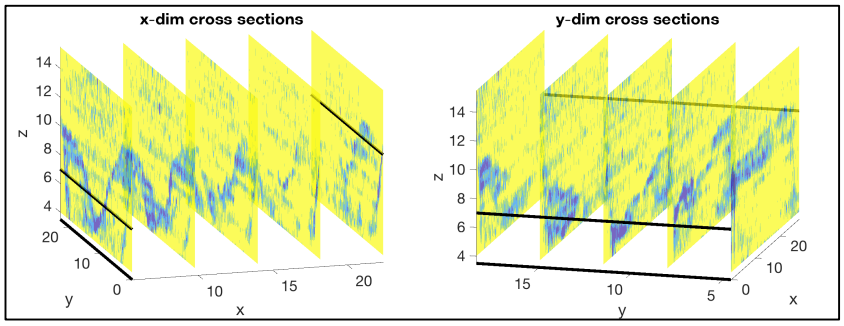

Figure 4.23: Matlab interpretation scenario H.2

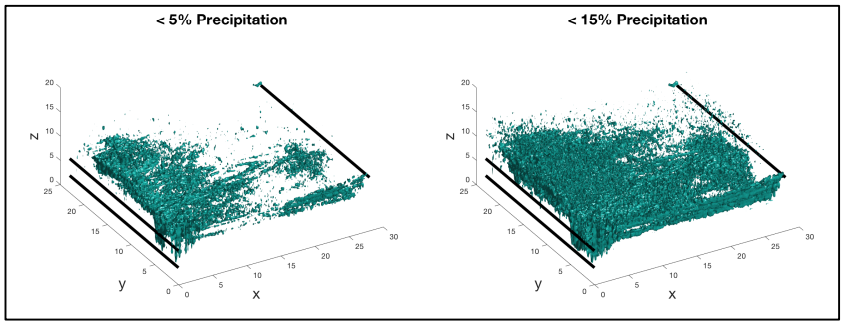

Figure 4.24: Precipitation visualisation scenario H.2

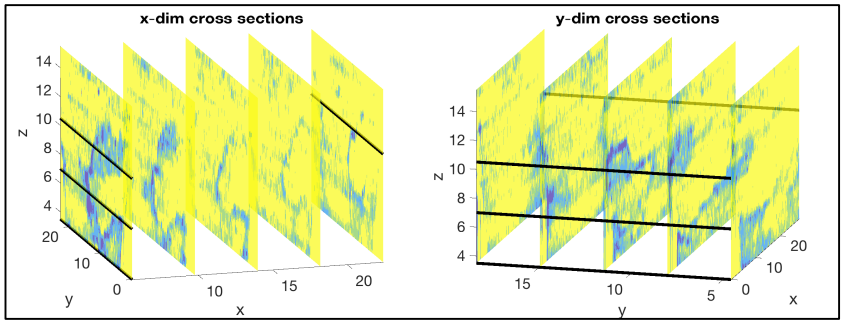

Figure 4.25: Matlab interpretation scenario H.5

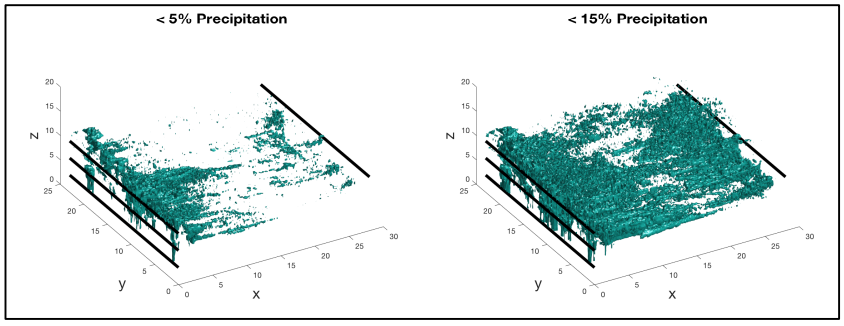

Figure 4.26: Precipitation visualisation scenario H.5

4.2.4 Hydraulic Conductivity Reduction

In Figure 4.27 the results of the falling-head test before the start of the test-scenarios are shown. The logarithm plot shows an almost linear decrease of the logarithm of the head over time. This implies that the hydraulic conductivity does not change significantly during the test and that the sample is completely saturated.

The hydraulic conductivity was determined based on 200 measurements of the diver. The first 20 measurements were not taken into account since there was a significant variability of the calculated hydraulic conductivity in these first measurements. The average calculated hydraulic conductivity before the experiments was equal to 0.003 cm/s ($3*10^{-5}$ m/s). This conductivity indicates a fine sand. The average hydraulic conductivity measured with the falling-head drains 1 and 2 separately, was 0.002 cm/s. For this value, it needs to be taken into account that the parameters which were used to calculate the hydraulic conductivity, were kept identical to the situation in which both falling-head drains were used. This is not completely correct since when using only one falling-head drain the width through which the water flows towards the surface is different.

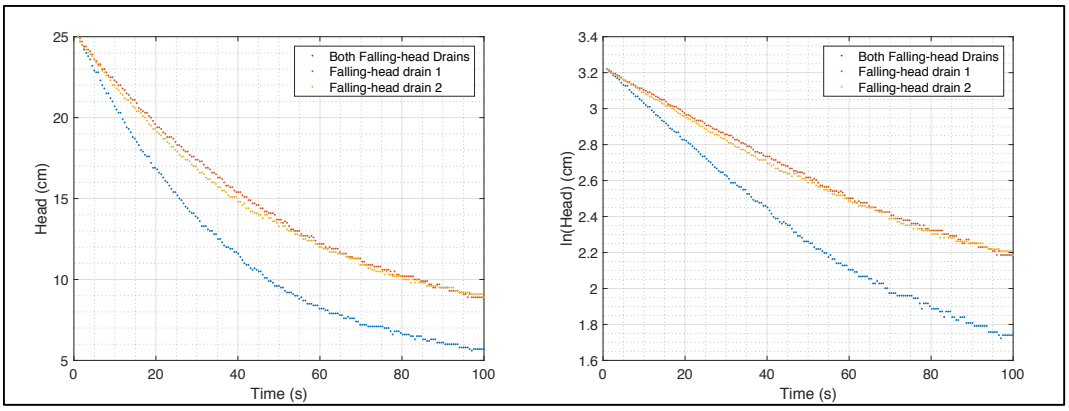

Figure 4.27: Falling-Head data before AI-DOM precipitation
On the left the head measurements over time are depicted. On the right the logarithm of the head measurements is depicted.

In Table 4.1 the hydraulic conductivities before and after the test-scenarios are listed. The average difference and maximum difference are given to give an indication of the reduction of hydraulic conductivity. The test scenarios H.1 and H.4 were conducted twice so two different before and after measurements were generated.

There was a wide variety of measurements of the hydraulic conductivity reduction. In scenarios H.1 till H.3 an increase in hydraulic conductivity was measured. This was mainly caused by erroneous ‘before’ measurements which were all lower as 0.003 cm/s. This could probably be caused by the set-up. In all other scenarios, falling-head drains and overflow drain were replaced and the measurements were again closer to 0.003 cm/s.

The average reduction in hydraulic conductivity when using two injections drains was approximately 5-10% (maximum 10-20%). When using three injection drains this average value was approximately 25-30% (maximum 30-35%). In the scenarios were three injection drains were used the Al-DOM precipitation was more randomly distributed in the set-up, which influenced the flow properties in the complete set-up and so a larger reduction was measured. In scenario H.6, three injection drains were used but water was injection in injection drain 1. Therefore, there was only one precipitation front which lead to a negligible measured reduction in permeability.

The different measurements of scenario H.1 show a significant difference, the two measurements of scenario H.4 were comparable with each other. The variability in measurements was probably caused by preferential flow paths and flow paths along the plastic sides of the set-up. The preferential flow paths occur through unaffected areas. As seen in the 3D Matlab interpretation, unaffected areas were present because there was no area-covering layer. The local reduction might therefore be higher as the measured reduction.

The assumption that a difference between falling-head drain 1 and 2 could be measured, seems not true. Only in scenario H.1 (2) and H.4 (1) a significant difference between falling-head drains 1 and 2 was measured. In most scenario's, the measurements more or less yielded the same values. Preferential flow paths and the lack of an area-covering layer caused that no difference was measured.

Table 4.1: Hydraulic conductivity reduction by Al-DOM precipitation

Scenario		Falling-Head drain					
		1-2	avg (max)	1	avg (max)	2	avg (max)
H.1	Before:	0.0020	1%	0.0013	-46%	0.0021	3%
	After	0.0020	(9%)	0.0019	(-30%)	0.0021	(12%)
H.1	Before	0.0027	12%	0.0023	6%	0.0024	52%
	After	0.0024	(22%)	0.0022	(13%)	0.0012	(58%)
H.2	Before	0.0018	-53%	0.0014	-31%	0.0013	-70%
	After	0.0027	(-40%)	0.0018	(-19%)	0.0022	(-58%)
H.3	Before	0.0023	6%	0.0012	2%	0.0017	-7%
	After	0.0022	(12%)	0.0012	(23%)	0.0018	(0%)
H.4	Before	0.0042	23%	0.0031	26%	0.0031	46%
	After	0.0032	(30%)	0.0023	(31%)	0.0018	(51%)
H.4	Before	0.0029	25%	0.0022	37%	0.0021	26%
	After	0.0022	(29%)	0.0014	(44%)	0.0016	(34%)
H.5	Before	0.0031	27%	0.0022	25%	0.0023	30%
	After	0.0023	(34%)	0.0016	(34%)	0.0016	(34%)
H.6	Before	0.0026	1%	0.0021	16%	0.0020	-7%
	After	0.0025	(6%)	0.0017	(20%)	0.0022	(-1%)
H.7	Before	0.0030	5%	0.0019	-2%	0.0020	-3%
	After	0.0029	(12%)	0.0020	(3%)	0.0021	(2%)

4.3 Oil-Tanking Case

In this section, the results of the reactive transport experiments using the sand from the location of Oil-Tanking Amsterdam are described. A vertical cross-section is depicted in Figure 4.28. It is shown that Al-DOM precipitation took place in the sample and two horizontal lines were created. The created lines were only a 3-5 millimetres thick.

Figure 4.28: Vertical cross-section Oil-Tanking Amsterdam case

In Figure 4.29 and Figure 4.30 the 3D Matlab interpretations are given. The results show a similar distribution of Al-DOM precipitation as found in the previous experiments. In the middle of the sample there were some unaffected areas and therefore no area-covering layer was created.

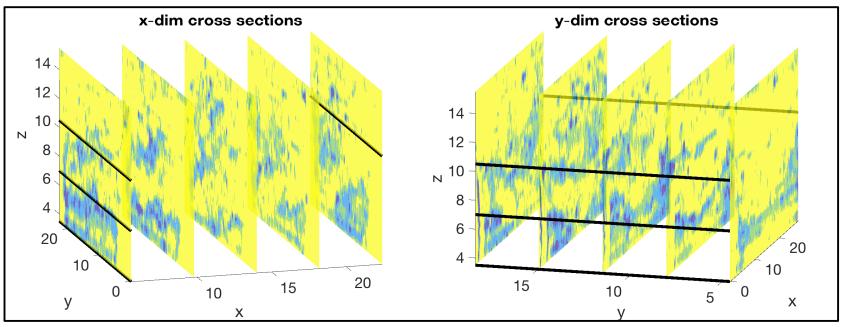

Figure 4.29: Matlab interpretation Oil-Tanking Amsterdam case

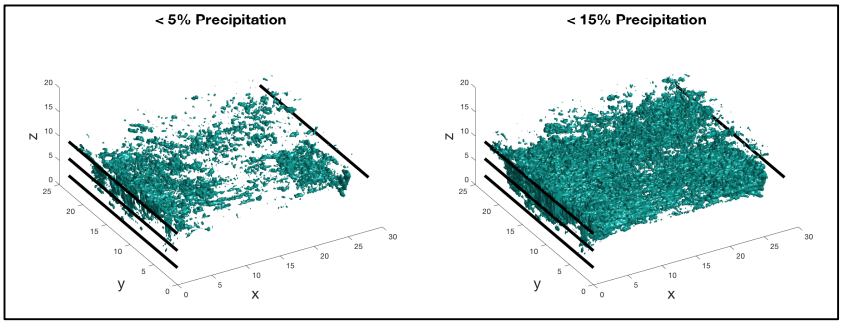

Figure 4.30: Precipitation visualisation Oil-Tanking Amsterdam case

Because no area-covering layer was created, the hydraulic conductivity reduction was difficult to measure. Besides that, the different sand caused problems in performing the falling-head test. At certain points during the test, a breakthrough of the flow was observed near falling-head drain 2. This meant that a preferential flow path was established with a sudden change in hydraulic conductivity as a result. This is depicted in Figure 4.31 where a sudden change in head is seen. The logarithm plot does not show a linear relationship meaning that the test was unreliable.

In Figure 4.32 the head measurements are given. In Table 4.2 the calculated hydraulic conductivities are listed. Due to the observed breakthroughs above falling-head drain 2, an increase in hydraulic conductivity was measured. The other two measurements yield an average hydraulic conductivity reduction of 5-10%. For engineering purposes this reduction of hydraulic conductivity is negligible. However, the reliability of the falling-head test results must be questioned due to the observation of breakthroughs.

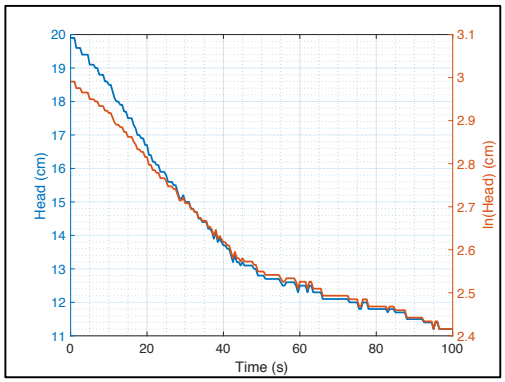

Figure 4.31: Breakthrough in hydraulic conductivity Oil-Tanking case

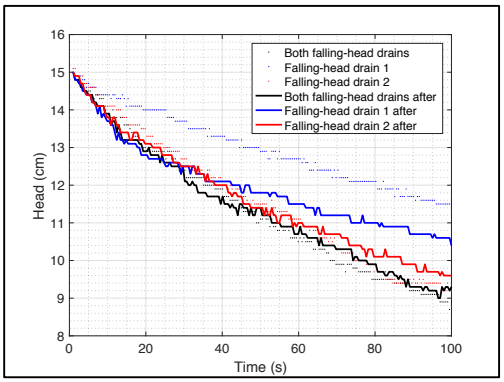

Figure 4.32: Falling-head test results Oil-Tanking case

Table 4.2: Hydraulic conductivity reduction by AI-DOM precipitation Oil-Tanking case

Scenario		Falling-Head drain					
		1-2 x $1*10^{-3}$	avg (max)	1 x $1*10^{-3}$	avg (max)	2 x $1*10^{-3}$	avg (max)
Oil-Tanking	Before:	0.9279	5%	0.8716	7%	0.4656	-44%
	After	0.8826	(14%)	0.8101	(19%)	0.6694	(-29%)

Chapter 5

Conclusions

This page is intentionally left blank

In this research, the possibility to use the interaction between aluminium-chloride and organic matter for engineering a horizontal layer of reduced permeability in the context of the SoSEAL project was discussed. The aim of this thesis was to give a proof of principle that a layer with reduced permeability could be engineered by using Al-DOM precipitation to counteract leakage problems. A three-dimensional set-up was created in which reactive transport experiments were conducted. The two solutions were injected via the drains at a constant rate.

The reactive transport experiments showed that horizontal Al-DOM precipitation took place. In a 3D Matlab interpretation it was shown that the Al-DOM precipitation took place over the complete width of the set-up but was concentrated near the injection- and overflow drains, leaving the middle part of the set-up unaffected. Near the injection- and overflow drains the Al-DOM precipitation was concentrated in a 3-4 mm precipitation band. This precipitation band caused a separation of flow. Since the flows were further apart from each other towards the middle of the set-up, the mixing due to dispersion was not concentrated to a small area and a wider and vaguer area of precipitates was observed. It can therefore be stated that separation of flow plays an important role in the accumulation of precipitates.

Although Al-DOM precipitation took place, this did not lead to a significant measurable reduction in hydraulic conductivity. This was mainly caused by the separation of flow due to which no area-covering Al-DOM precipitation layer was created. Due to the lack of this area-covering layer, preferential flow occurs through unaffected areas. The measured reduction in hydraulic conductivity was 25-30%, which is far from worthwhile for engineering purposes. In a COMSOL Multiphysics model it was estimated that the reduction over the complete domain could be two orders of magnitude. When the Al-DOM precipitation in the set-up can create an area-covering layer, it is likely that the reduction in permeability is more like this two order of magnitude. Although other boundary conditions might play a role.

The presence of an unsaturated layer of soil, showed that it is a tough challenge to create an Al-DOM precipitation layer in this unsaturated part. In the unsaturated layer the flow is less predictable and therefore no constant flow of the chemicals was established. Due to the unsaturated layer in the set-up, the upper injection drain was not as effective as thought. Due to a hydraulic gradient, there is an upwards flow to the surface. The flow via upper injection drain is affected the most by this hydraulic gradient. This was shown in scenarios in which only the lower two injection drains were used. These drains were less affected by the upwards flow and therefore a better visible Al-DOM precipitation layer was formed.

In the current set-up, the Al-DOM precipitation layer was formed in between the injection drains as was expected from the COMSOL Multiphysics model. However, in some cases the precipitation line was not formed horizontally but had a curly or tilted shape. Probably this was cause by clogging of the injection drains either by Al-DOM precipitation or insoluble organic matter.

In characterization experiments, it was found that approximately 15% of the organic matter was not soluble which could clog the drains. By UV254 measurements it was shown that 85% of organic matter could form complexes. The $AlCl_3$/OM ratio at which this 85% reacted organic matter was reached is dependent of the pH of the organic matter solution. At each initial pH value, the same amount of undissolved organic matter and organic matter concentration was found. It can therefore be concluded that deprotonation of binding sites in HUMIN-P 775 is not depending on pH in the pH range 5-9. This pH range has more influence in the aluminium solubility, causing more precipitation at lower pH.

The results in this research show that it is possible to use Al-DOM precipitation to engineer horizontal layer of reduced permeability but that it is a challenge to create this layer to be area-covering. The injected chemicals must remain close to each other to ensure that mixing via dispersion occurs in a small width and no separation of flow occurs. At this point, it is therefore better to engineer this horizontal layer under completely saturated conditions since in the unsaturated zone the flow is more difficult to predict. When these problems can be overcome, Al-DOM precipitation can potentially be used in the creation of horizontal layers of reduced permeability.

Chapter 6

Recommendations

This page is intentionally left blank

6.1.1 Reactive Transport Experiments

Saturation

The experimental set-up gave a proof of concept that the podsolization concept can be applied to create a horizontal layer of reduced permeability. However, since the unsaturated zone has a significant effect on the streamlines in the box, in new experiments complete saturation must be ensured. When the sample is completely saturated, the streamlines can be predicted better and therefore the mixing area of the chemicals has better control options.

To achieve a completely saturated sample, the outflow drain needs to be situated significantly above the input drains. In the current set-up, the upper drain was situated almost at the same height as the outflow drain, causing the flow to stream to/in the unsaturated layer. Another option is the use of a suction pump at the outflow drain and putting a ponding layer of water on top of the sand sample. In this way, the sample is completely saturated and the outflow is regulated with the flow rate of a pump. This set-up simulates an in-situ situation where the horizontal layer of reduced permeability is created underneath the groundwater table in saturated conditions.

Separation of Flow

In the conducted reactive transport experiments, it was found that the separation of flow has a significant effect on the mixing width and Al-DOM formation. In the current set-up, the injection drains were 3.5 centimetres apart. In investigate the effect of separation of flow in more detail, the experiments could be conducted with a variable length in between the injection drains. When the injection drains are closer to each other, the separation of flow due to Al-DOM precipitation might be less and therefore a larger area could be treated.

6.1.2 Measuring Hydraulic Conductivity

During the hydraulic conductivity measurements, no significant reduction could be measured. This could also be due to case that the falling-head drains were positioned to high. It was found that precipitates were formed at the same height as the drains, meaning that the flow did not need to pass this area which results in less resistance. In a new set up, the drains must be positioned further underneath the input of the chemicals to prevent precipitates to influence the area underneath the falling head test set-up.

To prevent a too high pressure on a small area of the sand, more input drains for the falling-head test must be constructed at the bottom of the box. In that way, the forced water flow into the box is divided over the complete area the box instead of only a few centimetres. This prevents bursting up of the sand in sand which has a lower hydraulic conductivity.

6.1.3 Field Applications

In field applications for the SoSEAL project, the 3D Matlab and COMSOL model showed that it is possible to create a horizontal mixing zone of the chemicals. However, it is difficult to create an area-covering layer in the 3D box. This is also due to side-effects which play a role in the set-up. In a pilot/full-scale test, these play a less significant role. In the box experiment it was possible that the drains were clogged, in reality this will probably not play a role since the injection can take place at a higher pressure.

Still, it will be a challenge to create an area-covering layer due to heterogeneity. Therefore, it is important to perform a ground investigation to pick a saturated aquifer in which the potential Al-OM precipitation layer can be created. It is important that the chemicals can easily flow through this aquifer to ensure mixing. To be able to predict the streamlines of the chemicals, it is preferred to have saturated conditions. To ensure mixing, it is probably preferred to use three drains. In this way, the aluminium solution in the middle drain is forced to mix. The drains could be 0.5 meters apart from each other, resulting in a total depth of 1 meter.

The concentrations of the Aluminium salt- and Organic matter solution should be kept at 1 g/L and 2 g/L respectively. It is not desirable to use higher Aluminium concentrations because then there will always be a discussion about the toxicity of Aluminium in the subsurface. When keeping these concentrations, the Metal/Carbon ratio will be about 0.1 which ensures an immediate reaction.

The challenge in creating a horizontal layer is probably the large area which needs to be treated. When for example an area of 100 m^2 needs to be treated, 30 m^3 of porous volume is treated (assuming a porosity of 30%). To get a better grip at the flush factor needed, further research is recommended in the forming of precipitates in a horizontal way. The relationship between the flush factor and the treated area should be investigated. For field applications, such a relationship would be interesting since this then gives an indication on the amount of solutions needed for injection to treat a certain area.

References

Appelo, C. A. J., & Postma, D. (2005). *Geochemistry, groundwater and pollution*.

Bear, J., & Cheng, H.-D. A. (2011). *Modeling Groundwater Flow and Contaminant Transport*. *Vadose Zone Journal* (Vol. 10). https://doi.org/10.1007/978-1-4020-6682-5

Bonfiglio, C. (2016). *MSc. Thesis: Hydraulic conducitivity reduction induced by precipitation of aluminium-organic matter flocs in porous*. Delft University of Technology.

Bourgault, R. R., Ross, D. S., & Bailey, S. W. (2015). Chemical and Morphological Distinctions between Vertical and Lateral Podzolization at Hubbard Brook. *Soil Science Society of America Journal*, *79*(2), 428. https://doi.org/10.2136/sssaj2014.05.0190

De Coninck, F. (1980). Major mechanisms in formation of spodic horizons. *Geoderma*, *24*(2), 101–128. https://doi.org/10.1016/0016-7061(80)90038-5

Deflandre, B., & Gagné, J. P. (2001). Estimation of dissolved organic carbon (DOC) concentrations in nanoliter samples using UV spectroscopy. *Water Research*, *35*(13), 3057–3062. https://doi.org/10.1016/S0043-1354(01)00024-0

Duan, J., & Gregory, J. (2003). Coagulation by hydrolysing metal salts. *Advances in Colloid and Interface Science*, *100–102*(SUPPL.), 475–502. https://doi.org/10.1016/S0001-8686(02)00067-2

Eusterhues, K., Hädrich, A., Neidhardt, J., Küsel, K., Keller, T. F., Jandt, K. D., & Totsche, K. U. (2014). Reduction of ferrihydrite with adsorbed and coprecipitated organic matter: Microbial reduction by Geobacter bremensis vs. abiotic reduction by Na-dithionite. *Biogeosciences*, *11*(18), 4953–4966. https://doi.org/10.5194/bg-11-4953-2014

Ferro-Vázquez, C., Nóvoa-Muñoz, J. C., Costa-Casais, M., Klaminder, J., & Martínez-Cortizas, A. (2014). Metal and organic matter immobilization in temperate podzols: A high resolution study. *Geoderma*, *217–218*, 225–234. https://doi.org/10.1016/j.geoderma.2013.10.006

Fitts, C. R. (2012). *Groundwater Science* (2nd ed.).

Hopman, J. (2016). *BSc. Thesis: First insights into Al-OM complexation and the effect of Al-OM flocs on porous mediapermeability*. Delft University of Technology.

Ivanov, V., & Chu, J. (2008). Applications of microorganisms to geotechnical engineering for bioclogging and biocementation of soil in situ. *Reviews in Environmental Science and Biotechnology*, *7*(2), 139–153. https://doi.org/10.1007/s11157-007-9126-3

Jankowski, M. (2014). The evidence of lateral podzolization in sandy soils of northern Poland. *Catena*, *112*, 139–147. https://doi.org/10.1016/j.catena.2013.03.013

Jansen, B., Nierop, K. G. J., & Verstraten, J. M. (2002). Influence of pH and metal / carbon ratios on soluble organic complexation of Fe (II), Fe (III) and Al (III) in soil solutions determined by diffusive gradients in thin films. *Analytca Chimica Acta*, *454*, 259–270.

Jansen, B., Nierop, K. G. J., & Verstraten, J. M. (2003). Mobility of Fe(II), Fe(III) and Al in acidic forest soils mediated by dissolved organic matter: Influence of solution pH and metal/organic carbon ratios. *Geoderma*, *113*(3–4), 323–340. https://doi.org/10.1016/S0016-7061(02)00368-3

Jansen, B., Nierop, K. G. J., & Verstraten, J. M. (2004). Mobilization of dissolved organic matter, aluminium and iron in podzol eluvial horizons as affected by formation of metal-organic complexes and interactions with solid soil material. *European Journal of Soil Science*, *55*(2), 287–297. https://doi.org/10.1111/j.1365-2389.2004.00598.x

Klučáková, M., & Kolajová, R. (2014). Dissociation ability of humic acids: Spectroscopic determination of pK a and comparison with multi-step mechanism. *Reactive and Functional Polymers*, *78*(1), 1–6. https://doi.org/10.1016/j.reactfunctpolym.2014.02.005

Lundström, U. S. (1993). The role of organic acids in the soil solution chemistry of a podzolized soil. *Journal of Soil Science*, *44*(1), 121–133. https://doi.org/10.1111/j.1365-2389.1993.tb00439.x

Lundström, U. S., Van Breemen, N., & Bain, D. (2000). The podzolization process. A review. *Geoderma*, *94*(2–4), 91–107. https://doi.org/10.1016/S0016-7061(99)00036-1

Lundström, U. S., Van Breemen, N., Bain, D. C., Van Hees, P. A. W., Giesler, R., Gustafsson, J. P., … Tau Strand, L. (2000). Advances in understanding the podzolization process resulting from a multidisciplinary study of three coniferous forest soils in the Nordic Countries. *Geoderma*, *94*(2–4), 335–353. https://doi.org/10.1016/S0016-7061(99)00077-4

Matilainen, A., Vepsäläinen, M., & Sillanpää, M. (2010). Natural organic matter removal by coagulation during drinking water treatment: A review. *Advances in Colloid and Interface Science*, *159*(2), 189–197. https://doi.org/10.1016/j.cis.2010.06.007

McKeague, J. a., Brydon, J. E., & Miles, N. M. (1971). Differentiation of Forms of Extractable Iron and Aluminum in Soils1. *Soil Science Society of America Journal*, *35*(1), 33. https://doi.org/10.2136/sssaj1971.03615995003500010016x

Nemati, M., & Voordouw, G. (2003). Modification of porous media permeability, using calcium carbonate produced enzymatically in situ. *Enzyme and Microbial Technology*, *33*(5), 635–642. https://doi.org/10.1016/S0141-0229(03)00191-1

Nierop, K. G. J., Jansen, B., & Verstraten, J. M. (2002). Dissolved organic matter, aluminium and iron interactions: Precipitation induced by metal/carbon ratio, pH and competition. *Science of the Total Environment*, *300*(1–3), 201–211. https://doi.org/10.1016/S0048-9697(02)00254-1

Pacheco Torgal, F., Labrincha, J. A., Diamanti, M. V., & Lee, H. K. (2015). *Biotechnologies and Biomimetics for Civil Engineering*.

Projectbureau PGS. (2012). PUBLICATIEREEKS GEVAARLIJKE STOFFEN. Retrieved March 1, 2017, from http://www.publicatiereeksgevaarlijkestoffen.nl/

Rashid, M. A., & King, L. H. (1970). Major oxygen-containing functional groups present in humic and fulvic acid fractions isolated from contrasting marine environments. *Geochimica et Cosmochimica Acta*, *34*(2), 193–201. https://doi.org/10.1016/0016-7037(70)90006-2

Sauer, D., Sponagel, H., Sommer, M., Giani, L., Jahn, R., & Stahr, K. (2007). Podzol: Soil of the year 2007. A review on its genesis, occurrence, and functions. *Journal of Plant Nutrition and Soil Science*, *170*(5), 581–597. https://doi.org/10.1002/jpln.200700135

Scheel, T., Haumaier, L., Ellerbrock, R. H., Rühlmann, J., & Kalbitz, K. (2008). Properties of organic matter precipitated from acidic forest soil solutions. *Organic Geochemistry*, *39*(10), 1439–1453. https://doi.org/10.1016/j.orggeochem.2008.06.007

Schulze-Makuch, D. (2009). Advection, Dispersion, Sorption, Degradation, Attenuation. In L. Silveira & E. J. Usunoff (Eds.), *Groundwater Encyclopedia of Life Support Systems* (Vol. II, pp. 55–69).

Sommer, M., Halm, D., Weller, U., Zarei, M., & Stahr, K. (2000). Lateral podzolization in a granite landscape. *Soil Science Society of America Journal*, *64*(4), 1434–1442. https://doi.org/10.2136/sssaj2000.6441434x

Stevenson, F. J. (1994). *Humus Chemistry Genesis, Composition and Reactions* (2nd ed.). New York.

Tang, Y., Zhou, J., Yang, P., Yan, J., & Zhou, N. (2016). *Groundwater Engineering*.

Tipping, E. (2002). *Cation Binding by Humic Substances*.

Tipping, E., Lofts, S., & Sonke, J. E. (2011). Humic Ion-Binding Model VII: A revised parameterisation of cation-binding by humic substances. *Environmental Chemistry*, *8*(3), 225–235. https://doi.org/10.1071/EN11016

tropicalbotany.wordpress.com. (n.d.). CalciumCarbonate. Retrieved from https://tropicalbotany.wordpress.com/2014/04/07/seminar-at-kew-by-mike-rowley-tropical-tree-converts-atmospheric-co2-into-mineralized-carbonate/

van Paassen, L. A., Daza, C. M., Staal, M., Sorokin, D. Y., van der Zon, W., & van Loosdrecht, M. C. M. (2010). Potential soil reinforcement by biological denitrification. *Ecological Engineering*, *36*(2), 168–175. https://doi.org/10.1016/j.ecoleng.2009.03.026

Vis, R. (2015). *MSc. Thesis: Control of Subsurface Flow The Effect of Al-OM Interactions on Hydraulic Conductivity*. Delft University of Technology.

www.geocaching.com. (n.d.). opbouwpodzol. Retrieved from https://www.geocaching.com/geocache/GC5Y65D_podzol-reindersmeer?guid=3e237b1a-e44d-4a15-b09d-7b0992817418

Zhang, H. (2013). *Rapid determination of dissolved organic carbon by persulfate oxidation vial and UV/VIS spectrophotometer*.

Zsolnay A. (2003). Dissolved organic matter: Artefacts, definitions, and functions. *Geoderma*, *113*(3–4), 187–209. https://doi.org/10.1016/S0016-7061(02)00361-0

This page is intentionally left blank

Appendices

This page is intentionally left blank

Appendix A Additional Background Theory

A.1 Lateral Podsolization

The classical theory of podsolization assumed vertical, unsaturated water flow and thus a horizontal podzol horizon development. In places where lateral subsurface water fluxes predominate also (hillslope-scale) lateral podsolization occurs (Bourgault et al., 2015; Jankowski, 2014; Sommer et al., 2000). Bourgault et al. (2015) investigated 99 podzols and found that laterally developed podzol horizons were twice as thick as vertically developed podzols. Laterally develop podzols contained higher concentrations of aluminium and lower concentrations of iron and carbon. In this study, it was concluded that vertical developed podzols had a more crumb microstructure with higher porosity, while lateral developed podzols were more infilled.

In Figure A.1 the lateral development of a podzol is depicted. Inhere it can be seen that the eluvial zone (E horizon) decreases in thickness downslope, while the opposite is true for the illuvial zone (B horizon). The exact transportation mechanism is still unsure. Bourgault et al. (2015) suggest that lateral podsolization occurs via solution transport of aluminium ions and dissolved organic carbon downslope with groundwater. It can however also be that complexes are formed uphill and are transported downhill physically through the pores.

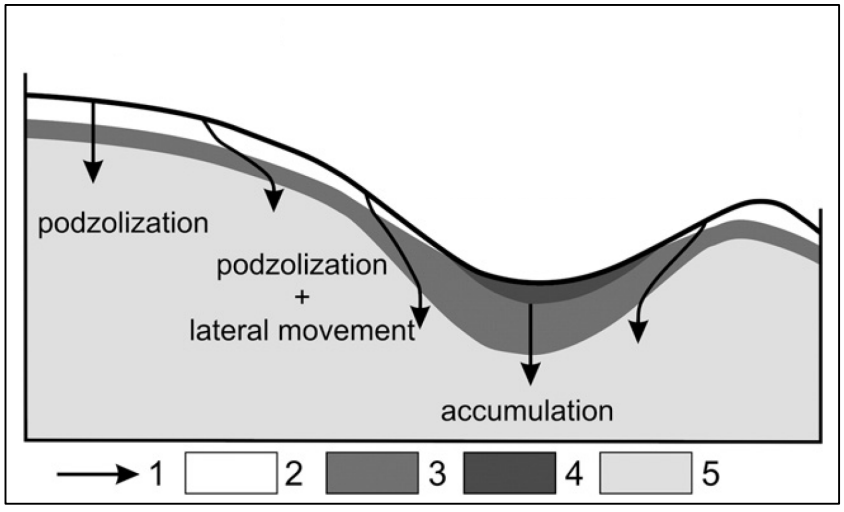

Figure A.1: Lateral podzol development
1 represent the direction of flow, 2 is the E horizont, 3 the B horizon, 4 the A horizon and 5 the C horizon. Copied from Jankowski (2014).

A.2 Chemical Composition of Humic Compounds

As mentioned in the main text, organic matter can be subdivided into humic acids, fulvic acids and humin. The chemical composition of different sources of these compounds is represented in Table A.1. The carbon content of humic substances is typically around 50%, fulvic acids may have less because they are better soluble.

Table A.1: Chemical Composition of Humic Compounds.
Table taken from Tipping (2002)

Humic Compound	C	H	O	N	S
Soil HA	52.8 – 58.7	2.2 – 6.2	32.8 – 38.3	0.8 – 4.3	0.1 – 1.5
Soil FA	40.7 – 50.7	2.8 – 7.0	39.7 – 49.8	0.9 – 2.3	0.1 – 2.6
Groundwater HA	65.5	5.2	24.8	2.4	1.0
Groundwater FA	60.4	6.0	32.0	0.9	0.7
Soil Humin	55.9	5.8	32.8	4.9	-

A.3 Effect of Organic Matter with Cations

The effect of organic matter on metal cations is shown in various works. Stevenson (1994) and Tipping (2002) did research in the metal cation binding capacity of organic matter. In Figure A.2 binding/complexation capacity of cupper is depicted. It can be seen that even at low concentrations of organic matter, fulvic acid in this case, a large portion of cupper ions have formed complexes. It can therefore be concluded that organic matter in solution with cations result in complexes and therefore have less free cations in solution than a similar solution lacking the organic material.

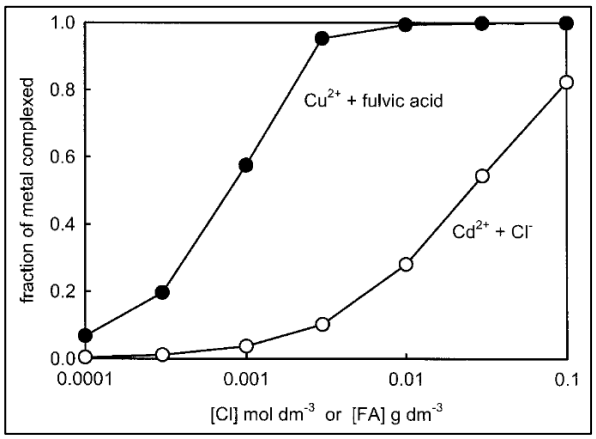

Figure A.2: Complexation of Cu by organic matter at pH 7
Copied from Tipping (2002)

A.4 Darcy Flow

When in the Richard's equation it is assumed that the relative permeability is equal to one, the sample is completely saturated. The Richard's equation than reduces to equation A.1. When then substituting the hydraulic head as the sum of the pressure head and elevation head, the equation reduces to equation A.2 which is the Darcy flow equation. Because flow occurs from a high to a low head value, a minus sign is needed to correct for the direction. The gradient in pressure head shows that for flow to occur the pressure must change.

$$\frac{\partial \theta_w}{\partial t} = -\nabla q = \nabla K_{sat}(\nabla h_w + \nabla z) \qquad (A.1)$$

$$q = -K_{sat}(\nabla H) \qquad (A.2)$$

A.5 Constant-head test

A constant-head test is different from the falling-head test because a constant head difference is maintained across the sample. This induces a steady discharge through the sample. The constant-head test set-up is depicted in Figure A.3. According to Darcy's flow equation, the hydraulic conductivity can be calculated with equation A.3. Because the Darcy flow equation is used, the sample must be completely saturated.

$$K = \frac{Q}{A}\frac{L}{dh} \qquad (A.3)$$

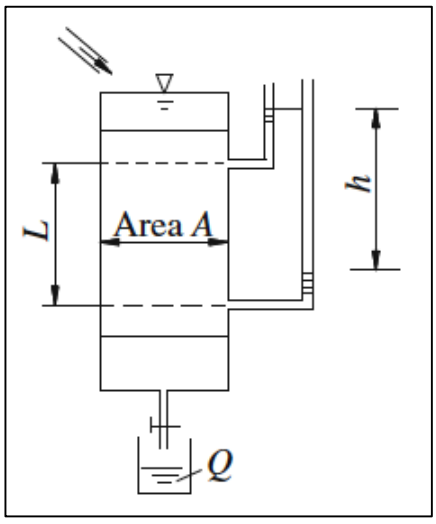

Figure A.3: Constant-head test set-up
Copied from Fitts (2012)

A.6 Kozeny-Carman Equation

In the Kozeny-Carman equation the change in porosity is related to a change in hydraulic-conductivity. Hydraulic conductivity estimates based on such an empirical relationship are rough and should only be used as to giving sens of the order of magnitude. The Kozeny-Carman relationship is given in equation A.5. When assuming the density, viscosity and mean grain size do not change, the new hydraulic conductivity can be estimated with equation A.6 in which *n* represents the new values, and *i* the initial values.

$$K = \left(\frac{\rho_w g}{\mu}\right)\left(\frac{n^3}{(1-n)^2}\right)\left(\frac{{d_{50}}^2}{180}\right) \qquad (A.5)$$

$$K_n = K_i \left(\frac{\frac{{n_n}^3}{(1-n_n)^2}}{\frac{{n_i}^3}{(1-n_i)^2}} \right) \qquad (A.6)$$

Appendix B Chemical Datasheets

HUMIN-P 775

MATERIAL SAFETY DATA SHEET
acc. to 91/155/EEC - ISO 11014-1:1994(E)

Trade Name: HUMIN - P 775

Printing date 08/08/2003 Reviewed on 06/08/2003

1. IDENTIFICATION OF SUBSTANCE

- **Product details**
- **Trade name:** HUMIN - P 775
- **Article number:** 4 036964 003036
- **Application of the substance / the preparation:** Intermediate
- **Manufacturer/Supplier:**
  Humintech GmbH
  Heerdter Landstr. 189/D
  D-40549 Düsseldorf/ Germany
  www.humintech.com
  info@humintech.com
  Tel: +49 211 50 66 57 0
  Fax: +49 211 50 66 57 22
- **Information:** see: Section 16 (Contact)
- **Emergency information:** see: Manufacturer/Supplier

2. COMPOSITION/ DATA ON COMPONENTS

- **Chemical characterization:** Potassium salt of humic acids
- **Chemical state:** Solid
- **CAS No. Designation:** 68514-28-3
- **Identification number(s):**
- **EINECS number:** 271-030-1
- **Dangerous components:**

CAS: 1310-58-2 EINECS : 215-181-3	Potassium hydroxide	C ; R 35	< 2%

- **Additional information**
  For the wording of the listed risk phrases refer to section 16.

Figure B.1: Material Safety Datasheet HUMIN-P 775

Aluminium-Chloride Hexahydrate

ScienceLab.com
Chemicals & Laboratory Equipment

Health	2
Fire	0
Reactivity	0
Personal Protection	E

Material Safety Data Sheet
Aluminum chloride hexahydrate MSDS

Section 1: Chemical Product and Company Identification

Product Name: Aluminum chloride hexahydrate

Catalog Codes: SLA1855, SLA3358

CAS#: 7784-13-6

RTECS: BD0530000

TSCA: TSCA 8(b) inventory: No products were found.

CI#: Not applicable.

Synonym: Aluminum (III) chloride, hexahydrate

Chemical Name: Aluminium trichloride hexahydrate

Chemical Formula: AlCl3.6H2O

Contact Information:

Sciencelab.com, Inc.
14025 Smith Rd.
Houston, Texas 77396

US Sales: **1-800-901-7247**
International Sales: **1-281-441-4400**

Order Online: ScienceLab.com

CHEMTREC (24HR Emergency Telephone), call: 1-800-424-9300

International CHEMTREC, call: 1-703-527-3887

For non-emergency assistance, call: 1-281-441-4400

Section 2: Composition and Information on Ingredients

Composition:

Name	CAS #	% by Weight
Aluminum chloride hexahydrate	7784-13-6	100

Toxicological Data on Ingredients: Aluminum chloride hexahydrate: ORAL (LD50): Acute: 3311 mg/kg [Rat]. 1990 mg/kg [Mouse].

Figure B.2: Material Safety Datasheet Aluminium-Chloride Hexahydrate

Appendix C Characterization Results as Function of M/C-ratio

In the results and discussion chapter, the results of the fundamental research have been given as a function of the Aluminium Salt over Organic Matter concentration ratio. Since in literature the M/C ratio is often used, the results as a function of the M/C ratio are given in this attachment. Since the dissolved carbon content cannot be determined precisely, this M/C ratio cannot be determined precisely exact. In , it can be seen that the turning points lie around an M/C ratio of 0.03 which is also reported in literature as an important M/C turning point.

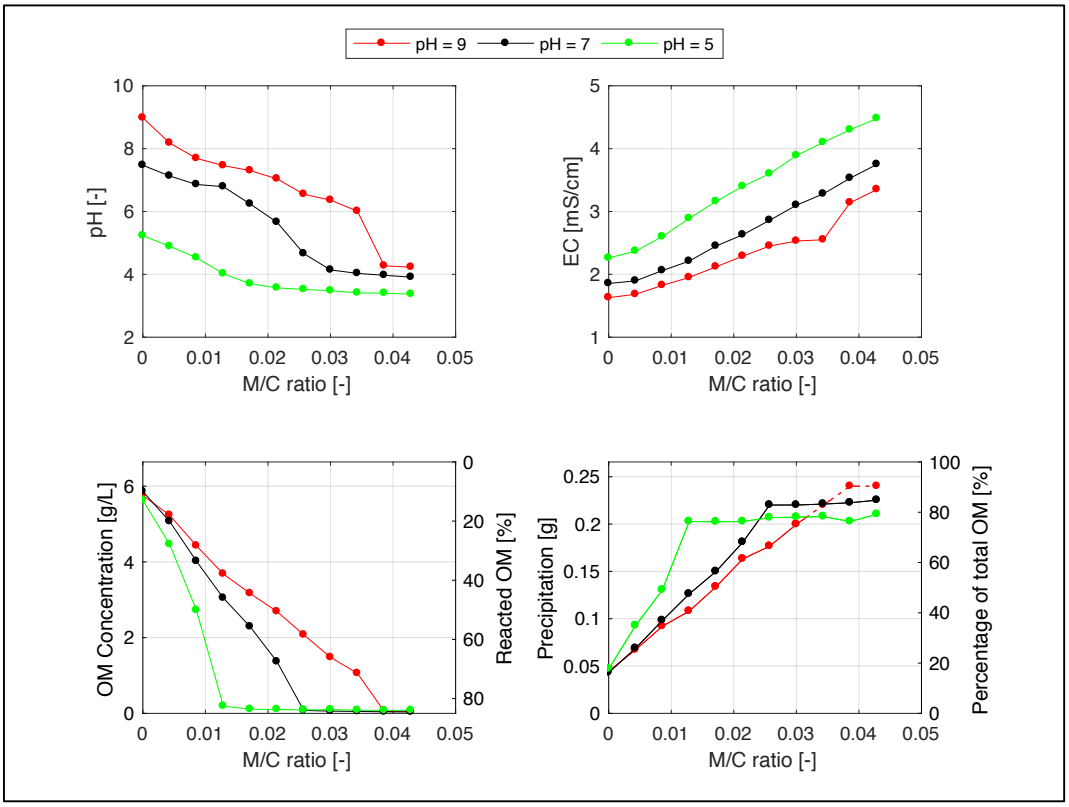

Figure C.1: Characterization results as function of M/C ratio

This page is intentionally left blank

Appendix D Matlab Code 3D Interpretation

Data Access

```
clear, clc, close all, imtool close all

photostart = 5330;                          % Start Photo
photoend = 5354;                            % End Photo
photos = photoend - photostart + 1;

prefix = 'SAM_';
fnum = photostart:photoend;
ext = '.jpg';

% Import Pictures
hWaitBar = waitbar(0,'Reading jpg files');
for i = 1:length(fnum)
    fname = [prefix num2str(fnum(i)) ext];  % Name of the Photo
    jpg = rgb2gray(imread(fname));          % Load the Photo and convert
to grey scale
    jpg = imcrop(jpg,[550 400, 1900, 1800]);% Crop the image to area of
interest
    jpg = imresize(jpg, 0.1);               % Resize the image for
computing speed
    jpg = double(jpg);                      % Change to data type double
to make calculations
    D(:,:,length(fnum)+1-i) = jpg;          % Storte image to 3D Volume
Data matrix
    waitbar((i)/length(fnum))
end
delete(hWaitBar)
whos D
D = flipud(D);                              % Turn the y-axis for
representation
```

Statistical Analysis

```
figure(), hold on

yyaxis left
histogram(D(:))
xlabel('grey scale intensity')
ylabel('Counts')


stats = datastats(D(:));                    % The data statistics of the
volume data
pd = fitdist(D(:),'Normal');                % Fit a normal distribution
x = 0:1:255;
y=normpdf(x, stats.mean, stats.std);
```

```
percentages = [1.0 0.30, 0.15, 0.05];       % The percentages for the
critical values
criteria = icdf(pd, percentages);           % Back calculate the critical
values

colors = {[1 1 1]
    [1 0.8 0.8]
    [1 0.5 0.5]
    [1 0.0 0.0]};

yyaxis right
plot(x,y)


for i=1:4
patchX = [linspace(0,criteria(i),50),criteria(i),0];
patchY = [normpdf(linspace(0,criteria(i),50),stats.mean,stats.std),0,0];
pa(i) = patch(patchX,patchY,colors{i});
end

legend([pa(4) pa(3),pa(2),pa(1)],' 5% Precipitation','10% Most likely
precipitation','15% adsorption and precipitation', '70% Normal Sand')
ylabel('pdf')
xtext = [criteria(2:4)];
ytext = [pdf(pd,criteria(2:4))];
string = {[num2str(criteria(2),4) '  \rightarrow'],
[num2str(criteria(3),4) '  \rightarrow'],[num2str(criteria(4),4) '
\rightarrow']};
text(xtext, ytext, string,'HorizontalAlignment','right')

title('Histogram / probability density function')
figure()
k1 = slice(D, [],[],[1:3:photos]);
set(k1, 'edgecolor', 'none')
```

Interpolation in z-direction

```
[x, y, z] = size(D);
[xq, yq, zq] = meshgrid(1:y,1:x,1:0.2:z);
D = interp3(D,xq,yq,zq,'cubic');            % Interpolate the matrix
along the z dimension
whos D
```

Discretization into classes

```
contournumber = 3;                          % The number of contour lines

nbins = contournumber + 1;                  % Number of categories
binEdges = [stats.min criteria(4) criteria(3) criteria(2)  stats.max];
% Intensity edges for the categories
P = discretize(D,binEdges);         % discretize the volume matrix into
the categories
```

Contourlines

```
contoursfor = [1 size(D,3)];                % Draw contours for these
photos

for i = contoursfor
    figure()
    figurenumber = num2str(i);
    [C,h] = contourf(P(:,:,i), contournumber,'EdgeColor','none'); % Check
if discretized matrix yields the same contour as D
    set(gca, 'ydir','reverse');
    title(['Discretized ' figurenumber])
end
```

2D slices

```
[x, y, z] = size(P);

Xl = 28;
Yl = 23;
Z0 = 3.5;
Z1 = 15.5;

X = linspace(0, Xl, y);
Y = linspace(0, Yl, x);
Z = linspace(Z0, Z1, z);

figure(), hold on
k1 = slice(X,Y,Z,P,[],[4.*Yl./5, 13.*Yl./20, Yl./2, 7.*Yl./20,
Yl./5],[],'nearest');
set(k1, 'edgecolor', 'none','FaceAlpha', 0.7)
line([0 0],[Yl./5 4.*Yl./5], [10.5 10.5], 'Color','k','LineWidth',4)
line([0 0],[Yl./5 4.*Yl./5], [7 7], 'Color','k','LineWidth',4)
line([0 0],[Yl./5 4.*Yl./5], [3.5 3.5], 'Color','k','LineWidth',4)
line([Xl Xl],[Yl./5 4.*Yl./5], [11 11], 'Color','k','LineWidth',4)
xlabel('x')
ylabel('y')
zlabel('z')
title('y-dim cross sections')
view(-75,20)

figure(), hold on
k1 = slice(X,Y,Z,P,[4.*Xl./5, 13.*Xl./20, Xl./2, 7.*Xl./20,
Xl./5],[],[],'nearest');
set(k1, 'edgecolor', 'none','FaceAlpha', 0.7)
line([Xl./5 Xl./5],[0 Yl], [10.5 10.5], 'Color','k','LineWidth',4)
line([Xl./5 Xl./5],[0 Yl], [7 7], 'Color','k','LineWidth',4)
line([Xl./5 Xl./5],[0 Yl], [3.5 3.5], 'Color','k','LineWidth',4)
line([4.*Xl./5 4.*Xl./5],[0 Yl], [11 11], 'Color','k','LineWidth',4)
xlabel('x')
ylabel('y')
zlabel('z')
title('x-dim cross sections')
view(-16,20)
```

Precipitation

```
figure()
isosurface(X,Y,Z,D,criteria(4),'noshare')

line([0 0],[0 Yl], [10.5 10.5], 'Color','k','LineWidth',4)
line([0 0],[0 Yl], [7 7], 'Color','k','LineWidth',4)
line([0 0],[0 Yl], [3.5 3.5], 'Color','k','LineWidth',4)
line([Xl Xl],[0 Yl], [11 11], 'Color','k','LineWidth',4)
xlabel('x')
ylabel('y')
zlabel('z')
title('< 5% Precipitation')
view(-30,50)

figure()
isosurface(X,Y,Z,D,criteria(3),'noshare')

line([0 0],[0 Yl], [10.5 10.5], 'Color','k','LineWidth',4)
line([0 0],[0 Yl], [7 7], 'Color','k','LineWidth',4)
line([0 0],[0 Yl], [3.5 3.5], 'Color','k','LineWidth',4)
line([Xl Xl],[0 Yl], [11 11], 'Color','k','LineWidth',4)
xlabel('x')
ylabel('y')
zlabel('z')
title('< 15% Precipitation')
view(-30,50)
```

movie y-direction

```
v = VideoWriter('5_ydir.avi');
v.FrameRate = 2;
v.Quality = 100;
open(v);

figure('renderer','zbuffer');
nframes = x;
view([-90 0 0])

for j = 1:5:nframes
    k = slice(X,Y,Z,P,[Xl],j./x.*Yl,[Z0],'nearest');
    set(k, 'edgecolor', 'none')
    line([0 0],[0 Yl], [10.5 10.5], 'Color','k','LineWidth',4)
    line([0 0],[0 Yl], [7 7], 'Color','k','LineWidth',4)
    line([0 0],[0 Yl], [3.5 3.5], 'Color','k','LineWidth',4)
    line([Xl Xl],[0 Yl], [11 11], 'Color','k','LineWidth',4)
    xlabel('x')
    ylabel('y')
    zlabel('z')
    title('y-dim cross sections')
    M = getframe;
    writeVideo(v,M);
end
movie(M,1,1)
close(v);
```

Appendix E Sensitivity Analysis Discretization Classes

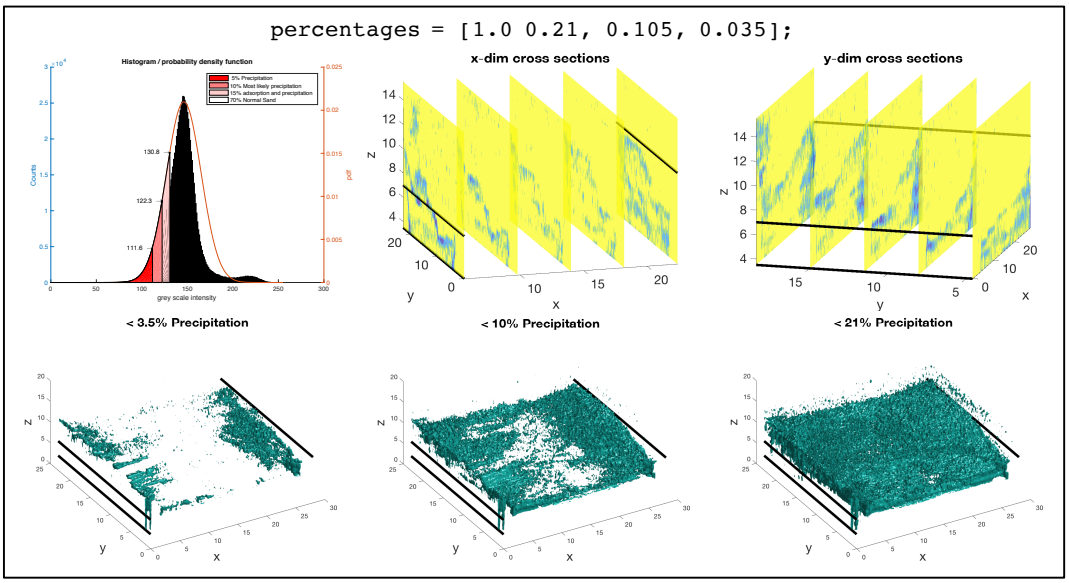

Figure E.1: Sensitivity Analysis Discretization into classes: -30%

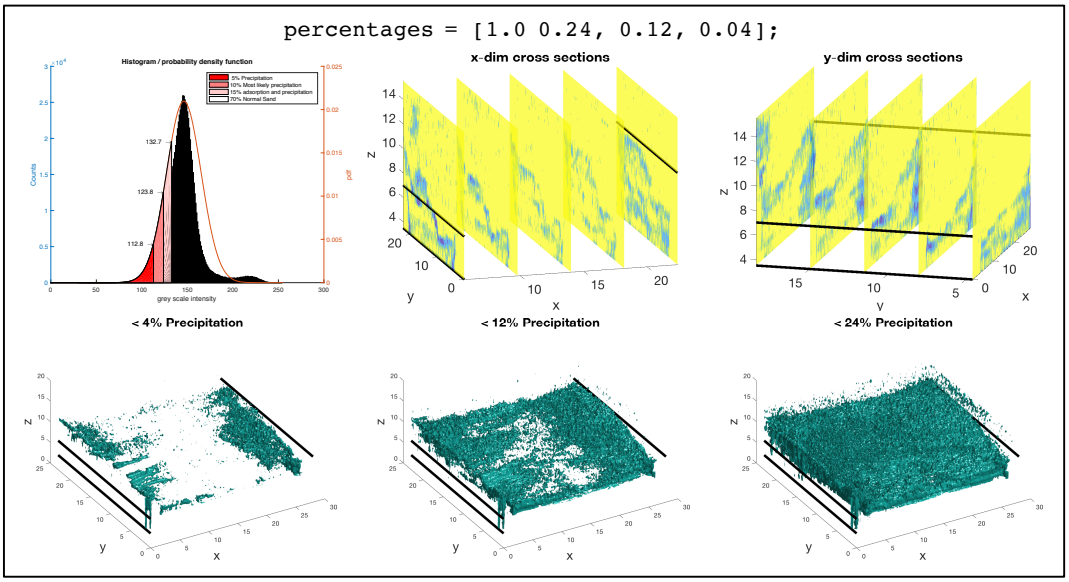

Figure E.2: Sensitivity Analysis Discretization into classes: -20%

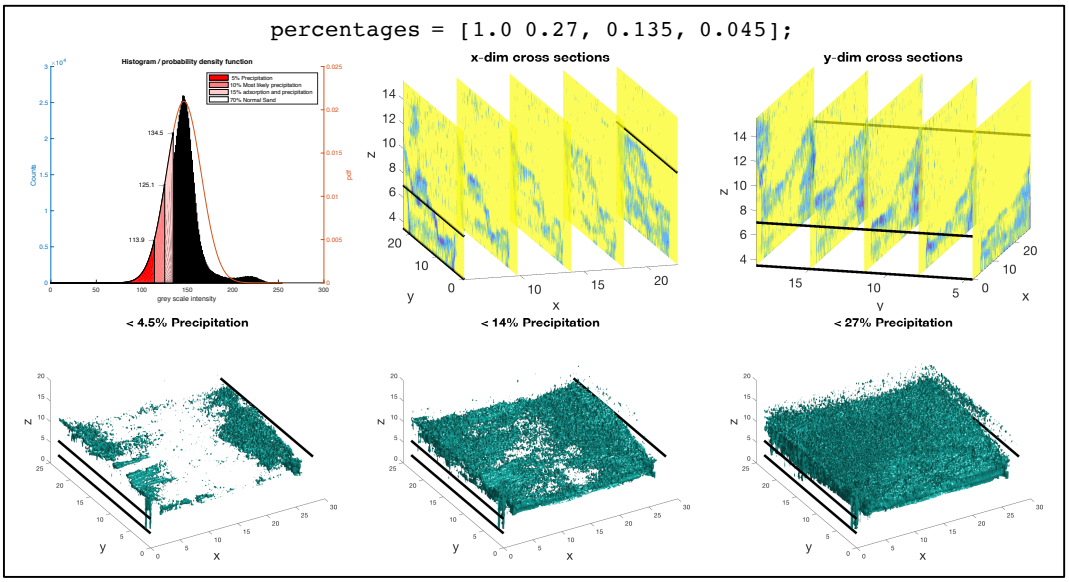

Figure E.3: Sensitivity Analysis Discretization into classes: -10%

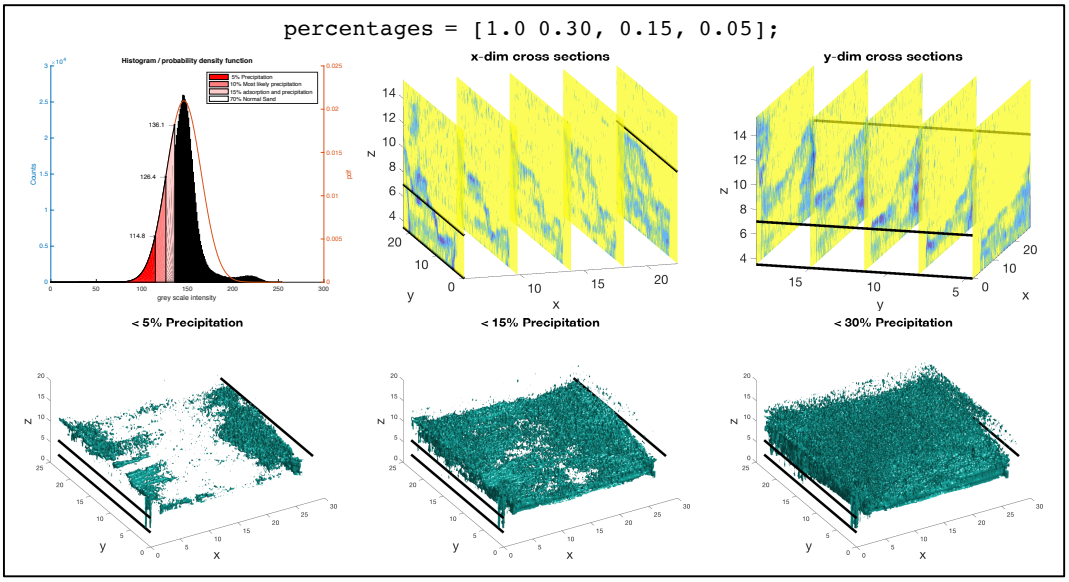

Figure E.4: Sensitivity Analysis Discretization into classes: 0%

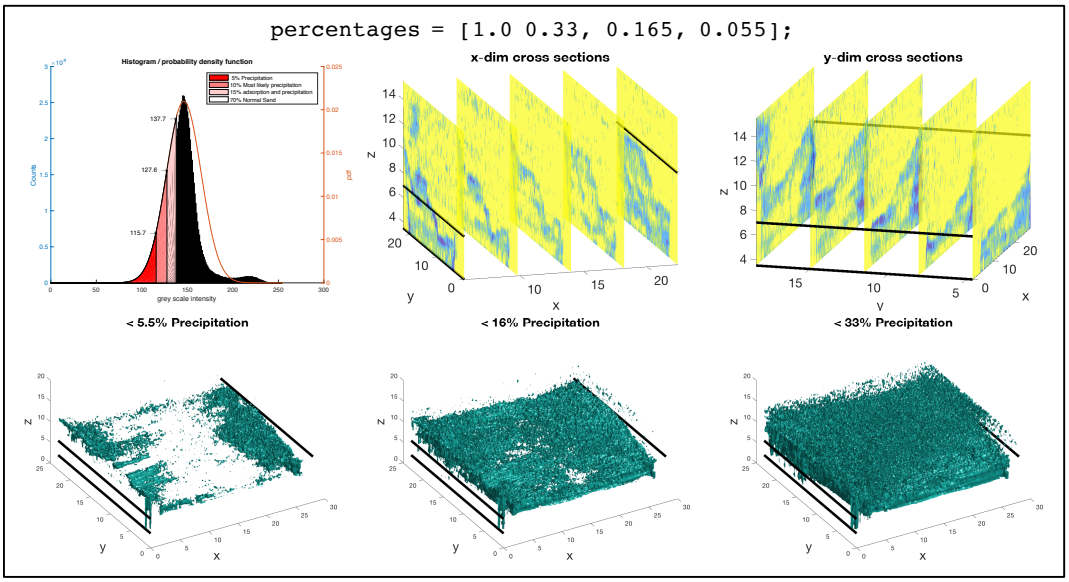

Figure E.5: Sensitivity Analysis Discretization into classes: +10%

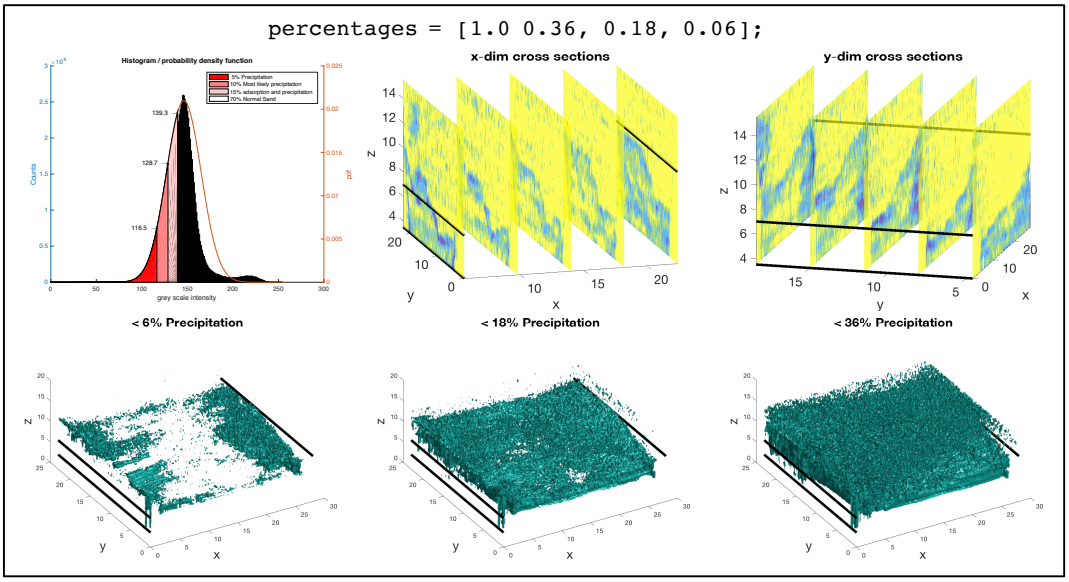

Figure E.6: Sensitivity Analysis Discretization into classes: +20%

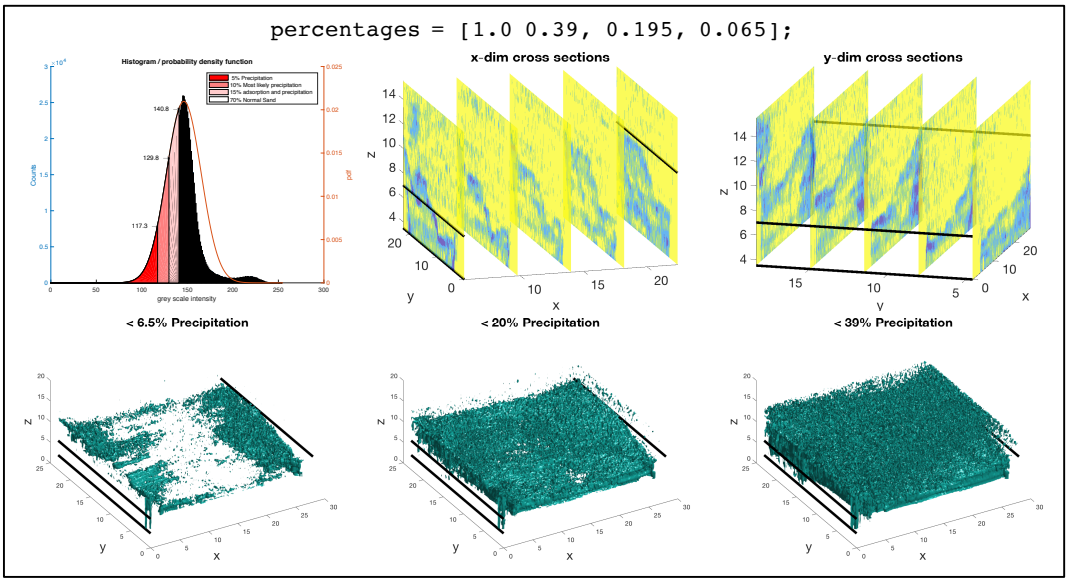

Figure E.7: Sensitivity Analysis Discretization into classes: +30%

Appendix F Results 3D Matlab Interpretation

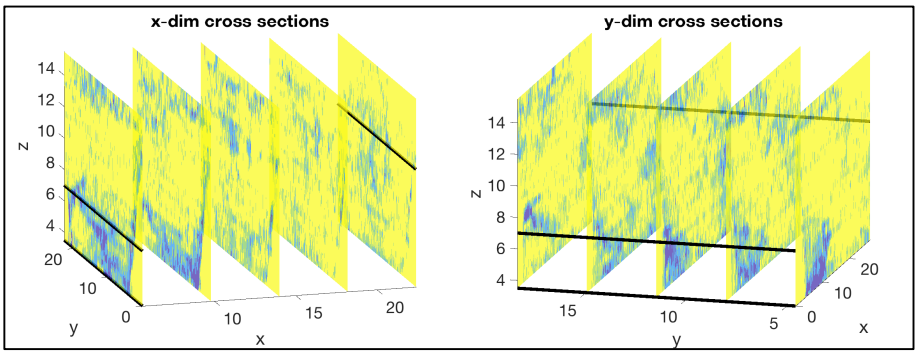

Figure F.1: Matlab interpretation scenario H.1

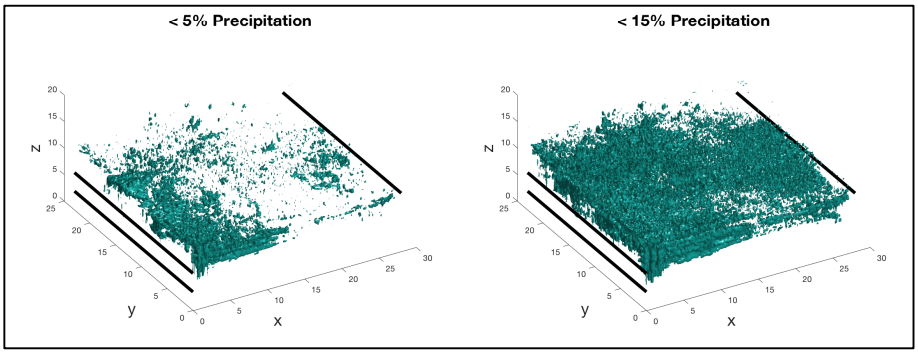

Figure F.2: Precipitation visualisation scenario H.1

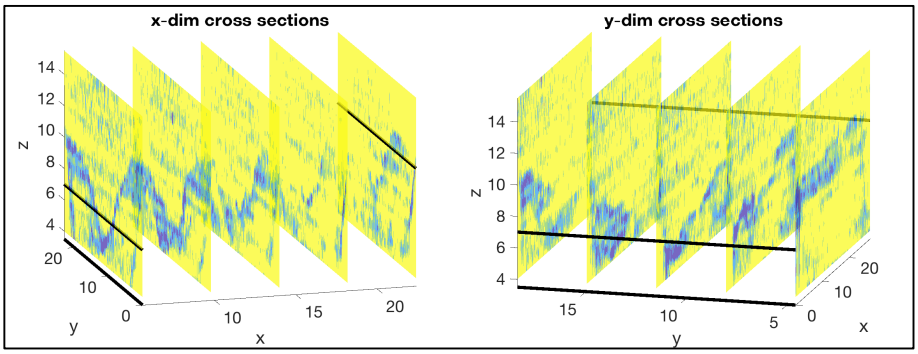

Figure F.3: Matlab interpretation scenario H.2

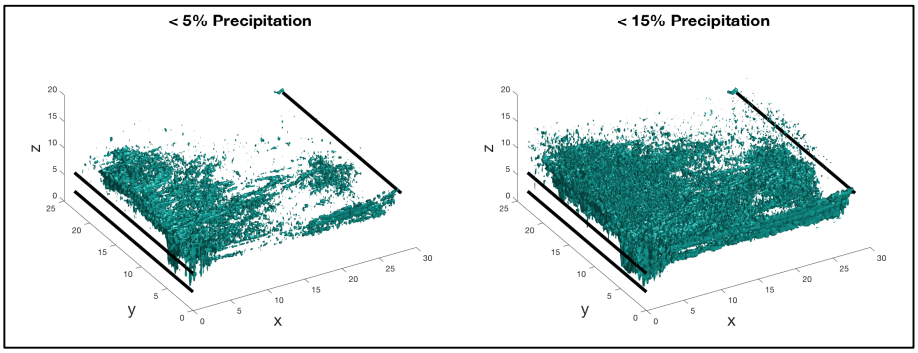

Figure F.4: Precipitation visualisation scenario H.2

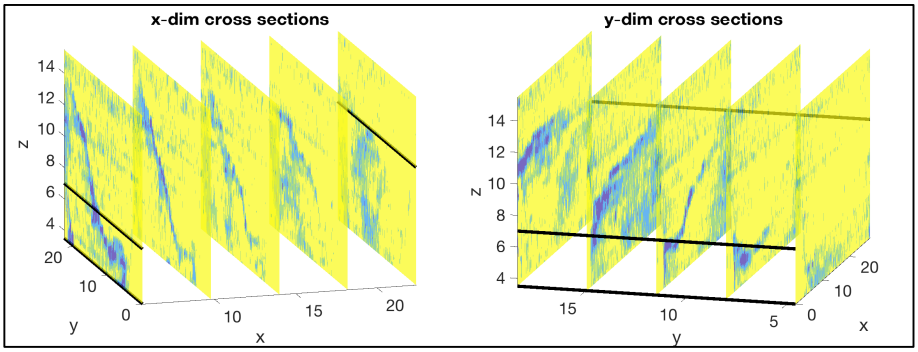

Figure F.5: Matlab interpretation scenario H.3

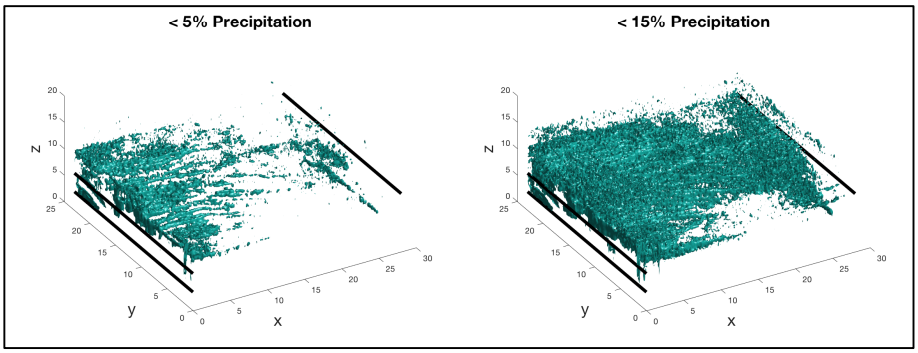

Figure F.6: Precipitation visualisation scenario H.3

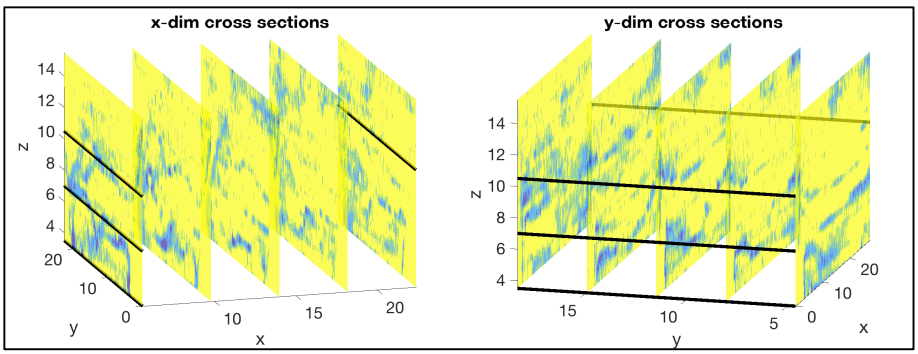

Figure F.7: Matlab interpretation scenario H.4

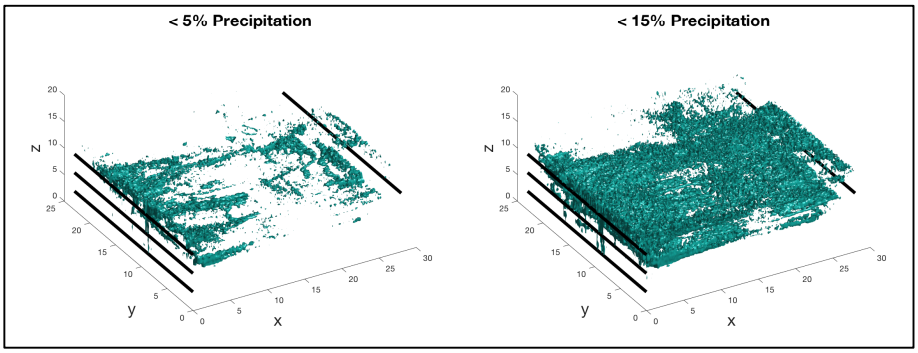

Figure F.8: Precipitation visualisation scenario H.4

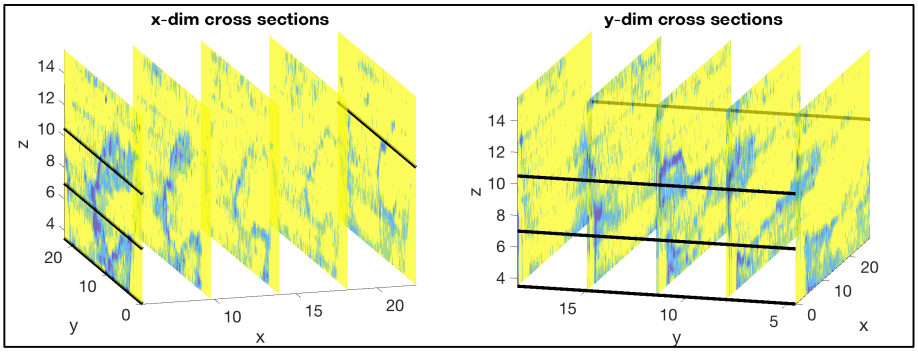

Figure F.9: Matlab interpretation scenario H.5

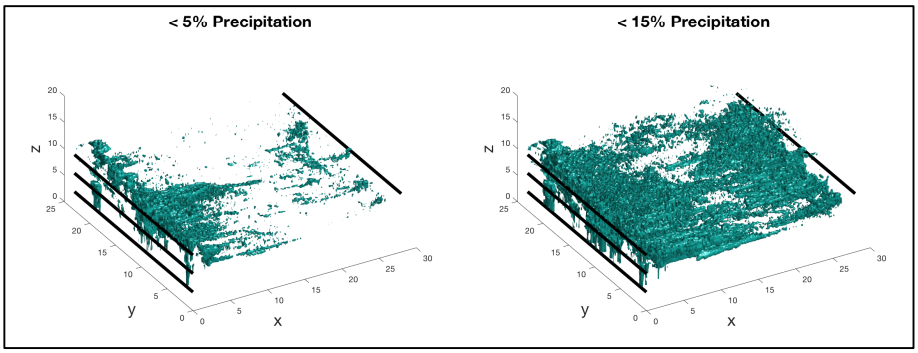

Figure F.10: Precipitation visualisation scenario H.5

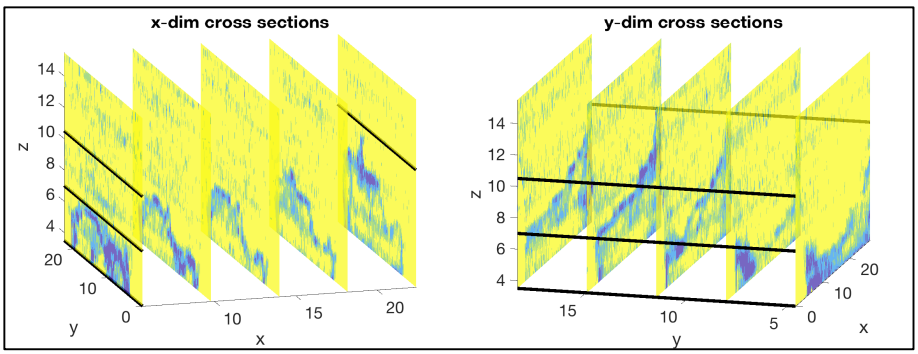

Figure F.11: Matlab interpretation scenario H.6

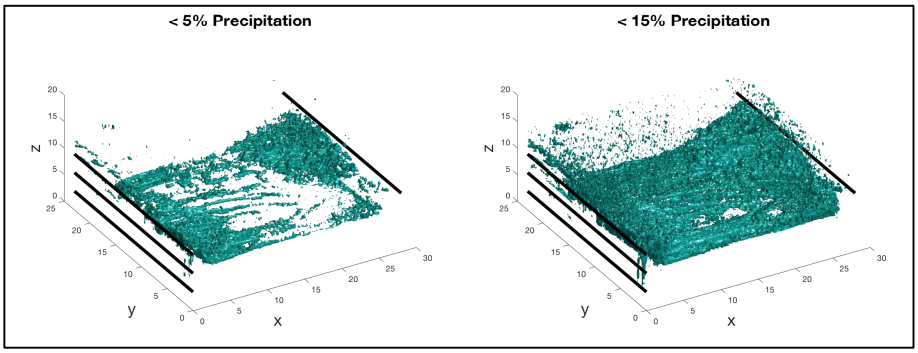

Figure F.12: Precipitation visualisation scenario H.6

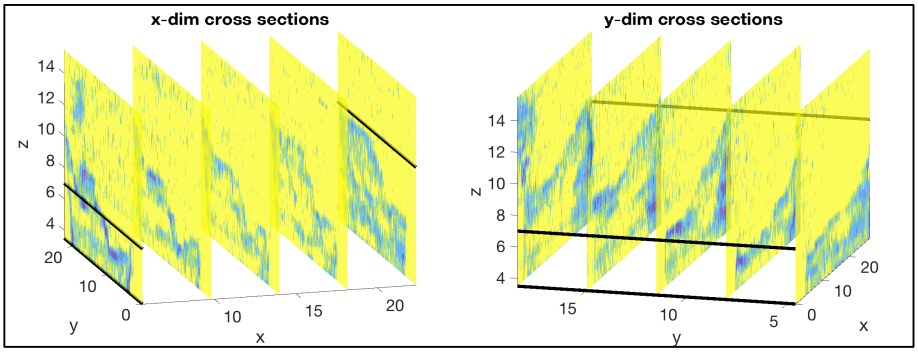

Figure F.13: Matlab interpretation scenario H.7

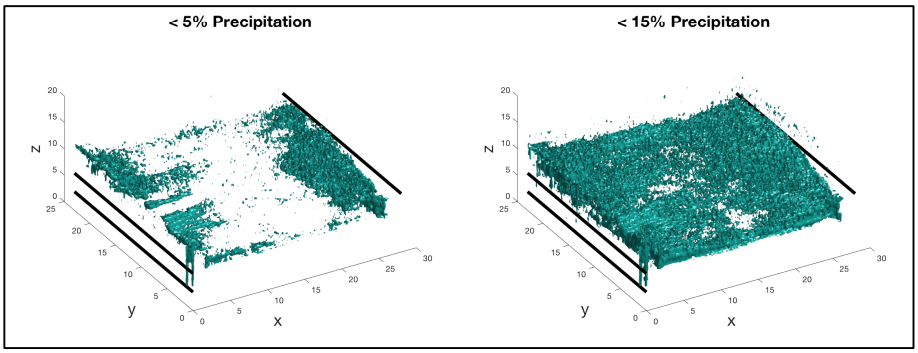

Figure F.14: Precipitation visualisation scenario H.7

Appendix G Results Falling-head Tests

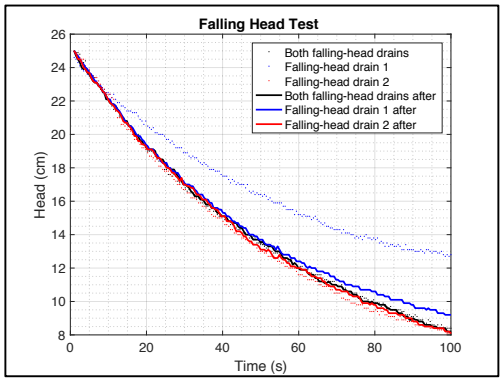

Figure G.1: Falling-head test scenario H.1 (1)

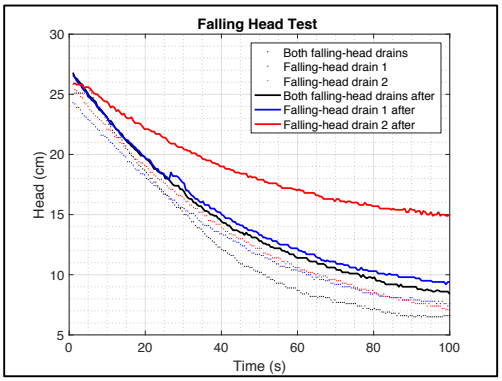

Figure G.2: Falling-head test scenario H.1 (2)

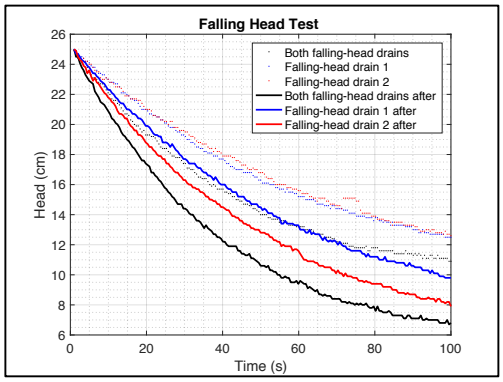

Figure G.3: Falling-head test scenario H.2

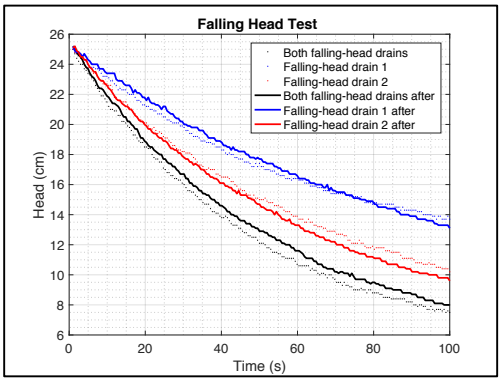

Figure G.4: Falling-head test scenario H.3

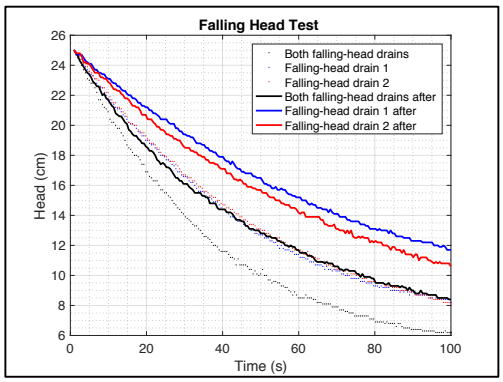

Figure G.5: Falling-head test scenario H.4 (1)

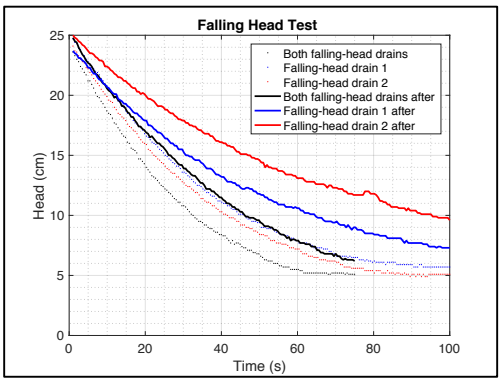

Figure G.6: Falling-head test scenario H.4 (2)

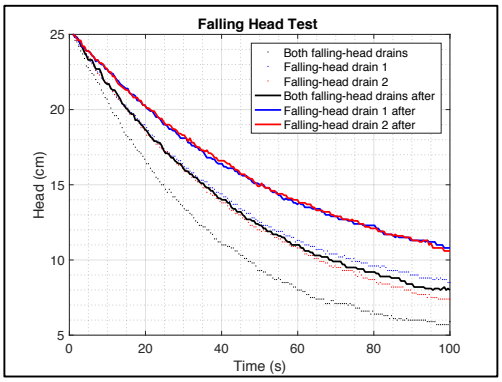

Figure G.7: Falling-head test scenario H.5

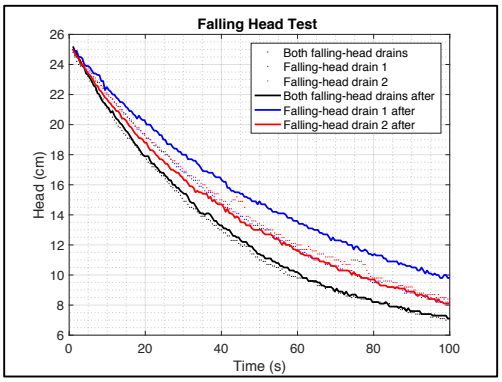

Figure G.8: Falling-head test scenario H.6

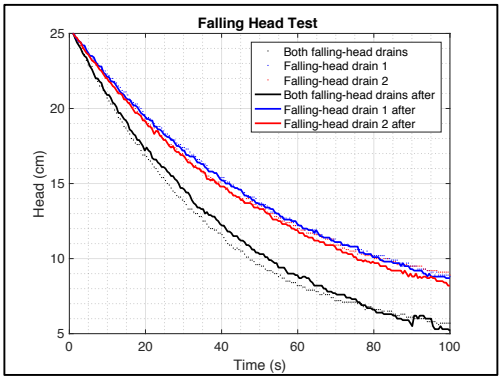

Figure G.9: Falling-head test scenario H.7

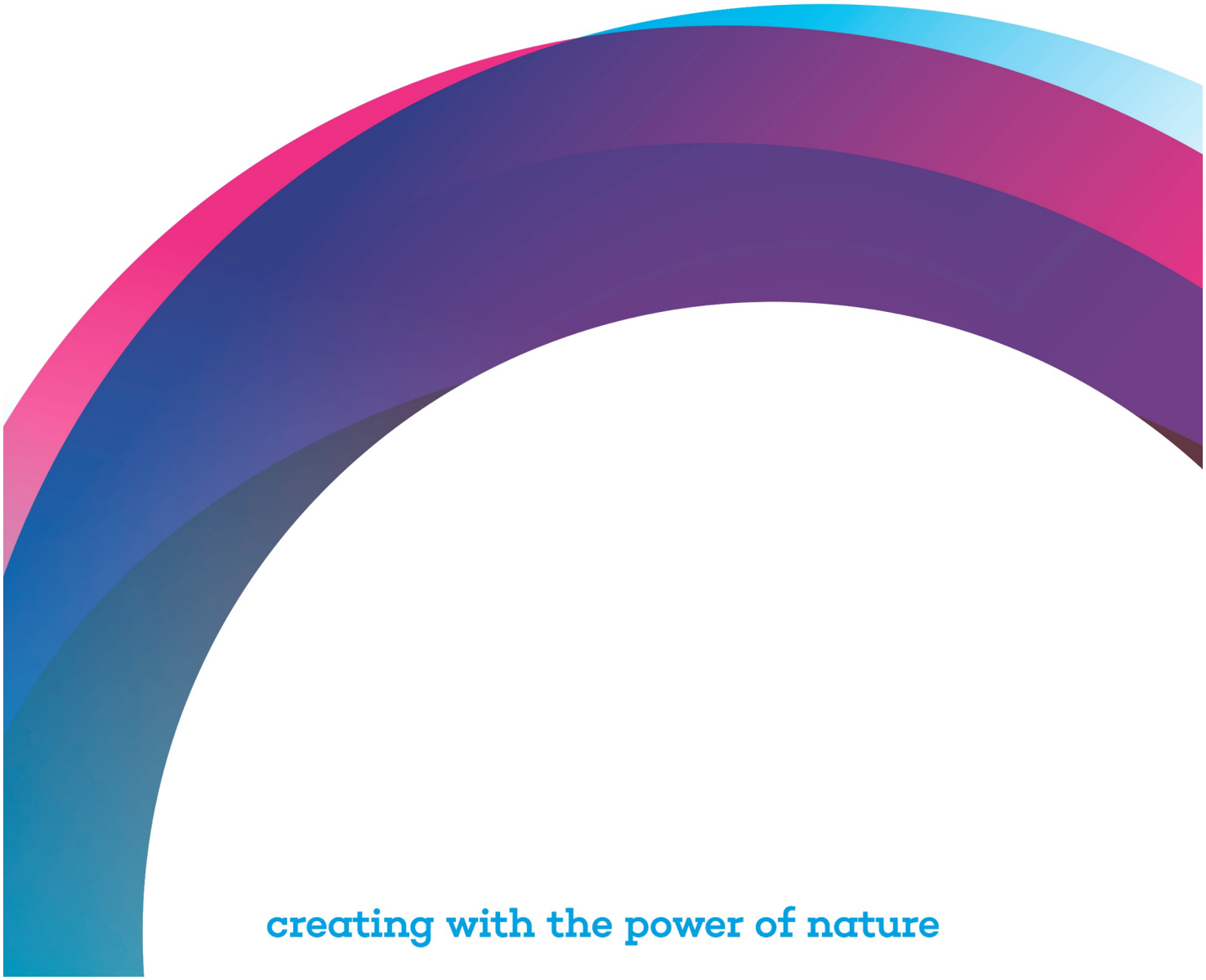

creating with the power of nature